Electrical Stimulation of Rat Primary Motor Cortex for Neurorehabilitation and Neuroprosthetic Applications

by

Azadeh Yazdan-Shahmorad

A dissertation submitted in partial fulfillment
of the requirements for the degree of
Doctor of Philosophy
(Biomedical Engineering)
in The University of Michigan
2011

Doctoral Committee:

      Professor Daryl R. Kipke, Chair
      Associate Professor Edward L. Ionides
      Assistant Professor Parag G. Patil
      Research Associate Mark J. Lehmkuhle

To My Family

Acknowledgement

I would like to thank my advisor, Daryl Kipke, for his support throughout my graduate career. In particular, I am grateful for the opportunity to have been a member of the excellent group of researchers he has brought together over the past years. I am also grateful for the understanding he displayed during a traumatic event that occurred during the course of my research, forcing me to leave the lab for weeks and even months at a time to deal with this issue. His advice to me was: "All we have to think about is your health. Don't even think about your research; just take care of yourself. We can take care of your research later." In addition I'd like to thank the members of my committee, Dr. Patil and Dr. Ionides, for their time and for the helpful discussions we've had about this work.

I would also like to give a special thanks to Dr. Mark Lehmkuhle another member of my committee, for being a great mentor in the past five years. He has helped me in different aspects of my project from the beginning. His guidance has had huge impacts on the progress of my work. In addition to mentoring me, he and his wife have been great friends and have helped me in difficult times. Thanks to Greg Gage who has been a great friend and mentor in the lab from the very first day that I stepped into the Kipke lab. In addition to being a good friend, Greg has always been there to help with an experiment, an idea, a review of a paper, a piece matlab code, etc. Rachel Miriani is another great colleague that I would like to thank. She has helped me a lot with my experiments, especially at the beginning when I was scared of working with rats. I would like to thank

Table of contents

Chapter 2: Polarity of cortical electrical stimulation differentially affects neuronal activity of deep and superficial layers of rat motor cortex

Chapter 4: Estimation of electrode location in rat motor cortex by laminar analysis of electrophysiology and intracortical electrical stimulation

List of Figures

List of Tables

List of Appendices

Chapter 1

Introduction

1.1. Overview

The first description of the electrical excitability of the human cortex was reported by Bartholow in 1874[1]. Since then electrical stimulation of the cortex has been a tool used extensively in experimental neuroscience to elicit neuronal or behavioral responses in a large variety of experiments[2-4]. One of the major focuses has been in neurologic injury and recovery[5-6]. Cortical stimulation techniques can provide insight into the physiological mechanisms of cortical functionality and are under investigation as a possible auxiliary intervention to modulate cortical excitability and enhance training effects[7]. Although a wide range of electrical stimulation parameters have been successfully used for a number of neuroprosthetics and neurorehabilitation applications, the effect of these parameters on the affected brain region is still unknown. Because the cortex and the surrounding anatomy have irregular geometries and inhomogeneous and anisotropic electrical properties, the distribution of electric field and current density generated during cortical stimulation cannot be easily predicted. It is also unclear how the distribution of the electric field and current affect the different neuronal elements in the cortex, because cortical neurons vary in shape, size, location, and orientation. The purpose of this dissertation is to investigate the effects of cortical stimulation on various modalities of

brain signals such as spiking activity, local field potentials (LFP) and electrocorticograms (ECoG) and their contributions to the future neuroprosthetic and neurorehabilitation techniques. The findings of these studies will help to understand and interpret the underlying mechanisms of stimulation effects.

1.2. Cortical Stimulation Methods

At present there are non-invasive and invasive methods for cortical stimulation applicable in settings of experimental procedures that modulate the level of cortical excitability. Transcranial Magnetic Stimulation (TMS) and more recently Transcranial direct current stimulation (tDCS) are two approaches that allow noninvasive and painless central nervous system (CNS) stimulation in living and awake humans [7]. TMS uses a rapidly changing magnetic field to elicit electric currents running parallel to the cortical surface via electromagnetic induction (Figure 1.1a). It is delivered in the form of single, paired and repetitive pulses, each of which can be applied for different experimental purposes[7]. tDCS is a non-invasive non-painful technique that modulates cortical excitability and aspects of behavior by applying prolonged, low-intensity electric current over the scalp[3] (Figure 1.1b). It has been shown that transcranial current application can induce an intracerebral current flow sufficiently large to achieve changes in cortical excitability. Thus, tDCS can be applied to humans non-invasively and painlessly to induce focal, lasting but reversible shifts of cortical excitability. The duration and direction of shifts of excitability depends on stimulus duration, strength and polarity[8].

a

b

Active
Electrode

Reference
Electrode

Anodal

Cathodal

Constant Current
Stimulator
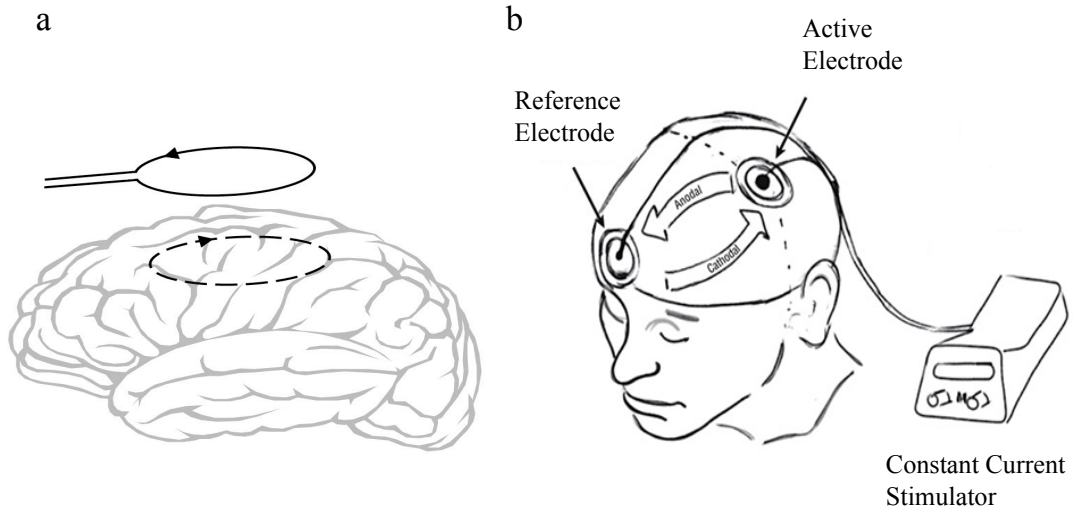
Figure 1.1: Non-invasive cortical stimulation methods. a) The basic principle of transcranial magnetic stimulation showing a time-varying pulse of current in an external coil causing inducing currents in the brain. b) Transcranial direct current stimulation setup and montage. The setup using a mobile battery-operated direct current stimulator connected with 2 electrodes. One electrode (active) is positioned over C3 (corresponding to the precentral gyrus), and the reference electrode is positioned over the contralateral supraorbital region[8].

a

b
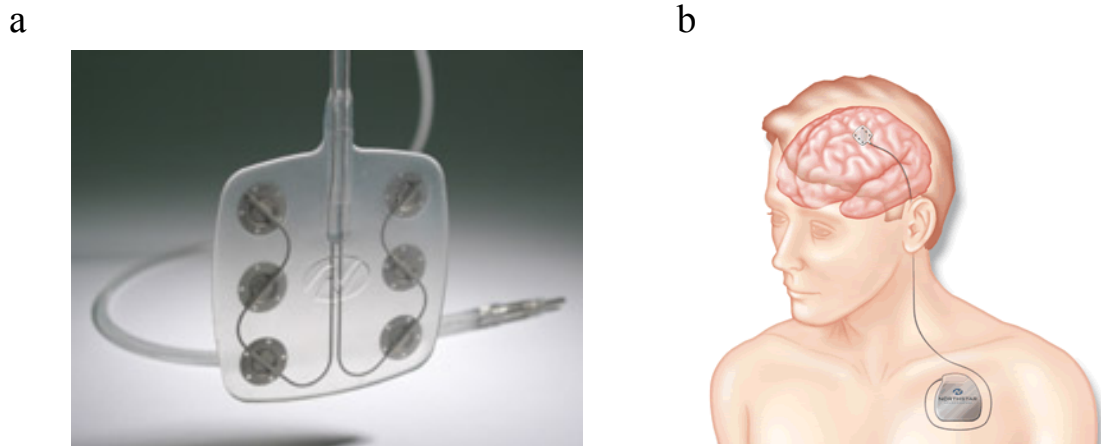
Figure 1.2. a) Surface electrode b) Cortical stimulation investigational device delivering targeted electrical stimulation to the outer surface of the brain (Renova™ Cortical Stimulation Device).
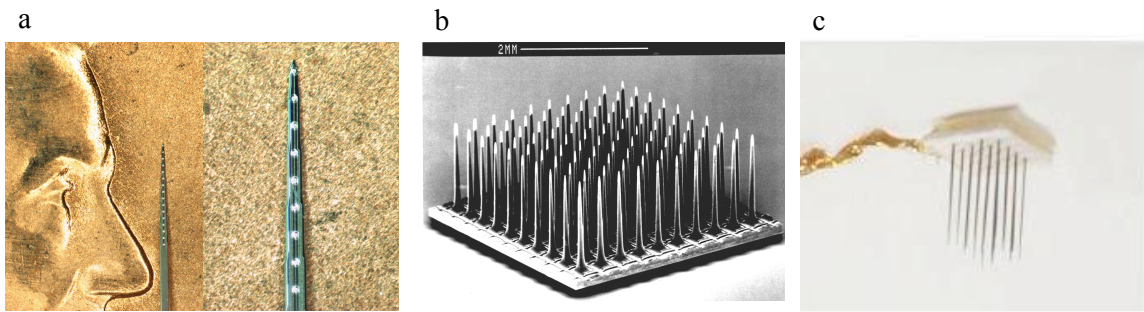
Figure 1.3. Microelectrode arrays used for ICMS. a) Linear electrode array (Michigan probe). b) Utah array. c) Floating microelectrode array (FMA).

Although the focus of cortical stimulation experiments has been on non-invasive techniques to date, their lack in focality and spatial resolution has led this research to invasive methods recently. So far two invasive techniques have been used in cortical stimulation experiments in animals and humans: surface stimulation and intracortical microscimulation (ICMS)[9-18]. Surface stimulation is an invasive technique which produces no damage to the cortical integrity[9] and can be implanted suburally and epidurally[10-12] (Figure 1.2). Subdural "grids" increase spatial resolution as compared to extracranial techniques and have been used to separate functionally distinct subdivision of cortex[11-12]. Instead of subdural placement, electrode grids can be implanted onto the dura (epidurally) which results in less focal stimulation due to greater electrode–tissue distance, but is less invasive with respect to cortex[9]. Placing electrodes into cortex increases spatial resolution and focality of stimulation. Intracortical microstimulation (ICMS) delivers small electrical fields in the immediate vicinity of neurons[13,14]. Linear[15,16] and grid multielectrode arrays[17,18] have been used to stimulate cortical architecture in ICMS to date (Figure 1.3). Needle penetration in ICMS may cause

network dysfunction and slow the diffuse of stimulating current by formation of a nonconductive glial scar [9]. Similar to non-invasive methods, the stimulation patterns (frequency, amplitude and pulse width) varies from different experimental purposes in invasive techniques[9-18].

1.3. Cortical Stimulation Applications

Cortical Stimulation techniques have shown to enhance the beneficial effects of motor training[19], visuomotor coordination[20,21], implicit motor learning[22], skilled finger movements[23], probabilistic classification learning[24], working memory[25] and sleep-dependent consolidation of declarative memories[26] in healthy volunteers.

These findings have led cortical stimulation techniques to move from the research laboratories to the clinical environments. In humans, non-invasive and invasive (epidural) cortical electrical stimulation combined with rehabilitative training has been widely used for the enhancement of recovery from stroke[27-31]. There is also significant evidence in the literature for the use of non-invasive cortical stimulation for epileptic patients[32]. In addition, both high and low frequency subdural cortical stimulation showed a suppressive effect on seizures in human epilepsy[33-35]. TMS and epidural stimulation at low intensities have shown to ameliorate chronic neuropathic pain[36-39]. Primary motor cortex stimulation applied to treat patients with chronic pain lead to concomitant improvement of motor disorders, mainly tremor, related to the underlying neurological lesion at the origin of pain. All these data lead to consider primary motor cortex stimulation as an alternative therapeutic strategy to deep brain stimulation for Parkinson's disease[40]. In addition,

cortical stimulation studies using TMS and tDCS showed an important association between the modulation of the cortex activity and positive emotional processing which makes them good candidates for depression treatment[41,42]. Currently there are several groups working on depression treatment methods using epidural stimulations. Although there has been several experiments done on the therapeutic effect of cortical stimulation on schizophrenia, the experience is still limited and the efficacy has remained as a matter of debate[43]. In addition to the mentioned applications, a major part of cortical stimulation research has been focused on Electrical Stimulation Functional Mapping (ESFM)[9, 44-48].

1.4. Closed-loop cortical stimulation

Although a wide range of electrical stimulation parameters have been successfully used for a number of neuroprosthetics applications, their employment has been in an open-loop fashion. Open-loop refers to stimulation that is independent of brain activity at any particular point in time such that the dynamics of neuronal behavior are not incorporated in the generation of stimulation protocols[49]. Unlike cardiac pacemakers that regulate a rhythmic heartbeat, the brain is a much more complicated dynamical system with trillions of neurons firing in complicated and dissynchronous patterns that require much more complex stimulation protocols to manipulate. In open-loop stimulation systems the stimulation is kept periodically on and off following preset programming, regardless of what the state of the brain is[49]. However the exact nature and timing of these cycles are sometimes very critical. Under normal conditions in which no pathologic state is present, chronically stimulated neurons could easily get fatigued under such long term activation,

resulting in alteration of normal brain function[49-51]. Alternatively, constant stimulation could lead to an alteration in synaptic efficacy in the affected region, changing network characteristics in possibly a deleterious way[49-52]. To address such concerns, studies have been done to incorporate "feedback" in seizure control for epilepsy patients[49, 53-56] and pain control[57] in a number of ways using EEG signals. In general closing the loop would permit precisely timed stimulation with specific parameters that could adjust appropriately to the dynamic of the brain region of interest. Such a control protocol is the most flexible and it can respond to the actual brain activity in a timely fashion. But is also the most demanding in terms of processing ability to adapt to changing neuronal states[49].

1.5. Stimulation parameters

As mentioned before, cortical stimulation has been used in a large number of neuroprosthetic and neurorehabilitation applications. The stimulation parameters used for these applications were chosen based on theoretical considerations, modeling studies or practical experiments. As varying the stimulation parameters such as frequency, amplitude and pulse shape can have significantly different effects on the affected cortical region, choosing the proper stimulation parameters is of high importance. It is also important to keep in mind that for each neuroprosthetic and neurorehabilitation application, specific effects on the neural population are desired.

1.5.1. Stimulation electrode configuration and pulse shape

In the cortical stimulation studies, both bipolar and monopolar electrode configurations have been applied to the cortex[58]. Normally rectangular waveforms have been used for the current or voltage pulses employed in neural stimulators. In the rectangular pulses the rate of current injection is constant for the duration of the pulse. However other pulse shapes have been also used and proposed for neural stimulation purposes. A non-rectangular waveform implies a non-uniform current injection rate. In neural stimulation applications, current pulses are preferred over voltage pulses to eliminate variations in the stimulation threshold as a result of the changes in the electrode–tissue impedance. For rectangular stimuli, the amplitude and duration together determine the stimulus strength and therefore the volume of activation around the tip of the electrode[59]. There have been several investigations to optimize the stimulus waveform in order to maximize the injected charge through the electrode interface while keeping the activation threshold at a minimum [59-61]. It has been shown that this optimization varies as a function of the stimulus waveform and stimulating electrode material[59].

1.5.2. Stimulation pulse polarity

Modeling studies have shown that stimulation pulse polarity have a large and distinct influence on the response of cortical neural elements to stimuli. It has been shown that while neural elements perpendicular to the electrode surface are preferentially excited by anodal stimulation, cathodal stimulation excites those with a direction component parallel to its surface (Figure 1.4). When stimulating bipolarly, the excitation of neural elements

8

parallel to the bipole axis is additionally facilitated[62].
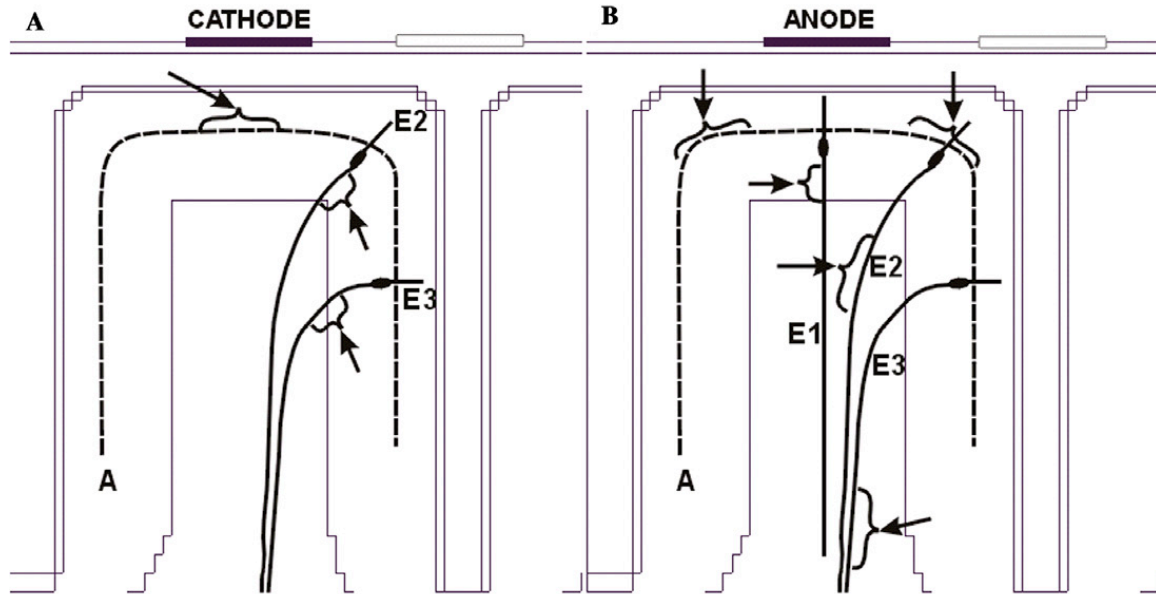
Figure 1.4. Sites of excitation in the 'A' fiber and 'E' neurons when stimulated by the surface electrodes having different polarities. For each electrode configuration, only those neurons that are activated below 30 V are shown. Often a few nodes have a similar threshold; therefore a span of excitation sites is indicated for each neural element[62].

1.5.3. Stimulation Frequency and amplitude

A large number of stimulation frequencies and amplitudes have been used for cortical stimulation in neurorehabilitation and neuroprosthetic applications. These parameters varied based on the stimulation method used. For extra-cranial methods, the stimulation amplitude used was usually higher because the high resistance of the skull shunts most of the current through the scalp[63]. Low and high frequencies of stimulation have been used in these applications. Frequencies up to 250 Hz have been investigated in the

9

neurorehabilitation studies and the therapeutic effects were tracked following the stimulation.

1.6. Dissertation Outline

This dissertation includes three studies which are either in press, submission or preparation for submission to peer-review journals. The first chapter is intended to introduce the reader to the relevant concepts and history not explicitly covered in each of the three studies. The last chapter of the dissertation summarizes the findings of all three studies as a whole and discusses future work and preliminary results stemming directly from these initial studies. All studies in this dissertation are focused on electrical stimulation of the rat motor cortex and evaluating the effects of stimulation on the affected neural population.

In chapter 2, we investigated the effects of CES on unit activity of different neuronal elements in layers of rat primary motor cortex after the offset of stimulation. We evaluated the effects of monopolar CES pulse polarity (anodic versus cathodic) using various stimulation frequencies and amplitudes on unit activity following stimulation. Neural spiking activity before the onset and after the offset of CES was modeled using point processes fit to capture neural spiking dynamics as a function of extrinsic stimuli based on generalized linear model methods. We found that neurons in lower layers have a higher probability of being excited following anodic CES. Conversely, neurons located in upper cortical layers have a higher probability of being excited following cathodic stimulation. The opposing effects observed following anodic vs. cathodic stimulation in

upper and lower layers were frequency- and amplitude-dependent. The data demonstrate that the post-stimulus changes in neural activity following manipulation of CES parameters changes according to the location (depth) of the recorded units in rat primary motor cortex. Chapter 2 was published in the *Brain Stimulation Journal,* 2011.

The purpose of the study reported in Chapter 3 was to investigate the effects of CES on local field potentials (LFP) and electrocorticograms (ECoG) recorded from the rat primary motor cortex and correlate them with the CES effects on the simultaneously recorded unit activity (reported in chapter 2). We investigated these effects after the offset of stimulation on unit activity, LFP and ECoG in rat primary motor cortex by changing the stimulation pulse polarity in various frequencies and amplitudes. Time-frequency spectral analysis was performed on LFPs and ECoGs recorded before the onset and after the offset of CES based on multitaper spectral analysis techniques. Our results showed a high temporal correlation between the effects of CES on unit activity change with the change in the gamma power of the simultaneous recorded LFPs. In addition the time-frequency analysis on ECoG data showed a high temporal correlation between the effects of CES on unit activity change in lower layers (V- VI) with the change in the high gamma power of the simultaneous recorded ECoGs. Chapter 3 is in preparation for submission.

In chapter 4, we have compared two in vivo methods for identifying the placement of electrodes in a linear array spaced 100 μm apart based on in situ laminar analysis of (1) ketamine-xylazine-induced field potential oscillations in rat motor cortex and (2) intracortical electrical stimulation-induced movement threshold. The first method is based on finding the polarity reversal in laminar oscillations which is reported to appear

11

at the transition between layer IV/V in laminar "high voltage spindles" of the rat cortical column. The second method compares the intracortical microstimulation currents that elicit a physical movement for anodic versus cathodic stimulation. Our results showed that the polarity reversal method estimates the beginning of layer V within ±90 μm with 95% confidence and the intracortical stimulation method estimates it within ±69.3 μm. We propose that these methods can be used to estimate the in situ location of laminar electrodes implanted in rat motor cortex. Chapter 4 is under revision for the *Journal of Neural Engineering*.

Chapter 5 summarizes the conclusions from the previous chapters, and places these results in the context of neurorehabilitation and neuroprosthetic applications as a whole. In addition, potential future work stemming from these earlier studies is described.

This dissertation provides several novel improvements to the current understanding of the cortical electrical stimulation in neurorehabilitation and neuroprosthetic applications, which have been evaluated in-vivo. These findings might go a long way toward developing new treatments that are more precisely targeted to the specific cortical systems affected. The results presented here not only improve the current stimulation parameters used for practical neurorehabilitation and neuroprosthetic applications, but contributes to the fundamental understanding of the effects of stimulation effects in the cortex.

1.7. References

1. Barthlow R. Experimental investigations into the function of the human brain. American journal of the medical sciences. 1874; 134: 305-313.

2. Butovas S, Schwarz C. Spatiotemporal Effects of Microstimulation in Rat Neocortex: A Parametric Study Using Multielectrode Recordings. Journal of neurophysiology. 2003;90(5):3024.

3. Harris-Love ML, Cohen LG. Noninvasive Cortical Stimulation in Neurorehabilitation: A Review. Archives of physical medicine and rehabilitation. 2006;87(2):84.

4. Ilic TV, Ziemann U. Exploring motor cortical plasticity using transcranial magnetic stimulation in humans. Biophysics from molecules to brain: In memory of Radoslav K Andjus. 2005;1048:175-84.

5. Ranck JB. Which elements are excited in electrical stimulation of mammalian central nervous system – Review. Brain Research. 1975;98(3):417-40.

6. Rossini PM, Martino G, Narici L, Pasquarelli A, Peresson M. Short-term brain pÌ€lasticity' in humans: transient finger representation changes in sensory cortex somatotopy following ischemic anesthesia. Brain research. 1994;642(1-2):169-2.

7. Tehovnik EJ. Electrical stimulation of neural tissue to evoke behavioral responses. Journal of neuroscience methods. 1996;65(1):1.

8. Schlaug G, Renga V. Transcranial direct current stimulation: a noninvasive tool to facilitate stroke recovery. Expert Rev. Med. Devices. 2008; 5(6): 759-768.

9. Molina-Luna K, Buitrago MM, Hertler B, Schubring M, Haiss F, Nisch W, et al. Cortical stimulation mapping using epidurally implanted thin-film microelectrode arrays. Journal of neuroscience methods. 2007;161(1):118.

10. Lee W-s, Lee J-K, Lee S-A, Kang J-K, Ko T-s. Complications and results of subdural grid electrode implantation in epilepsy surgery. Surgical neurology. 2000;54(5):346.

11. Nii Y, Uematsu S, Lesser RP, Gordon B. Does the central sulcus divide motor and sensory functions? Cortical mapping of human hand areas as revealed by electrical stimulation through subdural grid electrodes. NEUROLOGY. 1996;46(2):360-7.

12. Kitzmiller J, Beversdorf D, Hansford D. Fabrication and testing of microelectrodes for small-field cortical surface recordings. Biomedical Microdevices. 2006;8(1):81-5.

13. Neafsey EJ, Bold EL, Haas G, Hurleygius KM, Quirk G, Sievert CF, et al. The organization of the rat motor cortex- A microstimulation mapping study. Brain Research reviews. 1986;11(1):77-96.

14. Suner S, Fellows MR, Vargas-Irwin C, Nakata GK, Donoghue JP. Reliability of Signals From a Chronically Implanted, Silicon-Based Electrode Array in Non-Human Primate Primary Motor Cortex. IEEE transactions on neural systems and rehabilitation engineering : a publication of the IEEE Engineering in Medicine and Biology Society. 2005;13(4):524.

15. Jensen W, Yoshida K, Hofmann UG. In-vivo implant mechanics of flexible, silicon-based ACREO microelectrode arrays in rat cerebral cortex. IEEE Transactions on Biomedical Engineering. 2006;53(5):934-40.

16. Kipke DR, Vetter RJ, Williams JC, Hetke JF. COMMUNICATIONS - Silicon-Substrate Intracortical Microelectrode Arrays for Long-Term Recording of Neuronal Spike Activity in Cerebral Cortex. IEEE transactions on neural systems and rehabilitation engineering : a publication of the IEEE Engineering in Medicine and Biology Society. 2003;11(2):151.

17. Kim S-J, Manyam S, Warren D, Normann R. Electrophysiological Mapping of Cat Primary Auditory Cortex with Multielectrode Arrays. Annals of Biomedical Engineering. 2006;34(2):300-9.

18. Warren DJ, Fernandez E, Normann RA. High-resolution two-dimensional spatial mapping of cat striate cortex using a 100-microelectrode array. Neuroscience. 2001;105(1):19-31.

19. Antal A, Nitsche MA, Kincses TsZ, Kruse W, Hoffmann K-P, Paulus W. Facilitation of visuo-motor learning by transcranial direct current stimulation of the motor and extrastriate visual areas in humans. European Journal of Neuroscience. 2004;19(10):2888-92.

20. Antal A, Nitsche MA, Kruse W, Kincses TsZ, Hoffmann K-P, Paulus W. Direct Current Stimulation over V5 Enhances Visuomotor Coordination by Improving Motion Perception in Humans. Journal of Cognitive Neuroscience. 2004;16(4):521-7.

21. Butefisch CM, Khurana V, Kopylev L, Cohen LG. Enhancing Encoding of a Motor Memory in the Primary Motor Cortex By Cortical Stimulation. Journal of neurophysiology. 2004;91(5):2110.

22. Fregni F, Boggio PS, Nitsche M, Bermpohl F, Antal A, Feredoes E, et al. Anodal transcranial direct current stimulation of prefrontal cortex enhances working memory. Experimental Brain Research. 2005;166(1):23-30.

23. Kincses TZ, Antal A, Nitsche MA, Bartfai O, Paulus W. Facilitation of probabilistic classification learning by transcranial direct current stimulation of the prefrontal cortex in the human. Neuropsychologia. 2004;42(1):113-7.

24. Kobayashi M, Hutchinson S, Theoret H, Schlaug G, Pascual-Leone A. Repetitive TMS of the motor cortex improves ipsilateral sequential simple finger movements. NEUROLOGY. 2004;62(1):91-8.

25. Marshall L, Molle M, Hallschmid M, Born J. Transcranial direct current stimulation during sleep improves declarative memory. Journal of Neuroscience. 2004;24(44):9985-92.

26. Nitsche MA, Schauenburg A, Lang N, Liebetanz D, Exner C, Paulus W, et al. Facilitation of implicit motor learning by weak transcranial direct current stimulation of the primary motor cortex in the human. Journal of Cognitive Neuroscience. 2003;15(4):619-26.

27. Adkins-Muir DL. Cortical electrical stimulation combined with rehabilitative training: Enhanced functional recovery and dendritic plasticity following focal cortical ischemia in rats. Neurological research. 2003;25(8):780.

28. Blanke O. Electrical Cortical Stimulation of the Human Prefrontal Cortex Evokes Complex Visual Hallucinations. Epilepsy & Behavior. 2000;1(5):356-61.

29. Blanke O. Simple and complex vestibular responses induced by electrical cortical stimulation of the parietal cortex in humans. Journal od Neurology, Neurosurgery and Psychiatry. 2000;69(10):553-6.

30. Brown JA. Motor Cortex Stimulation for the Enhancement of Recovery from Stroke: A Prospective, Multicenter Safety Study. Neurosurgery. 2006;58(3):464.

31. Canavero. Transcranial Magnetic Cortical Stimulation Relieves Central Pain. Stereotactic and Functional Neurosurgery. 2002;78(3-4):192-4.

32. Corina DP. Dissociation of action and object naming: Evidence from cortical stimulation mapping. Human brain mapping. 2005;24(1):1.

33. Lazzaro V. Comparison of descending volleys evoked by monophasic and biphasic magnetic stimulation of the motor cortex in conscious humans. Experimental brain research. 2001;141(1):121.

34. Fitzgerald PB, Huntsman S, Gunewardene R, Kulkarni J, Daskalakis ZJ. A randomized trial of low-frequency right-prefrontal-cortex transcranial magnetic stimulation as augmentation in treatment-resistant major depression. The International Journal of Neuropsychopharmacology. 2006;9(6):655-66.

35. Hummel F. Effects of non-invasive cortical stimulation on skilled motor function in chronic stroke. Brain. 2005;128(3):490-9.

36. Hummel F. Improvement of Motor Function with Noninvasive Cortical Stimulation in a Patient with Chronic Stroke. Neurorehabilitation and Neural Repair. 2005;19(1):14-9.

37. Loo CK. Applications of transcranial magnetic stimulation (TMS) in psychiatry. Journal of ECT. 2002;18(1):62.

38. Kinoshita M, Ikeda A, Matsuhashi M, et al. Electric cortical stimulation suppresses epileptic and background activities in neocortical epilepsy and mesial temporal lobe epilepsy. Clinical neurophysiology : official journal of the International Federation of Clinical Neurophysiology. 2005;116(6):1291.

39. Lefaucheur J-P. New insights into the therapeutic potential of non-invasive transcranial cortical stimulation in chronic neuropathic pain. Pain. 2006;122(1):11.

40. Lefaucheur JP. Repetitive transcranial magnetic stimulation (rTMS): insights into the treatment of Parkinson's disease by cortical stimulation. Clinical Neurophysiology. 2006;36(3):125-33.

41. Lefaucheur JP. Repetitive transcranial magnetic stimulation (rTMS): insights into the treatment of Parkinson's disease by cortical stimulation. Clinical Neurophysiology. 2006;36(3):125-33.

42. Lubrano V. Writing-specific sites in frontal areas: A cortical stimulation study. Journal of neurosurgery. 2004;101(5):787.

43. Plautz EJ. Post-infarct cortical plasticity and behavioral recovery using concurrent cortical stimulation and rehabilitative training: A feasibility study in primates. Neurological research. 2003;25(8):801.

44. Saba G. Therapeutic and neurophysiologic aspects of transcranial magnetic stimulation in schizophrenia. Clinical Neurophysiology. 2006;36(3):185-94.

45. Schrader LM, Stern JM, Wilson CL, Fields TA, Salamon N, Nuwer MR, et al. Low frequency electrical stimulation through subdural electrodes in a case of refractory status epilepticus. Clinical Neurophysiology. 2006;117(4):781-8.

46. Tassinari CA, Cincotta M, Zaccara G, and Michelucci R. Transcranial magnetic stimulation and epilepsy. Clinical Neurophysiology. 2003; 114: 777-798.

47. Xiong Y. Effects of cortical stimulation on auditory-responsive thalamic neurones in anaesthetized guinea pigs. The Journal of Physiology. 2004;560(1):207-17.

48. Yamamoto J. Low-frequency electric cortical stimulation decreases interictal and ictal activity in human epilepsy. Seizure- European Journal of Epilapsy. 2006;15(7):520-7.

49. Li Y. Electrical Control of Epileptic Seizures. Journal of clinical neurophysiology : official publication of the American Electroencephalographic Society. 2007;24(2):197.

50. Fregni F. Rapid-rate repetitive transcranial magnetic stimulation and cognitive function in Parkinson's disease patients: A safety study. Movement disorders. 2004;19:S240-S1.

51. Michelucci R. Rapid-rate transcranial magnetic stimulation and hemispheric language dominance: Usefulness and safety in epilepsy. Neurology. 1994;44(9):1697.

52. Jahanshahi M. Rapid rate transcranial magnetic stimulation - a safety study. Electroencephalography and clinical neurophysiology. 1997;105(6):422.

53. Nakagawa M. Suppression of spontaneous epileptiform activity with applied currents. Brain research. 1991;567(2):241-7.

54. Krauss G. Cerebellar and Thalamic Stimulation for Epilepsy. Advances in neurology. 1994;63:231-46.

55. Warren RJ. Effects of applied currents on spontaneous epileptiform activity induced by low calcium in the rat hippocampus. Brain research. 1998;806(2):186.

56. Sun FT. Responsive cortical stimulation for the treatment of epilepsy. Neurotheraoeutics. 2008;5(1):68-74.

57. Ativanichayaphong T, He JW, Hagains CE, Peng YB, Chiao JC. A combined wireless neural stimulating and recording system for study of pain processing. Journal of Neuroscience methods. 2008;170(1):25-34.

58. Kombos T. Comparison Between Monopolar and Bipolar Electrical Stimulation of the Motor Cortex. Acta neurochirurgica. 1999;141(12):1295.

59. Sahin M, Tie Y. Non-rectangular waveforms for neural stimulation with practical electrodes. Journal of Neural Engineering. 2007;4(3):227-33.

60. Blair HA. On the intensity-time relations for stimulation by electric currents. I: The Rockefeller University Press.

61. Ayers GM, Aronson SW, Geddes LA. Comparison of the ability of the lapicque and exponential strength-duration curves to fit experimentally obtained perception threshold data. Australasian Physical and Engineering Sciences in Medicine. 1986;9(3):111-6.

62. Manola L. Anodal vs cathodal stimulation of motor cortex: A modeling study. Clinical neurophysiology : official journal of the International Federation of Clinical Neurophysiology. 2007;118(2):464.

63. Basser PJ. New currents in electrical stimulation of excitable tissues. Annual Review of Biomedical Engineering. 2000;2:377-97.

Chapter 2

Polarity of cortical electrical stimulation differentially affects neuronal activity of deep and superficial layers of rat motor cortex

2.1. Abstract

Cortical electrical stimulation (CES) techniques are practical tools in neurorehabilitation that are currently being used to test models of functional recovery after neurological injury. However, the mechanisms by which CES has therapeutic effects, is not fully understood. In this study we investigated the effects of CES on unit activity of different neuronal elements in layers of rat primary motor cortex after the offset of stimulation. We evaluated the effects of monopolar CES pulse polarity (anodic versus cathodic) using various stimulation frequencies and amplitudes on unit activity following stimulation. A penetrating single shank silicon microelectrode array enabled us to span the entirety of 6 layer motor cortex allowing simultaneous electrophysiological recordings from different depths following monopolar CES. Neural spiking activity before the onset and after the offset of CES was modeled using point processes fit to capture neural spiking dynamics as a function of extrinsic stimuli based on generalized linear model methods. We found that neurons in lower layers have a higher probability of being excited following anodic CES. Conversely, neurons located in upper cortical layers have a higher probability of being excited following cathodic stimulation. The opposing effects observed following anodic vs. cathodic stimulation in upper and lower layers were frequency- and amplitude-dependent. The data demonstrate that the post-stimulus changes in neural activity

following manipulation of CES parameters changes according to the location (depth) of the recorded units in rat primary motor cortex. The most effective pulse polarity for eliciting action potentials following stimulation in lower layers was not as effective in upper layers. Likewise, lower amplitudes and frequencies of CES were more effective than higher amplitudes and frequencies for eliciting action potentials. These results have important implications in the context of maximizing efficacy of CES for neurorehabilitation and neuroprosthetic applications.

2.2. Introduction

Cortical electrical stimulation (CES) has been used extensively in experimental neuroscience to modulate neuronal or behavioral activity which has led this technique to be considered in neurorehabilitation. In healthy volunteers, cortical stimulation techniques have been shown to affect a wide variety of cortical systems, enhancing the beneficial effects of motor training[1-2], implicit motor learning[3], skilled finger movements[4], probabilistic classification learning[5], working memory[6] and sleep-dependent consolidation of declarative memories[7]. Cortical stimulation techniques for use as neuroprosthetics have shown evidence for enhanced recovery from stroke[8], suppression of seizures in epilepsy[9], amelioration of chronic neuropathic pain[10], improved motor symptoms in Parkinson's disease[11] and reduced depression[12]. The mechanisms by which cortical stimulation has therapeutic effects is not fully understood. Because the cortex and the surrounding anatomy have irregular geometries and inhomogeneous and anisotropic electrical properties, the distribution of electric field and current density generated during cortical stimulation cannot be easily predicted. It is also

unclear how the distribution of the electric field and current affect the different neuronal elements in the cortex, since cortical neurons vary in shape, size, location and orientation[13-14]. Although there have been several modeling studies on current flow and neuronal polarization in the cortex[14-18], there is little knowledge on the effects of CES *in vivo*. The therapeutic effects of CES may be improved when the stimulation parameters (polarity, frequency, amplitude, etc) can be optimized based on knowledge of the neuronal elements to be targeted.

Modeling studies have shown that while neuronal elements perpendicular to the electrode surface are preferentially excited by anodic stimulation, cathodic stimulation excites those with a direction component parallel to its surface[14-15]. In this study we investigated these effects after the offset of stimulation on unit activity of different neuronal elements in rat primary motor cortex by changing the stimulation pulse polarity in various frequencies and amplitudes. A penetrating single shank silicon microelectrode array enabled us to span the entirety of 6 layer cortex allowing simultaneous electrophysiological recordings from different depths[19] following monopolar CES. Neural spiking activity before the onset and after the offset of CES was modeled using point processes fit to the neural spike trains based on generalized linear model methods[20]. The models characterized the differences in spiking propensity to capture temporal variations in neural spiking following the co-variation of CES parameters. Our results agree with previous modeling studies and show an increase in unit activity following anodic stimulation and a decrease in unit activity following cathodic stimulation in lower layers (V-VI) units after the offset of stimulation. The opposite post-stimulus effect was seen for the units in upper cortical layers (I-II). These opposing effects observed

22

following anodic vs. cathodic stimulation in upper and lower layers were frequency- and amplitude-dependent.

2.3. Methods

2.3.1. Subjects

Six normal male rats (Charles River Laboratories) were implanted with two bone screws used to deliver (source) monopolar CES to primary motor cortex as well as a much larger current return (sink). A micro-scale penetrating electrode array (NeuroNexus Technologies) consisting of 16-electrodes spaced 100μm apart (Figure 2.1a) was implanted to span the entirety of 6-layer motor cortex[19]. This electrode array was implanted to record extracellular action potentials from the forelimb representation of primary motor cortex and was angled toward the cortical stimulation electrode such that extracellular action potentials had a higher probability of being affected by the cortical stimulation (Figure 2.1b).

2.3.2. Electrophysiological Recordings and Stimulation protocol

Animals were placed in a faraday cage where all signals could be routed through a commutator to a wireless stimulation device (Northstar Neuroscience) and multichannel neural signal amplifier (MNAP, Plexon Inc., Dallas, TX). For spike recordings, the signals were filtered with a passband of 150-8000Hz, further amplified and sampled at 40kHz. Unit spiking activity was sorted offline from each channel using Offline Sorter software (Plexon Inc., Dallas, TX).
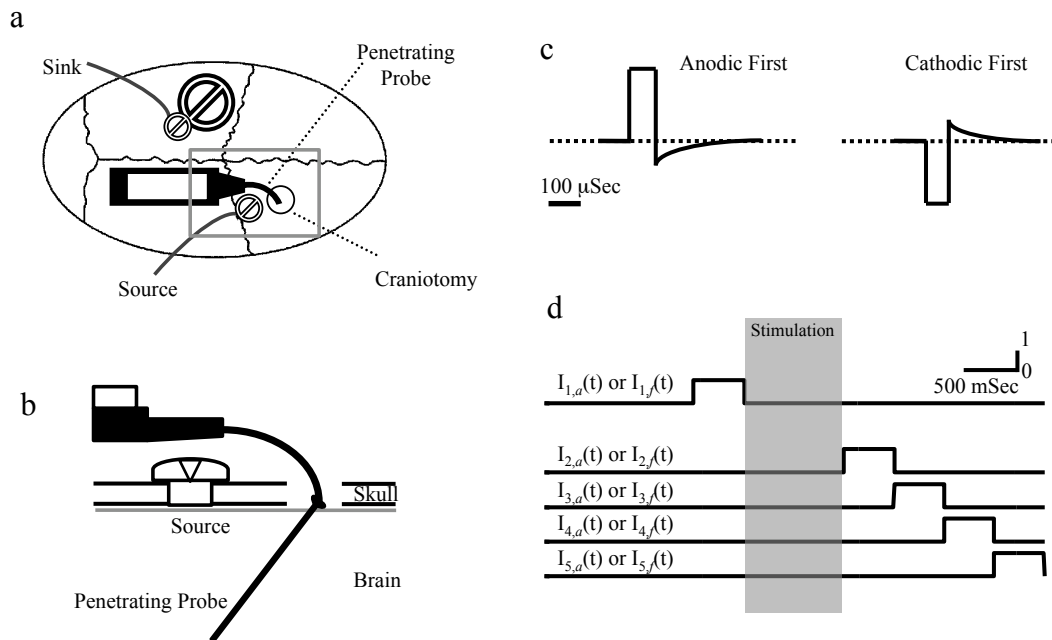
Figure 2.1. a) Horizontal schematic of the rat skull showing the locations of craniotomy, implanted CES screws and penetrating probe. The current sink was shorted to a much larger bone screw (depicted). Rostral is to the right. b) Conceptual cross section in the sagital plane of the implanted probe enlarged from the gray box in (a) (rostral is to the right). The penetrating electrode was angled toward the cortical stimulation electrode such that recorded extracellular action potentials had a high probability of being affected by the cortical stimulation (electrodes are on the side of the silicon shank that faces the current source). c) Pulse shapes: Constant current CES was delivered in two configurations, Cathodic or Anodic consisting of pulse trains. Pulses consisted of square leading phase (100μsec) followed by an exponentially decaying second phase to balance charge. The pulse width of the leading phase was fixed at 100μsec and the length of the trailing phase varied according to leading phase current in order to balance the charge. d) Time intervals $I_{i,a}(t)$ or $I_{i,f}(t)$ for i=1,2,3,4,5 with respect to stimulation time. Stimulation starts at time 0 and end at 1000 ms. i=1 corresponds to 500ms before the onset of the stimulation and i={2,3,4,5} correspond to the four 500 ms time intervals after the offset of the stimulation.

Constant current CES was delivered in two configurations, cathodic or anodic consisting of pulse trains at frequencies of 25, 50, 100, 250, or 500Hz. Pulses consisted of square leading phase (100μsec) followed by an exponentially decaying second phase to balance charge of length dependent upon the amplitude of the leading phase (Figure 2.1c). Prior to starting the stimulation, a Movement Inducing Current (MIC) was determined for each frequency. MICs were determined as the weakest current passed through the cortical electrode that caused a forced movement in 50 % of test pulses[8,21]. The average measured

MIC for anodic and cathodic was 2.33±0.21 and 2.44±0.21 mA respectively. Once MICs were determined, 25, 50, and 75% of MIC was calculated. Recording sessions proceeded as follows: An entire session consisted of either cathodic or anodic stimulation pulses. A random combination (without replacement) of stimulation frequency and percentage of MIC current was chosen to be presented to the animal in 25 repetitions of 1 sec of stimulation followed by 4 sec of recording. It is important to point out that for each frequency of stimulation there were different numbers of pulses in the 1 second duration of stimulation.
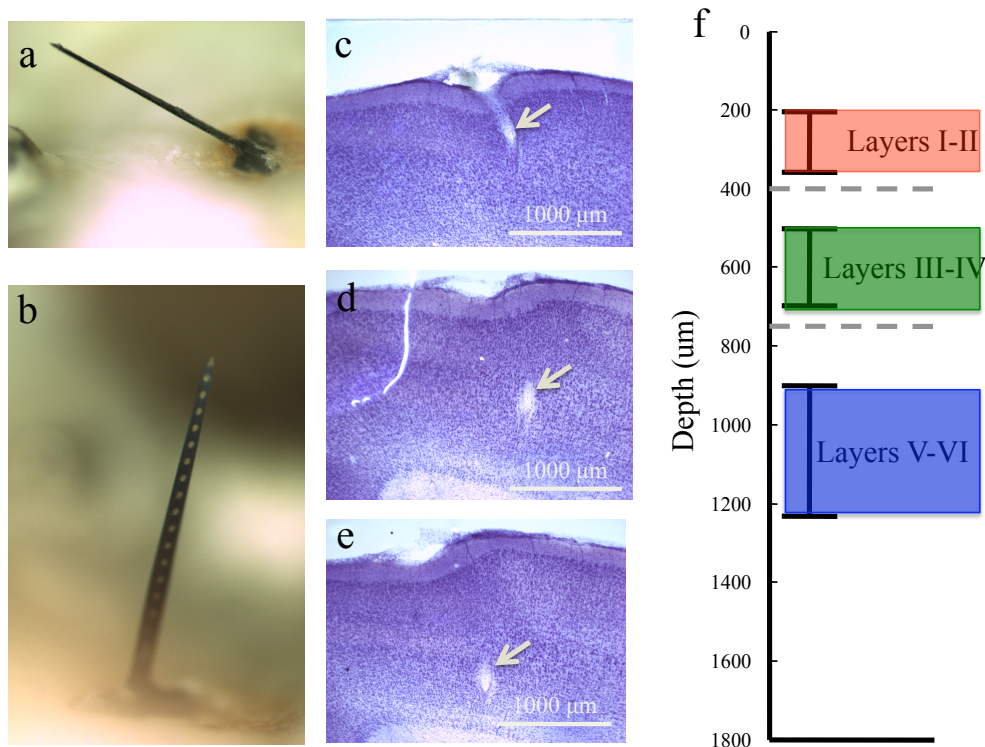
Figure 2.2. a,b) Images of explanted skulls: The angle and depth of the probe was estimated using these images. Individual electrodes can be seen along the silicon shank in (b). c-e) Images taken of histology from one rat. Three lesion marks are shown at different depths where the electrode was implanted in this series of serial slide sections. f) Depth distribution of the units in each of the layer categories used in the analyses. There were 19 units in Layers I-II (205-359μm). There were 19 units in Layers III-IV (502-698μm). There were 69 units located in Layers V-VI (900-1230μm).

2.3.3. Microlesioning and Histology

Upon completion of the experiment, electrolytic lesions were made followed by histological analysis to determine the electrode site locations within the different cortical layers[22]. In all cases, electrodes extracted from the brain were intact and were kept attached to the skull/headcap (Figure 2.2a-b). 100μm coronal slices were stained with a standard cresyl-violet (Nissl) staining method (Figure 2.2c-e). Exact stereotaxic positions of lesion marks and probe tracts were identified by co-registering histological images to the estimated probe locations from the images of the intact electrode arrays[22].

2.3.4. Point process model

A point process model was formulated to relate the spiking propensity of each unit to factors associated with the stimulation parameters (frequency and amplitude) in the time intervals before the onset and after the offset of stimulation. Point process models have been shown to be useful in characterizing neural spiking activity[20,23,24]. Conventional methods for analyzing the spiking activity of neurons are based on linear or nonlinear regression methods[25-27]. Although these methods have played an important role in characterizing the spiking properties in many neural systems, they could not be used to fully address several issues. First, neural spike trains form a sequence of discrete events or point process time series[20,28]. Standard linear or nonlinear regression methods are not designed for the analysis of discrete events and point process observations. To model spike trains with conventional regression methods the data are usually smoothed or binned which alters the stochastic structure of the data and, therefore, the inferences made from their analysis. Second, model goodness-of-fit assessment method should also

26

be appropriate for the discrete nature of neural spike trains[20]. To avoid the potential problems associated with these methods we used a point process likelihood framework to analyze the spiking activity in our dataset. The point process framework provides a flexible, computationally efficient approach for maximum likelihood estimation, goodness-of-fit assessment, model selection and neural coding[20]. A point process is a set of discrete events that occur in continuous time (e.g., the number of neuronal spikes in a given time interval) and is characterized entirely by the conditional intensity function (CIF) which is a history-dependent generalization of the rate function for the Poisson process. It provides a canonical representation of the stochastic properties of a neural spike train[20]. In this study, the time interval $(0,T]$ denotes the observation interval and $0 < t_1 < t_2... < t_n \leq T$ are a set of spike time measurements. If $N(t)$ is the number of spikes in $(0, t]$, then the conditional intensity function is defined for any $t \in (0,T]$ as:

$$(2.1) \qquad \lambda(t \mid H_t) = \lim_{\Delta t \to 0} \frac{\Pr(Spike \ \ in \ \ (t, t + \Delta t) \mid H_t)}{\Delta t}$$

Ht is the history of the spiking activity and that of any covariates up to time t. Consequently, equation (2.1) defines the probability of a spike in any small time interval $(t, t + \Delta)$ as follows:

$$(2.2) \qquad \Pr(Spike \ in \ (t, t+\Delta) \mid H_t) \approx \lambda(t \mid H_t)\Delta$$

When Δ is small, equation (2.2) is roughly the spiking propensity at any time t. To analyze the spiking propensity of the neurons, we define the CIF as a function of stimulation frequency $f \in \{1,2,3,4,5\}$ which corresponds to 25, 50, 100, 250 and 500Hz and stimulation amplitude $a \in \{1,2,3,4\}$ which corresponds to 25, 50, 75 and 100%MIC. Time was divided into five intervals of 500 ms with variable i, where i=1 corresponds to the 500ms before the onset of stimulation and i=\{2,3,4,5\} correspond to (0-500), (500-1000), (1000-1500) and (1500-2000)ms time intervals after the offset of the stimulation (Figure 2.1d).

$$(2.3) \qquad \lambda(t \mid H_t) = \exp\{\sum_{i=1}^{5}\sum_{a=1}^{4}\alpha_{i,a}I_{i,a}(t) + \sum_{i=1}^{5}\sum_{f=1}^{5}\beta_{i,f}I_{i,f}(t)\}$$

The following quantities are computed from data: $I_{i,a}(t)$ is equal to 1 for the time interval i and stimulation amplitude a and is equal to 0 otherwise. $I_{i,f}(t)$ is equal to 1 for the time interval i and stimulation frequency f and is equal to 0 otherwise (Figure 2.1d). Separate models were built for the anodic and cathodic stimulation sessions.

The model can be fit to the neural spike trains using general linear model (GLM) methods[17]. The GLM is an extension of the multiple linear regression model in which the variable being predicted, in this case spike times, need not be Gaussian[20]. GLM provides an efficient computational scheme for model parameter estimation and a likelihood framework for conducting statistical inferences based on the estimated model[23-24]. The maximum-likelihood estimates and confidence intervals of θ were computed for each neuron using the glmfit.m function in MATLAB.

The model parameter vector $\theta = \{\alpha_{i,a}, \beta_{i,f}\}$ was fitted to the data, where $\{\alpha_{i,a}\}$ measured the spiking probability for different amplitudes and $\{\beta_{i,f}\}$ measured the spiking probability for different frequencies. The $\{\alpha_{1,a}, \beta_{1,f}\}$ parameters measured the spiking probability 500ms before the onset of stimulation and $\{\alpha_{2-5,a}, \beta_{2-5,f}\}$ parameters measured the effects of CES in (0-500), (500-1000), (1000-1500), and (1500-2000)ms time intervals after the offset of stimulation on the spiking probability, respectively. Therefore the difference between $\{\alpha_{2-5,a}, \beta_{2-5,f}\}$ and $\{\alpha_{1,a}, \beta_{1,f}\}$ can capture the effects of different stimulation parameters on spiking probability at different time intervals after the offset of stimulation. To compare these effects across all units, the model parameters for anodic and cathodic stimulation models ($\{\alpha_{i,a}\}$ and $\{\beta_{i,f}\}$) were scaled to have values between -1 and 1 using the following equations:

$$(2.4) \quad \alpha_{i,a_{scaled}} = \frac{\alpha_{i,a}}{\max |\{\alpha_{i,a}\}|} \qquad \text{and} \qquad (2.5) \quad \beta_{i,f_{scaled}} = \frac{\beta_{i,f}}{\max |\{\beta_{i,f}\}|}$$

The differences of these scaled parameters for all of the four time intervals defined in the model were calculated:

$$(2.6) \qquad D_{j,a} = \alpha_{i,a_{scaled}} - \alpha_{1,a_{scaled}} \qquad , \qquad i=2,3,4,5$$

$$(2.7) \qquad D_{j,f} = \beta_{i,f_{scaled}} - \beta_{1,f_{scaled}} \qquad , \qquad i=2,3,4,5 \quad , \quad j=i\text{-}1$$

2.3.5. Statistical Analysis

To estimate the effect of various parameters in different depths of motor cortex the neuron populations were divided into three groups. Group 1 is defined as Layers I-II (0-400µm), Group 2 as Layers III-IV (400-750µm) and Group 3 as Layers V-VI (750-

1800μm) below the cortical surface. The distribution of the units over depth for each group can be seen in Figure 2.2f. The depth of these layers in motor cortex is reported in (29) and verified through histology.

The effects of stimulation parameters were divided between amplitude ($D_{j,a}$) and frequency ($D_{j,f}$) model parameters. A 2×4×3×4 ANOVA was constructed in SPSS Statistics 18 (IBM Company, Chicago, IL) for $D_{j,a}$ factors: pulse polarity (Anodic vs Cathodic), percent MIC (25,50,75,100%), Depth (Layers I-II, III-IV, V-VI) and time intervals (0-500,500-1000,1000-1500,1500-2000ms after the offset of the stimulation). Likewise, a 2×5×3×4 ANOVA was constructed for $D_{j,f}$ factors: pulse polarity (Anodic vs. Cathodic), Frequency (25, 50, 100, 250, 500Hz), Depth (Layers I-II, III-IV, V-VI) and time intervals (0-500, 500-1000, 1000-1500, 1500-2000ms after the offset of the stimulation). Based on significant interactions effects ($p < 0.05$, e.g. pulse polarity x frequency x layer) further ANOVA were constructed given that there were only two pulse polarities (e.g., 5x3x4 of factors frequency x depth x time for each pulse polarity) such that post-hoc tests could be performed to determine the significance of each factor (e.g. anodic pulse polarity in upper layers x frequency).

2.4. Results

We recorded from 110 units across six rats. For the both Anodic and Cathodic stimulation data, 107 models passed the goodness-of-fit assessment based on the 95% confidence bounds (Appendix Figure 1).

The effects of CES parameters on the neuron firing rates over time were investigated in four 500 ms intervals after the offset of stimulation (Figure 2.1d). Within the first 500 ms

after CES, unit activity was significantly different from the following three 500 ms intervals (p<0.01) which are described in the following sections:

2.4.1. CES pulse polarity

Our modeling results showed that Anodic and Cathodic stimulation pulses had a significantly different post-stimulus effect on neural spiking activity (p<0.01). In Figure 2.3, we show an example waveform, raster plots, post-stimulus time histogram (PSTH) of a unit, the normalized PSTH of all units, the population average PSTH and generalized linear modeling results to compare them across Anodic versus Cathodic stimulation. Our results demonstrated that the units located in lower layers (V-VI) of rat motor cortex have a significantly higher probability of being excited following anodic stimulation with respect to cathodic stimulation (p<0.01) in the first 500 ms (Figure 2.3a-b, lower panel). However in this interval, units located at the upper cortical layers (I-II) had a significantly higher probability of being excited following cathodic stimulation in comparison to anodic stimulation (p<0.005) (Figure 2.3a-b, upper panel). After the offset of stimulation, an increase in unit activity following anodic stimulation and a decrease following cathodic stimulation was seen in lower layer (V-VI) units (p<0.01) (Figure 2.3a-b, lower panel). The opposite effect was seen for the units in upper cortical layers (I-II) (p<0.01) (Figure 2.3a-b, upper panel). Both anodic and cathodic stimulation caused an increase (p<0.01) in activity of the units in layers III and IV (Figure 2.3a-b, middle panel) after the offset of stimulation.
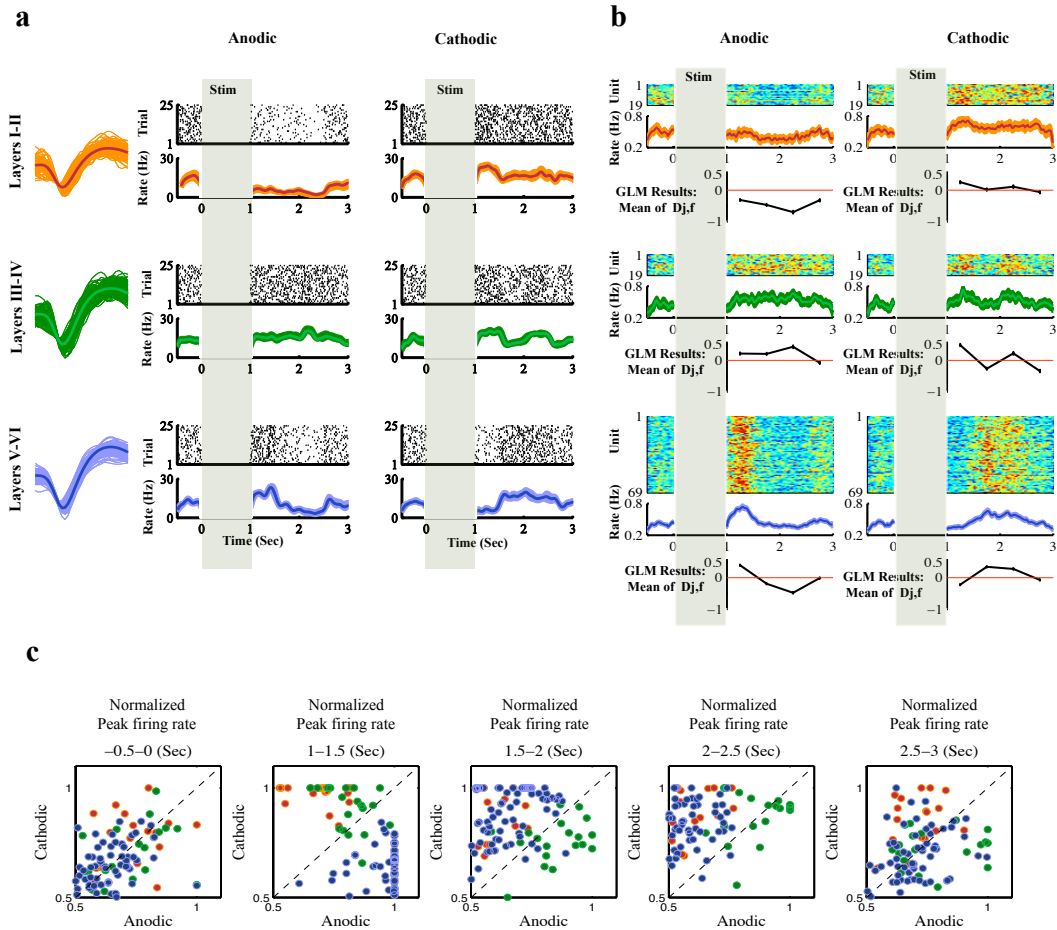
Figure 2.3. The effects of Anodic versus Cathodic stimulation regardless of stimulation frequency and amplitude. a) In each layer category an example waveform of a unit, raster plots and post-stimulus time histogram (PSTH) of the represented unit for both Anodic and Cathodic stimulation are shown. Each dot in the raster represents a single spike event. Each row of the raster represents a separate trial. Vertical shaded bars represent the 1 second stimulus pulse train in which no unit activity was recorded. The PSTH is the average firing rate of the unit in spike events per second in 10msec bins. Shaded area is standard error. These examples demonstrate the varying effects of stimulation polarity on unit activity in a range of cortical layers. b) In each layer category, the top plot shows the normalized PSTH of all units in false color. Each row represents a single unit. Each column is the unit firing rate in 10msec bins normalized to the maximum firing rate of each unit (hot colors represent high firing rates, cold colors represent low firing rates). The middle plots show the population average PSTH as the normalized mean firing rate (shaded area is standard error). The bottom plots show the generalized linear model (GLM) results which is the mean estimate of the normalized change in unit activity by the model (mean of Dj,f: equation 2.7) regardless of stimulation frequency and amplitude. Data points are the mean of the normalized change of unit activity (increase, positive deviation; decrease, negative deviation) from baseline in 500ms intervals after the offset of stimulation. c) Scatter plots of peak firing rate of units following Anodic versus Cathodic stimulation in five time intervals of -0.5-0, 1-1.5, 1.5-2, 2-2.5 and 2.5-3 seconds. The stimulation starts at time 0 and ends at 1 second. Three layer categories (I-II, III-IV, V-VI) are shown with red, green and blue dots, respectively, each dot representing the normalized firing rate of a single unit. The data in this figure demonstrate an increase in unit activity following anodic stimulation and a decrease in unit activity following cathodic stimulation in lower layers (V-VI, blue) in the first 500ms after the offset of stimulation. The opposite effect can be seen for the upper layers (I-II, red).

32

2.4.2. CES frequency

When varying the frequency of stimulation, our modeling results showed that the opposing post-stimulus effects observed after anodic vs. cathodic stimulation in upper and lower layers were frequency-dependent (Figure 2.4) ($p<0.01$). In addition, our results suggest that varying the stimulation frequency induces changes in the firing pattern of the units. The modeling response demonstrate that the probability of neurons firing increased ($p<0.05$) following low frequency stimulation (<100Hz) that decreased ($p<0.05$) as we increased the stimulation frequency (>100Hz) (Figure 2.4b). Figure 2.4a shows a raster plot and corresponding PSTH of a single unit for each layer category at frequencies of 50Hz (<100Hz) and 500Hz (>100Hz) following Anodic and Cathodic stimulation. Comparing the post-stimulus effects of these frequencies on Figure 2.4a across upper and lower layer units, show the opposite effects of anodic versus cathodic stimulation as well as the effects of changing the frequency.

By increasing the frequency of CES in layers I-II, we see a decrease in firing rate following cathodic stimulation ($p<0.05$). On the other hand, the decrease in activity observed following anodic stimulation is the same for all frequencies of CES up to 250Hz in these layers. Increasing the frequency from 250 to 500Hz causes a further significant decrease from other frequencies ($p<0.01$).
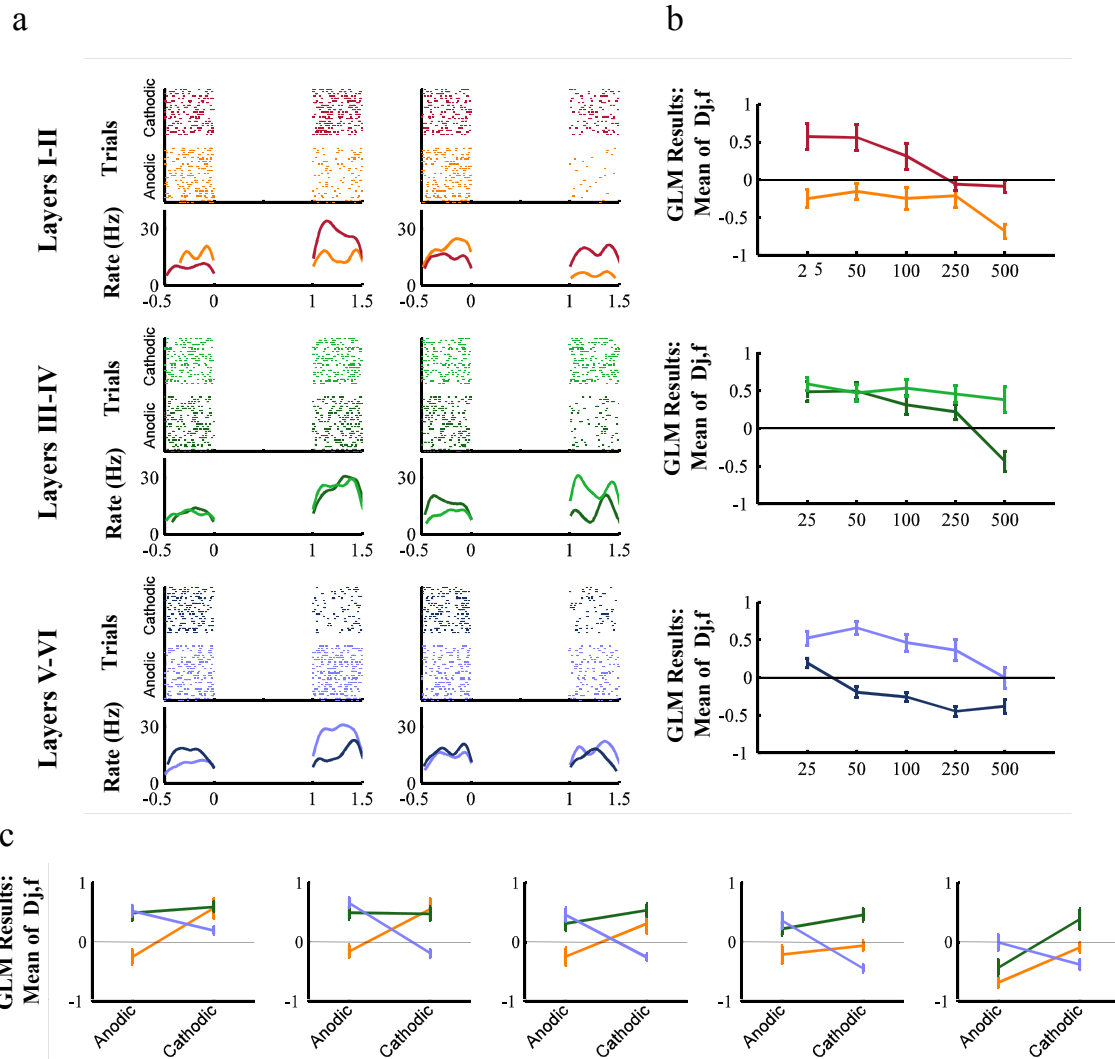
Figure 2.4. Effects of the frequency of stimulation on unit activity in layered cortex regardless of stimulation amplitude. a) A raster plot (top) and corresponding PSTH (bottom) is shown for each layer category of a single unit for frequencies of 50Hz (left column) and 500Hz (right column) following Anodic (light shading) and Cathodic (dark shading) stimulation. Each row of the raster represents a single trial and each dot in the raster represents a single spike event. The PSTH is the mean spike rate across trials in 10 ms bins. Color-coding is the same as Figure 2.3. b) GLM frequency results (Mean of Dj,f: equation 2.7) of units in each layer category following Anodic and Cathodic CES. Data points are the mean of the normalized change of unit activity (increase, positive deviation; decrease, negative deviation) from baseline in the first 500ms interval after the offset of different frequencies of stimulation. The error bars indicate 95% confidence intervals. Lines are used only for clarity and do not indicate continuous processes. c) Comparison of the GLM results for each stimulation frequency following Anodic and Cathodic stimulation. Data points are the mean of the normalized change of unit activity from baseline in the first 500ms interval after the offset of different frequencies of stimulation regardless of stimulation amplitude. The error bars indicate 95% confidence intervals. Lines are only used for clarity and do not indicate continuous processes. The opposing effects observed after anodic vs. cathodic stimulation in upper and lower layers are frequency-dependent. Stimulation pulses at lower frequencies caused an increase in activity compared to higher frequencies which caused a decrease in activity.

The probability of neuron firing increased following low frequency stimulation and decreased as we increased the stimulation frequency that we have seen in layers I-II also held true for neurons in layers V-VI (although with opposite pulse polarity)($p<0.01$). However, we don't see this trend in neurons located in layers III-IV, especially for the cathodic stimulation. Both anodic and cathodic stimulation cause an increase ($p<0.01$) in activity in the units located in these layers (except for 500Hz, anodic). As we increase the stimulation frequency, the increase in activity by these units remains consistent and we don't see a significant change affected by this parameter ($p>0.2$).

2.4.3. CES amplitude

Opposing post-stimulus effects on unit activity were observed after anodic vs. cathodic stimulation in upper and lower layers that were also amplitude-dependent (Figure 2.5) ($p<0.01$). Varying the stimulation amplitude induces changes in the firing pattern of the units as can be seen in the GLM amplitude results (Mean of $D_{j,a}$: equation 2.6) for each layer category following Anodic and Cathodic CES (Figure 2.5). Our results demonstrate that increasing the amplitude of stimulation from 25 to 50 and 75%MIC, caused a significant reduction in the depressive post-stimulus effects of Anodic pulses ($p<0.01$) and a significant increase in the excitatory post-stimulus effects of Cathodic pulses ($p<0.01$)(Figure 2.5b). However increasing the amplitude of stimulation from 50 and 75%MIC to 100% showed a decrease in both excitatory and inhibitory effects observed ($p<0.01$) (Figure 2.5b).
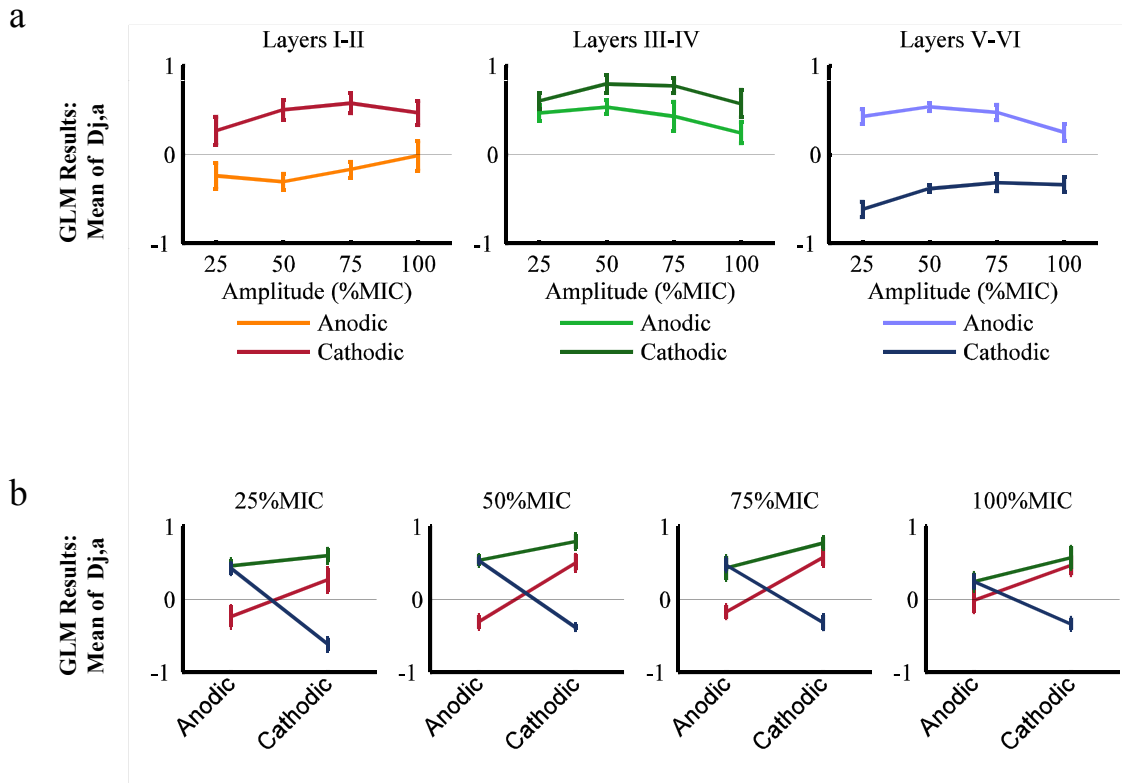
Figure 2.5. Effects of changing the amplitude of stimulation on unit activity in layered cortex regardless of stimulation frequency. a) GLM amplitude results (Mean of Dj,a: equation 2.6) for each layer category following Anodic and Cathodic CES. Data points are the mean of the normalized change of unit activity (increase, positive deviation; decrease, negative deviation) from baseline in the first 500ms interval after the offset of different amplitudes. The error bars indicate 95% confidence intervals. Lines are used only for clarity and do not indicate continuous processes.   b) Comparison of the GLM results for each stimulation amplitude following Anodic and Cathodic stimulation regardless of stimulation frequency. Data points are the mean of the normalized change of unit activity from baseline in the first 500 ms interval after the offset of different amplitudes of CES. The error bars indicate 95% confidence intervals. Lines are only used for clarity and do not indicate continuous processes.   Opposing effects on unit firing rate observed following anodic and cathodic stimulation in upper and lower layers are amplitude-dependent.

2.4.4. Short-term temporal effects of CES

The effects of CES parameters on the neuron firing rates over the first 500 ms after CES, was significantly different from the following three 500 ms intervals ($p<0.01$) which were described in the previous sections. The effects observed in the 500-1000 ms and 1000-1500 ms time interval showed no significant differences ($p=0.299$). We performed a t-test of the null hypothesis that data in the 1500-2000 ms after the offset of stimulation

36

are a random sample from a normal distribution with mean 0 and unknown variance, against the alternative that the mean is not 0. The null hypothesis was rejected for Cathodic stimulation (p<0.001) and was accepted for Anodic stimulation (p=0.48). This indicates that the effects of Cathodic CES on unit activity lasts at least 2 sec following the offset of stimulation while the effects of Anodic CES lasts up to 1.5 sec after the offset of stimulation. To investigate the post-stimulus effects of CES for cathodic stimulation after 2 seconds following the offset of stimulation, we have done further analysis. We have calculated the model parameters for 2000-2500 ms time interval after the offset of stimulation and performed the null hypothesis on them (see Supplementary materials). The results of our analysis revealed that the post-stimulus effects of cathodic stimulation last up to 2 seconds after the offset of stimulation.

These excitatory effects observed following the stimulation in our results were always followed by a decrease in activity that was observed 500 to 1500ms after the stimulation (p<0.01). In addition, our results demonstrated that the inhibitory effects observed in layers V-VI were followed by excitatory effects (p<0.01).

2.5. Discussion

In this study we have investigated the post-stimulus effects of CES pulse polarity of various frequencies and amplitudes on neural activity. It is important to point out that in stimulation studies, recording is generally difficult for the duration of the stimulus pulse train due to the substantial stimulation artifacts that corrupt the data and/or saturate the recording electronics[30-32]. Therefore, we were only able to have a high quality recording

after the offset of stimulation and report the post-stimulus effects observed. It has been shown that neuronal electrical stimulation results in two stages of conduction of the stimulation pulse[33-37]. These investigations have reported that effects observed directly after the stimulation are followed by a delayed series of stimulation-induced changes. Previous studies suggest that these indirect activities arise from retrograde, synaptic, or electrical transmission[38-43]. Since the results presented in this study are the post-stimulus effects after the one second train of stimulation pulses, the effects we have reported could be due to both of the above mechanisms and we cannot distinguish the effects of each separately.

2.5.1. Pulse polarity

When an electrical stimulus is applied within the CNS, cells and fibers over an unknown volume of tissue are activated[37]. To make accurate inferences about anatomical structures or physiological mechanisms involved in electrical stimulation, we must know which elements are stimulated. Our results showed a significantly different post-stimulus effect on neural spiking activity across different cortical layers following Anodic and Cathodic stimulation pulses. Previous clinical, animal, and modeling studies have suggested that neural elements perpendicular to the electrode surface are preferentially excited by anodic stimulation while cathodic stimulation excites those with a direction component parallel to its surface[14,15,44]. Previous studies on the effects of extracellular anodic and cathodic currents on cortical cells[45-49] have inferred that the differences obtained are, in part, due to the opposing membrane potential changes induced between oppositely directed poles (dendrite and axon) of vertically oriented cells. Accordingly, surface

38

anodal current is believed to hyperpolarize the dendrites while depolarizing cell body and axonal portions of neurons. An opposite sequence of depolarizing-hyperpolarizing events is believed to occur during surface cathodal current flow[50]. The neurons located in lower layers (V-VI) of rat motor cortex have elements that are primarily perpendicular to the stimulating electrode. The dendritic tree at the distal end of these neurons coalesces into the soma or cell body and the axon is at the proximal end. If an applied electric field is directed from the cortical surface inward, the dendrites are hyperpolarized, and the axon is depolarized, therefore this mode of stimulation is excitatory. On the other hand, if the applied electric field is directed outward from the cortical surface, the dendrites are depolarized, and the axon is hyperpolarized, resulting in no excitation[16,51]. In addition it has been reported that the site of excitation is dependent on the polarity of the stimulus, with cathodic stimuli resulting in lower thresholds for electrode positions closer to the axon and anodic stimuli resulting in lower thresholds for electrode positions closer to the cell body and dendrites[52]. These previous findings and the configurations of the surface stimulation in our experiments, lead us to hypothesize that neurons in these lower layers have a higher probability of being excited following anodic stimulation originating at the cortical surface. This hypothesis is confirmed by the evidence presented in our analysis and corroborated by modeling studies. Our results showed an increase in unit activity following anodic stimulation and a decrease in unit activity following cathodic stimulation in lower layer (V-VI) units.

As mentioned before, previous modeling studies have suggested that cathodic stimulation excites the neural elements with a direction component parallel to the surface of stimulation[14,15]. These studies have showed a positive activating function (an

approximation of the effect of stimulation induced potential fields on the membrane voltage of a nerve fiber[14]) as the result of surface cathodic stimulation in nerve fibers with a directional component parallel to the electrode surface. This positive activating function indicates membrane depolarization and possibly excitation induced by cathodic stimulation in these nerve fibers[14,15]. Therefore, it is expected to see the excitatory effects on upper cortical layers following cathodic stimulation in which the neuronal structure is primarily parallel to CES surface. Our results of unit activity following the first 500ms after the offset of stimulation in upper cortical layers (I-II) agree with these hypotheses. In addition it has been suggested that horizontally-running axons in the outer layers of the cortex are likely inhibited trans-synaptically as the result of anodic stimulation that polarizes the pyramidal cells[47]. This was also shown in our results in which a decrease in unit activity was observed in the upper cortical layers (I-II) following anodic stimulation. Both anodic and cathodic stimulation caused an increase in activity of the units in layers III and IV. This may also be attributed to the direction of the neuronal elements in these layers with respect to the stimulating electrode and the high degree of neural connections and neural interactions that causes both pulse polarities to increase unit firing rates after the offset of stimulation. It is important to point out that here we are reporting the post-stimulus effects and therefore cannot distinguish between direct and indirect activation of the recorded units.

2.5.2. CES frequency

The opposing post-stimulus effects observed after anodic vs. cathodic stimulation in upper and lower layers were frequency-dependent; our results suggest that varying the

stimulation frequency induces changes in the firing pattern of rat primary motor cortex neurons. Previous work has demonstrated frequency-dependent effects on brain activity following electrical stimulation. Studies have shown that within a large range of frequencies (at least up to 130Hz), neuronal fibers can be recruited by the stimulation, depolarized and hence, excited[53-55]. However, for high frequency stimulation (more than 130Hz), it was proposed that some synapses could not depolarize fast enough to follow the stimulus train, resulting in recurrent hyperpolarization that reduces the overall number of action potentials conveyed[53-56]. Also, high frequency stimulation induces a transient depression of excitatory synaptic currents in postsynaptic motor neurons[56]. Therefore, it is expected that by increasing the frequency of stimulation to high frequencies (>130Hz), the probability of neurons firing an action potential decrease. Our results agree with these hypotheses such that the response observed from the recorded units following different frequencies of stimulation demonstrate that the probability of neurons firing after the offset of stimulation, increased following low frequency stimulation (<100Hz) that decreased as we increased the stimulation frequency (>100Hz).

By increasing the frequency of CES in layers I-II, we see a decrease in firing rate following cathodic stimulation. On the other hand, the decrease in activity observed following anodic stimulation is the same for all frequencies of CES up to 250Hz. Increasing the frequency from 250 to 500Hz causes a further significant decrease from other frequencies. These post-stimulus results are probably due to different mechanisms involved in the excitatory and inhibitory effects observed in motor cortex neurons following cortical stimulation[57]. The inhibitory effects have been attributed to intracortical[58] or corticospinal[59] inhibitory mechanisms. The combination of these

inhibitory mechanisms in high frequencies of stimulation could cause higher recruitment of inhibition and therefore, at really high frequencies (in our case 500Hz), recurrent hyperpolarization.

The probability of neuron firing increased following low frequency stimulation and decreased as we increased the stimulation frequency that we have seen in layers I-II also held true for neurons in layers V-VI (although with opposite pulse polarity). However, we don't see this trend in neurons located in layers III-IV, especially for the cathodic stimulation. As shown above, both anodic and cathodic stimulation cause an increase in activity in the units located in these layers, except for 500Hz, anodic. As we increase the stimulation frequency, the increase in activity by these units remains consistent and we don't see a significant change affected by this parameter. These results suggest that there is a clear high frequency post-stimulus effect of anodic stimulation in the units in these cortical layers that will need further investigation to understand the mechanisms involved.

2.5.3. CES Amplitude

It has been shown that the probability for eliciting an action potential increases with increasing the amplitude of stimulation [60] because neuronal compartments polarize linearly with the amplitude of the applied electric field[52,61-62]. Although our results support this hypothesis, when we increase the amplitude of stimulation from 25 to 50 and 75%MIC, it does not agree for 100%MIC stimulation. Increasing the amplitude of stimulation from 50 and 75%MIC to 100% showed a decrease in both excitatory and inhibitory post-stimulus effects observed. It is important to point out that the cortical

architecture contains several excitatory and inhibitory cell types that are complexly interconnected locally as well as over longer distances[63-64]. Also, it is hypothesized that the amplitude of stimulation influences the distribution of the electric field induced into the brain[65]. This hypothesis and the high interconnectivity of the cortex predict that changing the stimulation amplitude can cause different populations of cell types to become activated as a result of electrical stimulation[66]. Previous modeling studies show that the threshold stimuli amplitude is lower for fibers with larger diameters[65]. This suggests that for lower current amplitudes (25 and 50%MIC) it is more probable to stimulate the pyramidal cell fibers while for higher amplitudes (75 and 100%MIC), neurons from inhibitory networks are being recruited[37]. Since inhibition can be transmitted by electrically (and synaptically) interconnected networks of interneuron[66-68], it is probable that higher amplitudes in CES can activate these networks and cause an inhibitory effect on the activity.

Previous in-vitro studies have shown that Layer V-VI neuron action potential thresholds are lower than upper layer pyramidal neurons and interneurons[69]. This is also shown in our results when comparing the responses of neurons located in layers V-VI with the ones located in layers I-II for 25%MIC. Increasing the amplitude, as mentioned before will recruit other networks of neurons that causes changes in firing rate that do not support this hypothesis.

2.5.4. Short-term temporal effects of CES

A large body of work from intracellular and extracellular recordings in the neocortex (*in vitro* and *in vivo*) describe a close correlation of both excitatory and inhibitory effects

after electrical stimulation[38-42]. Despite some variation across methods and preparations, the common finding was that excitation is evoked at short latencies and was always followed by an inhibitory response[43]. This post-stimulus effect was also observed in our results in the cases when we observed excitatory effects following the stimulation. These post-stimulus excitatory effects were always followed by a decrease in activity that was observed 500 to 1500ms after the stimulation. The reduction of excitation in the network could, be driven by two different mechanisms. First, intrinsic membrane currents could be triggered by the first wave of excitation and lead to a depression of firing rate[43]. Prominent candidates for such a mechanism are long-lasting after-hyperpolarizations in pyramidal neurons based on calcium or sodium-dependent currents[70-71]. Second, a decrement of network excitability could be based on short-term depression of excitatory intracortical synapses[72-75]. Both mechanisms would reduce excitatory drive from cortical neurons by suppressing firing rates in the population of postsynaptic neurons[43]. In addition, our results demonstrate that the post-stimulus inhibitory effects observed in layers V-VI were followed by excitatory effects. This can also be described with the mechanisms above since the dominant population of neurons are pyramidal cells in these layers.

2.6. Conclusion

The goal of this study was to design a set of experiments and test the influence of CES pulse polarity of various frequencies and amplitudes on the imposed volume of rat primary motor cortex. The results of this study suggested that neurons in lower layers have a higher probability of being excited following anodic stimulation. Similarly

neurons located in upper cortical layers have a higher probability of being excited following cathodic stimulation. The opposing effects observed after anodic vs. cathodic stimulation in upper and lower layers were frequency- and amplitude-dependent. In addition, our results demonstrate that the changes in neural activity following manipulation of CES parameters is time-dependent according to the location (depth) of the recorded units. It is clear that more quantitative data about intracortical distribution of projections and their target, as well as variation of electrical properties of cortical circuits are needed before the specific effects observed in the present study can be fully understood, especially in the context of maximizing efficacy of CES for neurorehabilitation and neuroprosthetic applications.

2.7. References

1.   Butefisch CM, Khurana V, Kopylev L, Cohen LG. Enhancing Encoding of a Motor Memory in the Primary Motor Cortex By Cortical Stimulation. Journal of neurophysiology. 2004;91(5):2110.

2.   Antal A, Nitsche MA, Kruse W, et al. Direct Current Stimulation over V5 Enhances Visuomotor Coordination by Improving Motion Perception in Humans. Journal of Cognitive Neuroscience. 2004;16(4):521-7.

3.   Nitsche MA, Schauenburg A, Lang N, et al. Facilitation of Implicit Motor Learning by Weak Transcranial Direct Current Stimulation of the Primary Motor Cortex in the Human. Journal of Cognitive Neuroscience. 2003;15(4):619-26.

4.   Kobayashi M, Ng J, Theoret H, Pascual-Leone A. Modulation of intracortical neuronal circuits in human hand motor area by digit stimulation. Experimental brain research. 2003;149(1):1.

5.   Kincses TZ, Antal A, Nitsche MA, Bartfai O, Paulus W. Facilitation of probabilistic classification learning by transcranial direct current stimulation of the prefrontal cortex in the human. Neuropsychologia. 2004;42(1):113-7.

6.   Fregni F, Boggio PS, Nitsche M, et al. Anodal transcranial direct current stimulation of prefrontal cortex enhances working memory. Experimental brain research. 2005;166(1):23.

7.   Marshall L, Molle M, Hallschmid M, Born J. Transcranial Direct Current Stimulation during Sleep Improves Declarative Memory. The journal of neuroscience: the official journal of the Society for Neuroscience. 2004;24(44):9985.

8.   Brown JA, Lutsep HL, Weinand M, Cramer SC. CLINICAL STUDIES - Motor Cortex Stimulation for the Enhancement of Recovery from Stroke: A Prospective, Multicenter Safety Study. Neurosurgery. 2006;58(3):464.

9.   Kinoshita M, Ikeda A, Matsuhashi M, et al. Electric cortical stimulation suppresses epileptic and background activities in neocortical epilepsy and mesial temporal lobe epilepsy. Clinical neurophysiology : official journal of the International Federation of Clinical Neurophysiology. 2005;116(6):1291.

10.   Ativanichayaphong T, He JW, Hagains CE, Peng YB, Chiao JC. A combined wireless neural stimulating and recording system for study of pain processing. Journal of Neuroscience methods. 2008;170(1):25-34.

11.   Lefaucheur JP. Repetitive transcranial magnetic stimulation (rTMS): insights into the treatment of Parkinson's disease by cortical stimulation. Clinical Neurophysiology. 2006;36(3):125-33.

12.   Fitzgerald PB, Huntsman S, Gunewardene R, Kulkarni J, Daskalakis ZJ. A randomized trial of low-frequency right-prefrontal-cortex transcranial magnetic stimulation as augmentation in treatment-resistant major depression. The International Journal of Neuropsychopharmacology. 2006;9(6):655-66.

13.   Nguyen JP, Lefaucheur JP, Keravel Y. Motor cortex stimulation. In: Simpson B, editor. Electrical Stimulation and the relief of Pain. Pain research and clinical management. Elsevier Science, 2003.

14.   Manola L, Holsheimer J, Veltink P, Buitenweg JR. Anodal vs cathodal stimulation of motor cortex: A modeling study. Clinical neurophysiology : official journal of the International Federation of Clinical Neurophysiology. 2007;118(2):464.

15.   Wongsarnpigoon A, Grill WM. Computational modeling of epidural cortical stimulation. Journal of Neural Engineering. 2008;5(4):443-54.

16.   Tranchina D, Nicholson C. A model for the polarization of neurons by extrinsically applied electric-fields. Biophysical Journal. 1986;50(6):1139-56.

17.   Amassian VE, Eberle L, Maccabee PJ, Cracco RQ. Modeling magnetic coil excitation of human cerebral-cortex with a peripheral-nerve immersed in a brain-shaped volume conductor – The significance of fiber bending in excitation. Electroencephalography and clinical neurophysiology. 1992;85(5):291-301.

18.   Iles JF. Simple models of stimulation of neurones in the brain by electric fields. Progress in biophysics and molecular biology. 2005;87(1):17-31. Electroencephalography and clinical neurophysiology. 1992;85(5):291-301.

19.   Kipke D, Vetter R, Williams J, Hetke J. Silicon-Substrate Intracortical Microelectrode Arrays for Long-Term Recording of Neuronal Spike Activity in Cerebral Cortex. IEEE transactions on neural systems and rehabilitation engineering : a publication of the IEEE Engineering in Medicine and Biology Society. 2003;11(2):151.

20.   Truccolo W, Eden UT, Fellows MR, Donoghue JP, Brown EN. A point process framework for relating neural spiking activity to spiking history, neural ensemble, and extrinsic covariate effects. Journal of Neurophysiology (Bethesda). 2005;93(2):1074-89.

21.   Teskey GC, Flynn C, Goertzen CD, Monfils MH, Young NA. Cortical stimulation improves skilled forelimb use following a focal ischemic infarct in the rat. Neurological research. 2003;25(8):794.

22.   Parikh H, Marzullo TC, Kipke DR. Lower layers in the motor cortex are more effective targets for penetrating microelectrodes in cortical prostheses: Institute of Physics Publishing; 2009.

23.   Brown EN, Barbieri R, Eden UT, Frank LM. Likelihood methods for neural spike train data analysis. Chapman & Hall/CRC Math Biol Med Ser. 2004:253-86.

24.   Brown EN, Barbieri R, Ventura V, Kass RE, Frank LM. The Time-Rescaling Theorem and Its Application to Neural Spike Train Data Analysis. Neural Computation. 2002;14(2):325-46.

25.   Ashe J. Movement parameters and neural activity in motor cortex and area-5. Cerebral cortex. 1994;4(6):590-600.

26.   Fu QG. Temporal Encoding of Movement Kinematics in the Discharge of Primate Primary Motor and Premotor Neurons. Journal of neurophysiology. 1995;73(2):836.

27.   Luczak A. Multivariate receptive field mapping in marmoset auditory cortex. Journal of neuroscience methods. 2004;136(1):77.

28.   Brillinger DR. Maximum-likelihood analysis of spike trains of interacting nerve-cells. Biological cybernetics. 1988;59(3):189-200.

29.   Skoglund T, Pascher R, Berthold C. The existence of a layer IV in the rat motor cortex. Cerebral Cortex. 1997;7(2):178-80.

30.   Wagenaar DA, Potter SM. Real-time multi-channel stimulus artifact suppression by local curve fitting. Journal of neuroscience methods. 2002;120(2):113.

31.   Wagenaar DA. Effective parameters for stimulation of dissociated cultures using multi-electrode arrays. Journal of neuroscience methods. 2004;138(1):27.

32.   Grumet AE, Wyatt JL, Rizzo JF. Multi-electrode stimulation and recording in the isolated retina. Journal of neuroscience methods. 2000;101(1):31.

33.   Kombos T, Suss O. Neurophysiological basis of direct cortical stimulation and applied neuroanatomy of the motor cortex: a review. Neurological focus. 2009;27(4).

34.   Parsons LM, Fox PT, Downs JH, Glass T, Hirsch TB. Use of implicit motor imagery for visual shape discrimination as revealed by PET. Nature. 1995;375(6526):54.

35.   Patton HD, Amassian VE. Single-unit and multiple-unit analysis of cortical stage of pyramidal tract activation. Journal of Neurophysiology. 1954;17(4):345-63.

36.   Phillips CG, Porter R. Unifocal and bifocal stimulation of motor cortex. Journal of Physiology-London. 1962;162(3):532-538.

37.   Ranck JB, Jr. Which elements are excited in electrical stimulation of mammalian central nervous system: A review: Elsevier; 2006.

38.   Butovas S. Effects of Electrically Coupled Inhibitory Networks on Local Neuronal Responses to Intracortical Microstimulation. Journal of neurophysiology. 2006;96(3):1227.

39.   Berman N, Douglas RJ, Martin K, Whitteridge D. Mechanisms of inhibition in cat visual cortex. The Journal of physiology. 1991;440:697-722.

40.   Li CL. The Inhibitory Effect of Stimulation of a Thalamic Nucleus on Neuronal Activity in the Motor Cortex. Journal of Physiology-London. 1956;133(1):40-53.

41.   Chagnacamitai Y, Connors BW. Synchronized Excitation and Inhibition Driven by Intrinsically Bursting Neurons in Neocortex. Journal of Neurophysiology. 1989;62(5):1149-62.

42.   Porter JT, Johnson CK, Agmon A. Articles - Cellular/Molecular - Diverse Types of Interneurons Generate Thalamus-Evoked Feedforward Inhibition in the Mouse Barrel Cortex. The journal of neuroscience : the official journal of the Society for Neuroscience.

2001;21(8):2699.

43.	Butovas S, Schwarz C. Spatiotemporal Effects of Microstimulation in Rat Neocortex: A Parametric Study Using Multielectrode Recordings. Journal of neurophysiology. 2003;90(5):3024.

44.	Nitsche MA, Paulus W. Excitability changes induced in the human motor cortex by weak transcranial direct current stimulation. The Journal of physiology. 2000;527:633-40.

45.	Bishop GH, O'Leary JL. The effects of polarizing currents on cell potentials and their significance in the interpretation of central nervous system activity. Electroencephalography and Clinical Neurophysiology. 1950;2(1-4):401-16.

46.	Creutzfeldt O, Fromm GH, Kapp H. Influence of transcortical D-C current on cortical neuronal activity. Experimental Neurology. 1962;5(6):436-452.

47.	Hern JEC, Porter R, Landgren S, Phillips CG. Selective excitation of corticofugal neurons by surface-anodal stimulation of baboons motor cortex. Journal of physiology-London. 1962;161(1):73-90.

48.	Landau WM, Bishop GH, Clare MH. Analysis of form distribution of evoked cortical potentials under influence of polarizing currents. 1964;27(5):788-813.

49.	Libet B, Gerard RW. Steady potential fields and neurone activity. Journal of Neurophysiology. 1941;4(6):438-494.

50.	Gorman ALF. Differential patterns fo activation of pyramidal system elicited by surface anodal and cathodal cortical stimulation. Journal of Neurophysiology. 1966;29(4):547.

51.	Basser PJ, Roth BJ. New currents in electrical stimulation of excitable tissues. Annual review of Biomedical Engineering. 2000;2:377-97.

52.	McIntyre CC, Grill WM. Electrophysiology - Excitation of Central Nervous System Neurons by Nonuniform Electric Fields. Biophysical journal. 1999;76(2):878.

53.	Priori A, Lefaucheur JP. Chronic epidural motor cortical stimulation for movement

disorders. Lancet Neurology. 2007;6(3):279-86.

54.   Garcia L, D'Alessandro G, Bioulac B, Hammond C. High-frequency stimulation in Parkinson's disease: more or less? Trends in Neurosciences. 2005;28(4):209-16.

55.   Beurrier C, Bioulac B, Audin J, Hammond C. High-Frequency Stimulation Produces a Transient Blockade of Voltage-Gated Currents in Subthalamic Neurons. Journal of neurophysiology. 2001;85(4):1351.

56.   Anderson W, Kudela P, Cho J, Bergey G, Franaszczuk P. Studies of stimulus parameters for seizure disruption using neural network simulations. Biological Cybernetics. 2007;97(2):173-94.

57.   Triggs WJ. Motor Inhibition and Excitation are Independent Effects of Magnetic Cortical Stimulation. Annals of neurology. 1992;32(3):345.

58.   Fuhr P, Agostino R, Hallett M. Spinal Motor-Neuron Excitability During The Silent   Period after Cortical Stimulation. Electroencephalography and Clinical Neurophysiology. 1991;81(4):257-62.

59.   Mills KR. Excitatory and Inhibitory Effects on Human Spinal Motoneurones from Magnetic Brain-Stimulation. Neuroscience Letters. 1988;94(3):297-302.

60. Baker LL, McNeal DR, Benton L, Bowman BR, Waters RL. Neuro muscular electrical stimulation, 4th edition Canada, 2000.

61.   Tranchina D, Nicholson C. A model for the polarization of neurons by extrinsically applied electric fields.

62.   Plonsey R, Altman KW. Electrical-Stimulation of Excitable Cells - A Model Approach. Proceedings of the IEEE. 1988;76(9):1122-9.

63. Braitenberg V, Schuz A. Anatomy of the Cortex. New York: Springer-Verlag,1991.

64. Peters A, Jones EG. Classification of cortical neurons. In: Cerebral Cortex, edited by Peters A and Jones EG. New York: Plenum Press, 1984.

65.   Manola L, Roelofsen BH, Holsheimer J, Marani E, Geelen J. Modelling motor

cortex stimulation for chronic pain control: electrical potential field, activating functions and responses of simple nerve fiber models. Medical & biological engineering & computing. 2005;43(3):335-44.

66.   Nowak LG, Bullier J. Axons, but not cell bodies, are activated by electrical stimulation in cortical gray matter. II. Evidence from selective inactivation of cell bodies and axon initial segments. Experimental brain research. 1998;118(4):489.

67.   Galarreta M, Hestrin S. A network of fast-spiking cells in the neocortex connected by electrical synapses. Nature. 1999;402(6757):72-5.

68.   Gibson JR, Beierlein M, Connors BW. Two networks of electrically coupled Inhibitory neurons in neocortex. Nature. 1999;402(6757):75.

69.   Radman T, Ramos RL, Brumberg JC, Bikson M. Role of cortical cell type and morphology in subthreshold and suprathreshold uniform electric field stimulation in vitro. Brain Stimulation. 2009;2(4):215-28.

70.   Schwindt PC. Long-Lasting Reduction of Excitability by a Sodium-Dependent Potassium Current in Cat Neocortical Neurons. Journal of Neurophysiology. 1989;61(2):233-44.

71.   Schwindt PC, Spain WJ, Foehring RC, Chubb MC, Crill WE. Slow Conductances in Neurons from Cat Sensorimotor Cortex In-vitro and their Role in Slow Excitability Changes. Journal of Neurophysiology. 1988;59(2):450-67.

72.   Abbott LF, Varela JA, Sen K, Nelson SB. Synaptic Depression and Cortical Gain Control. Science. 1997;275(5297):220.

73.   Thomson AM, Deuchars J, West DC. Large, Deep Layer Pyramid-Pyramid Single Axon EPSPs in Slices of Rat Motor Cortex Display Paired Pulse and Frequency Dependent Depression, Mediated Presynaptically and Self-Facilitation, Mediated Postsynaptically. Journal of neurophysiology. 1993;70(6):2354.

74.   Tsodyks MV, Markram H. The neural code between neocortical pyramidal neurons depends on neurotransmitter release probability (Correction). Proceedings of the National Academy of Sciences of the United States of America. 1997;94(10):5495.

75.   Harvey RL, Nudo RJ. Cortical brain stimulation: A potential therapeutic agent for

upper limb motor recovery following stroke. Topics in Stoke Rehabilitation. 2007;14(6):54-67.

Chapter 3

Polarity of cortical electrical stimulation differentially affects Electrocorticographs and Local Field Potentials recorded from rat motor cortex and correlates with neuronal activity of deep and superficial layers

3.1. Abstract

Cortical electrical stimulation (CES) has been used extensively in experimental neuroscience to modulate neuronal or behavioral activity, which has led this technique to be considered in neurorehabilitation. Because the cortex and the surrounding anatomy have irregular geometries as well as inhomogeneous and anisotropic electrical properties, the mechanisms by which CES has therapeutic effects is poorly understood. Therapeutic effects of CES can be improved by optimizing the stimulation parameters based on the effects of various stimulation parameters on target brain regions. In this study the effects of CES pulse polarity, frequency, and amplitude were investigated on unit activity (spikes), local field potentials (LFP), and electrocorticograms (ECoG) recorded from rat primary motor cortex. The results showed that units located in lower cortical layers are preferentially excited by anodic stimulation, while cathodic stimulation excites those located in upper cortical layers. These opposing effects were also frequency- and amplitude-dependent. Time-frequency analysis of LFPs showed high correlation of gamma frequencies with unit activity in corresponding layers. On the other hand, high gamma power of ECoG signals only showed high correlation with the unit activity in lower layers. Time-frequency correlations, which were found between LFPs, ECoGs and unit activity were also frequency- and amplitudedependent. The data demonstrates that the poststimulus effects in

neural activity after manipulation of CES parameters changes according to the location (depth) of the recorded neural activity in motor cortex. The signature of the neural activity observed in LFP and ECoG signals provides a better understanding of the effects of stimulation on the affected network and has a promising potential to be used in closed-loop control stimulation systems. These results demonstrate that the neurorehabilitation and neuroprosthetic applications of CES can be further improved by optimizing CES parameters.

3.2. Introduction

Although a wide range of electrical stimulation parameters have been successfully used for a number of neuroprosthetics and neurorehabilitation applications, the effects of CES on neuronal activity are still unclear. It is critical to know the effects of CES on neuronal activity such as unit activity, local field potentials (LFP) and Electrocorticograms (ECoG) in the affected region of the brain using various stimulation parameters. In the previous chapter, we have investigated the effects of CES on unit activity of different neuronal elements in rat primary motor cortex by changing the stimulation pulse polarity in various frequencies and amplitudes. Our results showed an increase in unit activity following anodic stimulation and a decrease in unit activity following cathodic stimulation in lower layers (V-VI) units 500 ms following the offset of stimulation. The opposite effect was seen for the units in upper cortical layers (I-II). These opposing effects observed after anodic vs. cathodic stimulation in upper and lower layers was frequency- and amplitude-dependent. However, LFPs and ECoGs, which represent the summation of excitatory and inhibitory dendritic activity of a population of cells[1], can offer a different perspective on the effect of stimulation on local network activity. Towards these ends it is essential to perform simultaneous intracortical (unit activity and LFP) and epicortical

recordings (ECoG), under various stimulation parameters, to directly address what exact aspects of neural activity are affected by CES.

Numerous studies have described the patterns of ECoG activity associated with neuronal activity in different cortical areas (see references in 2). It has been suggested that high (>60 Hz) frequency components of these signals represent activation of neuronal populations in the underlying cortex[3], but experimental evidence is scarce. More data exist on the relationship between intracortical local field potentials (LFPs) and neuronal activity[4], but the picture is far from complete. Beltitski et al. reported that spikes and LFPs in V1 convey independent information and that stimulus dependent modulation occurs in the 1-8 Hz and 60-100 Hz (high gamma) frequency ranges of LFPs[5]. Furthermore, Pesaran et al. showed that the gamma band power in LFP from lateral intraparietal (LIP) area was spatially tuned, and that spiking and LFP activity are coherent at high frequencies (25-90 Hz) but not at lower frequencies[6]. In another work by Spinks et al, M1 LFPs showed selectivity to hand grasp of different objects[7]. "Hook" grips resulted in larger beta (15-30 Hz) power while "precision" grips resulted in lower beta power (ref). The spikes and LFPs showed reverse correlation in the beta range but positive correlation in the 30- 50 Hz (gamma) frequency range[7]. It has also been shown that a strong correlation exists in general between spike and LFPs in the high frequencies (20-300Hz)[8]. Despite the fact that ECoG and LFPs are thought to be generated by similar mechanisms operating at different spatial scales, their relationship is unclear.

The purpose of this chapter is to investigate the effects of CES on LFPs and ECoGs recorded from the rat primary motor cortex and correlate them with the CES effects on the simultaneous recorded unit activity (reported in chapter 2). We investigated these effects after the offset of stimulation on unit activity, LFPs and ECoGs in rat primary motor cortex by changing the

stimulation pulse polarity in various frequencies and amplitudes. A penetrating single shank silicon microelectrode array enabled us to span the entirety of 6 layer cortex allowing simultaneous unit activity and LFP recordings from different depths[9] following monopolar CES. In addition we implanted bone screws that allowed simultaneous ECoG recording over three locations of primary motor cortex. Time-frequency spectral analysis was performed on LFPs and ECoGs recorded before the onset and after the offset of CES based on multitaper spectral analysis techniques. The spectral analyses were designed to capture the temporal variations in frequency components of the recorded LFPs and ECoGs following the co-variation of CES parameters. These changes in frequency components were then compared with the effects of CES on the simultaneous unit activity recordings. Our results show an increase in gamma (30-120 Hz) power in LFPs following anodic stimulation and a decrease in gamma power in LFPs following cathodic stimulation in lower layers (V-VI) after the offset of stimulation. The opposite post-stimulus effect was seen for the upper cortical layers (I-II). These opposing effects observed following anodic vs. cathodic stimulation in upper and lower layers were frequency- and amplitude-dependent. In addition our results showed a high temporal correlation between the effects of CES on unit activity change with the change in the gamma power of the simultaneously recorded LFPs. The ECoG spectral analyses show an increase in high gamma (60-120 Hz) power in ECoGs following anodic stimulation and a decrease in high gamma power in ECoGs following cathodic stimulation after the offset of stimulation. These opposing effects observed following anodic vs. cathodic stimulation in upper and lower layers were also frequency- and amplitude-dependent. Our results showed a high temporal correlation between the effects of CES on unit activity change in lower layers (V- VI) with the change in the high gamma power of the simultaneous recorded ECoGs.

3.3. Methods

3.3.1. Subjects

Six normal male rats (Charles River Laboratories) were used in this study. Animals were implanted with six bone screws that allowed recording ECoG signal over three location of primary motor cortex. An additional bone screw was used to deliver cortical electrical stimulation to primary motor cortex (Figure 3.1a). Finally, a micro-scale penetrating electrode array (NeuroNexus Technologies) consisting of 16-electrodes spaced 100 μm apart (Figure 3.1a-b) was implanted to span the entirety of 6-layer neocortex. This electrode array was implanted to record extracellular action potentials and LFPs. It was angled toward the cortical stimulation electrode such that extracellular action potentials and LFP recordings had a high probability of being effected by the cortical stimulation (Figure 3.1b).

3.3.2. Electrophysiological Recordings and Stimulation protocol

Animals were placed in a faraday cage where all signals could be routed through a commutator to a wireless stimulation device (Northstar Neuroscience) and multichannel neural signal amplifier (MNAP, Plexon Inc., Dallas, TX). LFP and spike data were recorded using the penetrating electrode implanted beneath the stimulating electrode. The detail of spike recordings is described in chapter 1. LFP data were band pass filtered between 1 and 500Hz, and were digitally sampled at 500Hz (Plexon Inc, Dallas,TX). As described before, three bone screws were implanted in the right primary motor cortex for ECoG recordings. In our experiments the ECoG data were also recorded, band pass filtered between 1 and 500Hz, and were digitally sampled at 500Hz (Plexon Inc, Dallas,TX).
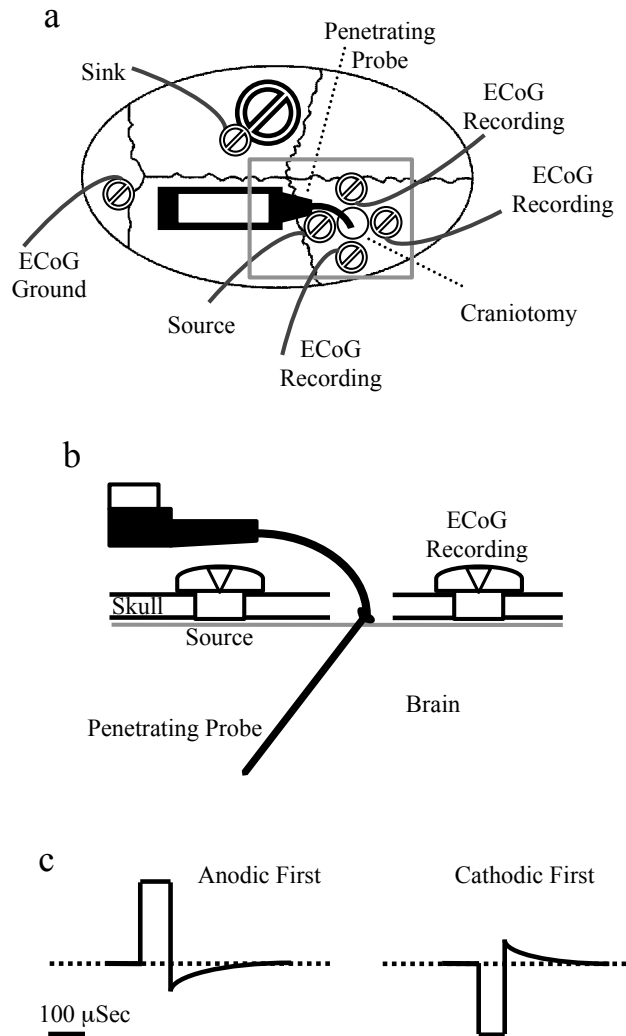
Figure 3.1. a) Horizontal schematic of the rat skull showing the locations of craniotomy, implanted CES screws, recording ECoGs and penetrating probe. The current sink was shorted to a much larger bone screw (depicted). Rostral is to the right. b) Conceptual cross section in the sagital plane of the implanted probe enlarged from the gray box in (a) (rostral is to the right). The penetrating electrode was angled toward the cortical stimulation electrode such that recorded extracellular action potentials and local field potentials had a high probability of being affected by the cortical stimulation (electrodes are on the side of the silicon shank that faces the current source). c) Pulse shapes: Constant current CES was delivered in two configurations, Cathodic-first or Anodic-first consisting of pulse trains. Pulses consisted of square leading phase (100μsec) followed by an exponentially decaying second phase to balance charge. The pulse width of the leading phase was fixed at 100μsec and the length of the trailing phase varied according to leading phase current in order to balance the charge.

The configuration of stimulation and the stimulation parameters were the same as reported in chapter 2. Constant current CES was delivered in both cathodic and anodic configurations consisting of pulse trains at frequencies of 25, 50, 100, 250, or 500Hz and amplitudes of 25, 50, 75 or 100% MIC. A random combination (without replacement) of stimulation frequency and percentage of MIC current was chosen to be presented to the animal in 25 repetitions of 1 sec of stimulation followed by 4 sec of recording. The detail of the histological analysis is also reported in chapter 2.

3.3.3. Time-Frequency Spectral Analysis

To compare the effects of CES parameters on unit activity (reported in chapter 1) with the effects on LFPs and ECoGs, we performed time-frequency spectral analysis on these signals recorded before the onset and after the offset of CES. We used multitaper methods of spectral analysis on the recorded ECoG and LFP data. These methods have been successfully applied to neurobiological data in recent work[6,10-12]. Multitaper methods involve the use of multiple data tapers for spectral estimation. A variety of tapers can be used, but an optimal family of orthogonal tapers is given by the prolate spheroidal functions or Slepian functions. These are parameterized by their length in time, T, and their bandwidth in frequency, W. For each choice of T and W, up to K=2TW-1 tapers are concentrated in frequency and suitable for use in spectral estimation[13]. The spectral analyses were designed to capture the temporal variations in frequency components of the recorded LFPs and ECoGs following the co-variation of CES parameters. The goal of these analyses was to find a signature of unit activity change in temporal variation of frequency components in these signals as the result of stimulation. We calculated the power of

the LFPs and ECoGs in different frequency bands such as beta (15-30Hz), gamma (30-120 Hz) and high gamma (60-120Hz) from the corresponding spectrograms in time intervals before the onset and after the offset of stimulation.

To compare the power across all LFPs and ECoGs, the power for each frequency band was normalized to have values between 0 and 1. We defined the power in the 500ms before the onset of stimulation as the baseline power of that frequency band and compared the power in the four 500 ms time intervals (0-500,500-1000,1000-1500,1500-2000ms) after the offset of stimulation with this baseline power to estimate the effects of CES on these frequency bands.

3.3.4. Statistical Analysis

As described in the previous chapter, to estimate the effect of various parameters in different depths of motor cortex the neuron populations were divided into three groups. Group 1 is defined as Layers I-II (0-400μm), Group 2 as Layers III-IV (400-750μm) and Group 3 as Layers V-VI (750-1800μm) below the cortical surface. To compare the effects of CES on different frequency bands of LFPs with unit activity, we used these groups for the LFP analysis. The effects of stimulation parameters on LFPs were divided between amplitude and frequency parameters. A 2×4×3×4 ANOVA was constructed in SPSS Statistics 18 (IBM Company, Chicago, IL) for *changes observed in the power of each frequency band in LFPs as the result of CES amplitude*: pulse polarity (Anodic vs Cathodic), percent movement induced current (MIC; 25,50,75,100%), Depth (Layers I-II, III-IV, V-VI) and time intervals (0-500,500-1000,1000-1500,1500-2000ms after the offset of the stimulation. Likewise, a 2×5×3×4 ANOVA was constructed for *changes observed in the power of each frequency band in LFPs as the result of CES frequency*: pulse

polarity (Anodic vs. Cathodic), Frequency (25, 50, 100, 250, 500Hz), Depth (Layers I-II, III-IV, V-VI) and time intervals (0-500, 500-1000, 1000-1500, 1500-2000ms after the offset of the stimulation). For ECoG data a 2×4×4 ANOVA was constructed for *changes observed in the power of each frequency band as the result of CES amplitude*: pulse polarity (Anodic vs Cathodic), percent CIM (25,50,75,100%) and time intervals (0-500,500-1000,1000-1500,1500-2000ms after the offset of the stimulation). Also a 2×5×4 ANOVA was constructed for *changes observed in the power of each frequency band in ECoGs as the result of CES frequency*: pulse polarity (Anodic vs. Cathodic), Frequency (25, 50, 100, 250, 500Hz) and time intervals (0-500, 500-1000, 1000-1500, 1500-2000ms after the offset of the stimulation). Based on significant interactions effects ($p < 0.05$, e.g. pulse polarity x frequency x layer) further ANOVA were constructed given that there were only two pulse polarities (e.g., 5x3x4 of factors frequency x depth x time for each pulse polarity) such that post-hoc tests could be performed to determine the significance of each factor (e.g. anodic pulse polarity in upper layers x frequency).

3.4. Results

3.4.1. CES pulse polarity

The results of time-frequency spectral analysis on LFPs showed that Anodic and Cathodic stimulation pulses had a significantly different post-stimulus effect on the gamma (30-120 Hz) power of LFPs ($p<0.01$). No significant changes were seen in the other frequency ranges ($P>0.2$). In addition the time-frequency analysis showed high correlation of gamma power change with the change in unit activity following CES in corresponding layers. These results are summarized in Figure 3.2. In this Figure, we show an example waveform of a unit, raster plots

and post-stimulus time histogram (PSTH) of the represented unit for both Anodic and Cathodic stimulation (Figure 3.2a). Also the normalized LFP spectrograms of the corresponding recording site of the unit shown in (Figure 3.2a) and the normalized gamma power (30-120 Hz) of the LFP averaged across trials are shown in Figure 3.2b for the represented electrode. Figure 3.2c shows the mean of the normalized change of unit activity from baseline in 500ms intervals after the offset of stimulation color-coded for each layer category for all units. The results shown in Figure 3.2c are also compared with the mean of the normalized change of gamma power from baseline in 500ms intervals after the offset of stimulation for LFPs recorded simultaneously from electrodes in each layer category (shown in black). Our results demonstrate that the gamma power of LFPs recorded from lower layers (V-VI) of rat motor cortex significantly increased following anodic stimulation ($p<0.01$) in the first 500 ms after the offset of stimulation (Figure 3.2b, right panel). However in this interval, gamma power in LFPs recorded from the upper cortical layers (I-II) deccreased significantly ($p<0.005$) in the first 500 ms after the offset of stimulation (Figure 3.2b, left panel). The opposite was observed for Cathodic stimulation in both layer categories, respectively (p-values). Both anodic and cathodic stimulation caused an increase ($p<0.01$) in the gamma power of LFPs in layers III and IV (Figure 3.2b, middle panel) after the offset of stimulation. Comparing the results of Figure 3.2a and 3.2b, as shown in Figure 3.2c, we see the effects of CES pulse polarity on unit activity change are highly correlated with the changes in gamma power of LFPs for all of the layer categories ($r>0.95$).
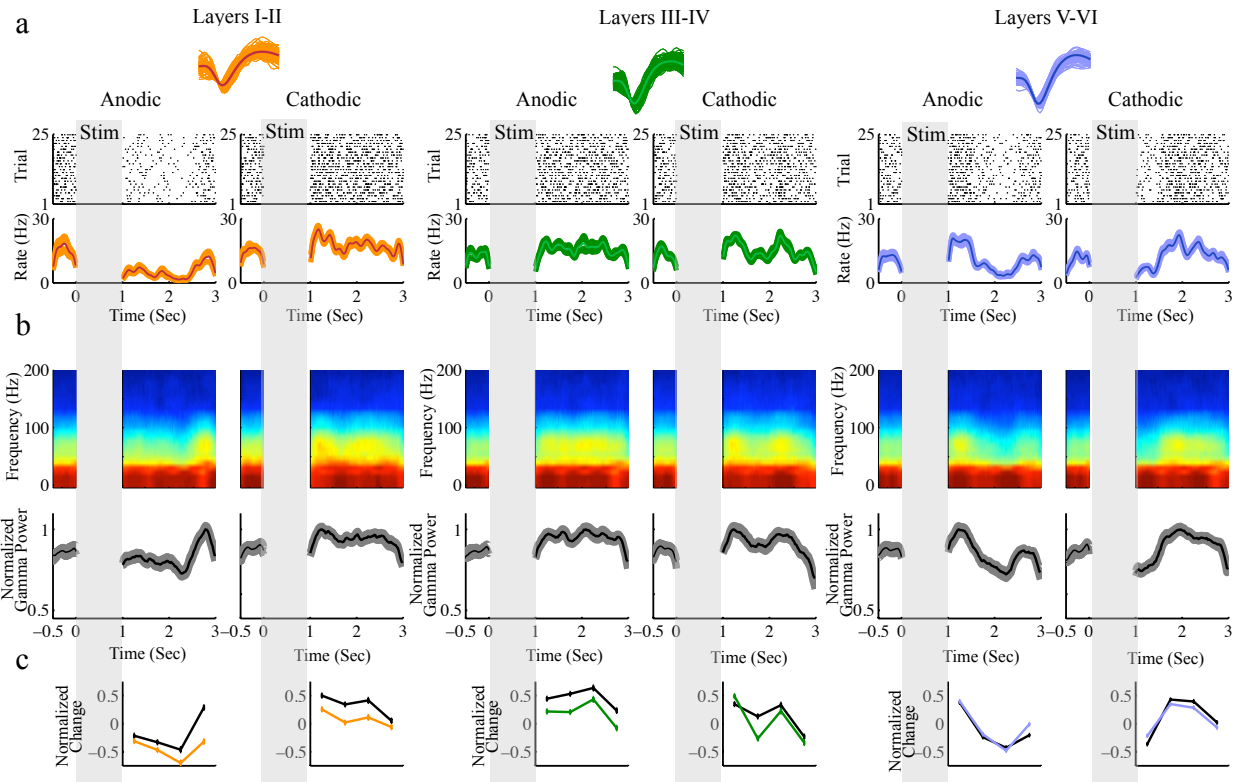
Figure 3.2. The effects of Anodic-first versus Cathodic-first stimulation on LFP regardless of stimulation frequency and amplitude. a) In each layer category an example waveform of a unit, raster plots and post-stimulus time histogram (PSTH) of the represented unit for both Anodic-first and Cathodic-first stimulation are shown. Each dot in the raster represents a single spike event. Each row of the raster represents a separate trial. Vertical shaded bars represent the 1 second stimulus pulse train in which no unit activity was recorded. The PSTH is the average firing rate of the unit in spike events per second in 10msec bins. Shaded area is standard error. These examples demonstrate the varying effects of stimulation polarity on unit activity in a range of cortical layers. b) In each layer category, the top plot shows the normalized LFP spectrograms of the corresponding recording site of the unit shown in (a) averaged across trials. Time is on the x-axis; frequency is on the y-axis; power is color-coded in a log scale (hot colors represent high power, cold colors represent low power). The bottom plot shows the normalized gamma power (30-120 Hz) of the LFP averaged across trials. Shaded area is standard error. c) These plots show the mean of the normalized change of unit activity (increase, positive deviation; decrease, negative deviation) from baseline in 500ms intervals after the offset of stimulation color-coded for each layer category for all units. Black lines show the mean of the normalized change of gamma power from baseline in 500ms intervals after the offset of stimulation for LFPs recorded from each layer category. The data in this figure demonstrate a correlation between the effects of stimulation polarity on unit activity with gamma power in LFP.

The results of time-frequency spectral analysis on ECoGs showed that Anodic and Cathodic stimulation pulses had a significantly different post-stimulus effect on the high gamma (60-120 Hz) power of ECoGs ($p < 0.05$). No significant changes were seen in the other frequency ranges

(P>0.3). In addition the time-frequency analysis showed high correlation of high gamma power change with the change in unit activity in lower layers (V-VI) following CES. These results are summarized in Figure 3.3. In this Figure, we show the normalized ECoG spectrograms recorded simultaneously with the units and LFPs shown in Figure 3.2 and the normalized high gamma power (60-120 Hz) of the ECoG averaged across trials (Figure 3.3a). Figure 3.3b shows the mean of the normalized change of unit activity from baseline in 500ms intervals after the offset of stimulation color-coded for each layer category for all units. The results shown in Figure 3.3b are also compared with the mean of the normalized change of high gamma power from baseline in 500ms intervals after the offset of stimulation for ECoGs recorded simultaneously from the surface of the brain (shown in black). In Figure 3.3c we compare the effects of CES pulse polarity on gamma power of LFPs (color coded for each layer category) with the effects on the high gamma power of ECoGs. After the offset of stimulation, an increase in high gamma power of ECoGs following anodic stimulation and a decrease following cathodic stimulation was seen (p<0.01). As shown in Figure 3.3b the effects of CES pulse polarity on the high gamma power of ECoGs are highly correlated with the effects on unit activity of lower layers (V-VI) (r>0.95). Likewise, as we see in Figure 3.3c, there is a high correlation between the effects of CES pulse polarity on high gamma power of ECoGs with the gamma power of LFPs recorded from lower layers (r>0.95). These result showed high correlation of gamma power in LFPs with unit activity in corresponding layers. On the other hand, high gamma power of ECoG signals only showed high correlation with the unit activity in lower layers (r>0.95).
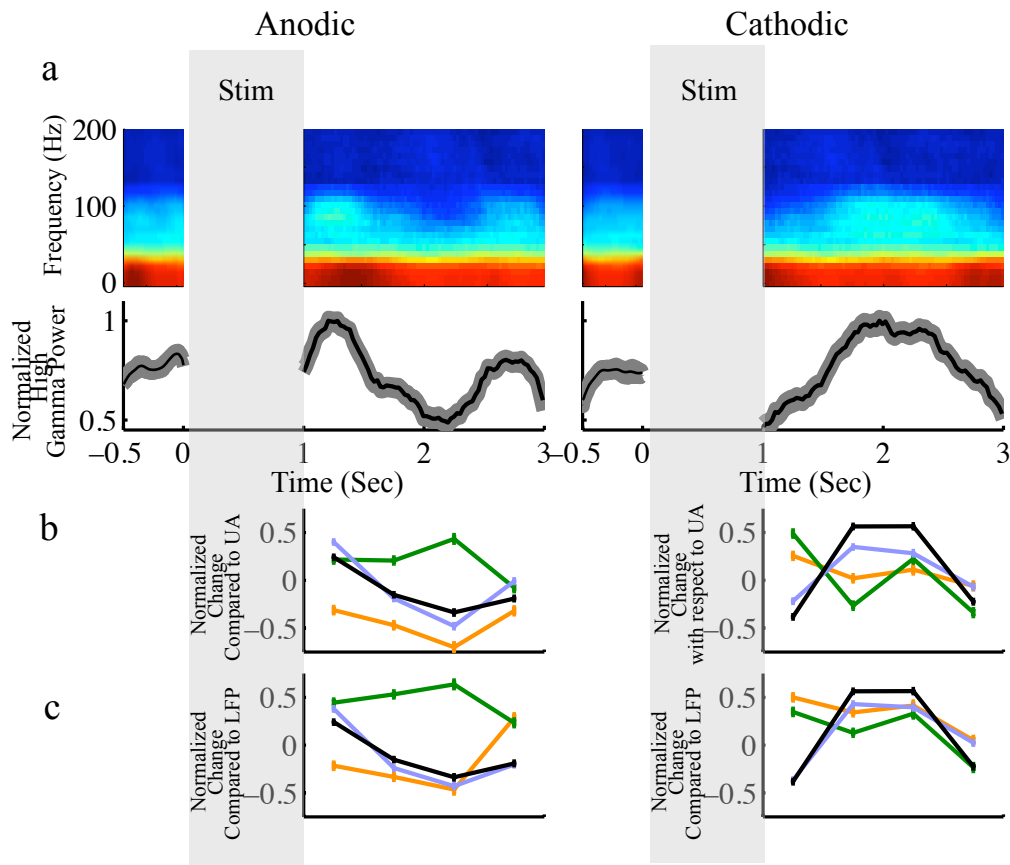
Figure 3.3. The effects of Anodic-first versus Cathodic-first stimulation on ECoG regardless of stimulation frequency and amplitude. a) The top plot shows the normalized ECoG spectrograms of the corresponding LFPs and units shown in Figure 2 averaged across trials. Time is on the x-axis; frequency is on the y-axis; power is color-coded in a log scale (hot colors represent high power, cold colors represent low power). The bottom plot shows the normalized high gamma power (60-120 Hz) of the ECoG averaged across trials. Shaded area is standard error. Vertical shaded bars represent the 1 second stimulus pulse train in which no activity was recorded. b) The mean of the averaged normalized change of high gamma power in all ECoG recorded signals (increase, positive deviation; decrease, negative deviation) from baseline in 500ms intervals after the offset of stimulation (shown in black) in comparison with unit activity (UA) which is color-coded (same as Figure 3.2) for each layer category for all units. c) The mean of the averaged normalized change of high gamma power in all ECoG recorded signals (increase, positive deviation; decrease, negative deviation) from baseline in 500ms intervals after the offset of stimulation (shown in black) in comparison with gamma power change in LFP which is color-coded for each layer category for all units. The data in this figure demonstrate a correlation between the effects of stimulation polarity on units located in layers V and VI with high gamma power in ECoG.

3.4.2. CES frequency

When varying the frequency of stimulation, our results showed that the opposing post-stimulus

effects on gamma power observed in LFPs after anodic vs. cathodic stimulation were frequency-dependent in both upper and lower layers (p<0.01, Figure 3.4). In Figure 4a we show a raster plot (top) and corresponding PSTH (bottom)for each layer category of a single unit for stimulation frequencies of 50 and 500Hz following Anodic and Cathodic stimulation . Below the unit responses are shown the normalized LFP spectrograms of the corresponding recording site of each unit averaged across trials (Figure 3.4b). Figure 3.4c summarizes these data. The mean of the normalized change of unit activity across all units (solid-colored bars) is plotted against LFP gamma power change (30-120 Hz) across all LFPs (white bars) as a function of stimulation frequency. As shown in this Figure, the change in the gamma power of the LFPs was highly correlated with the change in unit activity following all frequencies and pulse polarity for all of the layer categories (r>0.95).

Similarly, post-stimulus effects on ECoGs were frequency-dependent. When varying the frequency of stimulation, our results showed opposing anodic vs. cathodic effects observed in high gamma power of ECoGs (60 – 120Hz) (p<0.05, Figure 3.5). In this Figure we show the normalized ECoG spectrograms following Anodic and Cathodic stimulation at 50 and 500Hz (Figure 3.5a). These data are summarized in Figure 3.4b by showing the mean of the normalized change of unit activity across all units are compared with ECoG high-gamma power (60-120 Hz) across all ECoGs as the function of Anodic and Cathodic stimulation frequency . As can be seen in this Figure, the change in the high gamma power of ECoG was highly correlated with the change in unit activity of the lower layers (V-VI) following all frequencies of stimulation (r>0.95).
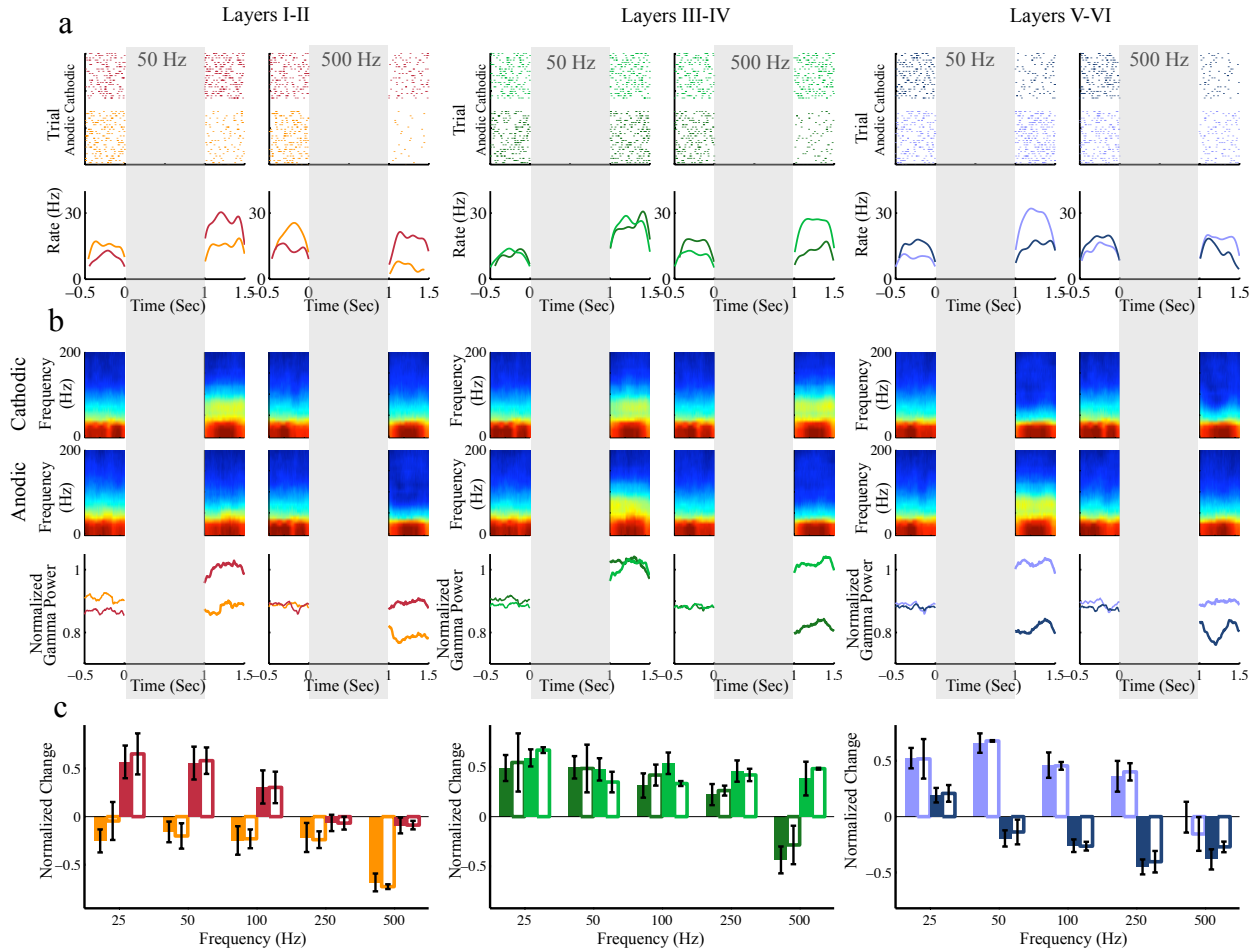
Figure 3.4. Effects of the frequency of stimulation on LFP in layered cortex regardless of stimulation amplitude. a) A raster plot (top) and corresponding PSTH (bottom) is shown for each layer category of a single unit for frequencies of 50Hz (left column) and 500Hz (right column) following Anodic-first (light shading) and Cathodic-first (dark shading) stimulation. Each row of the raster represents a single trial and each dot in the raster represents a single spike event. The PSTH is the mean spike rate across trials in 10 ms bins. Color-coding is the same as Figure 3.2. b) In each layer category, the top plot shows the normalized LFP spectrograms of the corresponding recording site of the shown unit in (a) averaged across trials for Cathodic stimulation and for frequencies of 50Hz (left column) and 500Hz (right column). The middle plot shows the normalized LFP spectrograms of the corresponding recording site of the unit shown in (a) averaged across trials for Anodic stimulation. Time is on the x-axis; frequency is on the y-axis; power is color-coded in a log scale (hot colors represent high power, cold colors represent low power). The bottom plot shows the normalized gamma power (30-120 Hz) of the LFP averaged across trials following Anodic-first (light shading) and Cathodic-first (dark shading) stimulation for frequencies of 50Hz (left column) and 500Hz (right column) of the unit shown in (a). c) The mean of the normalized change of unit activity (solid-colored bars) across all units and LFP gamma power (30-120 Hz) change (white bars) across all LFP as the function of stimulation frequencies for Anodic-first (light shading) and Cathodic-first (dark shading) stimulation consistent with the color coding in (a) and (b). The error bars indicate 95% confidence intervals. The data in this figure demonstrate a correlation between the effects of stimulation polarity on unit activity with gamma power in LFP for various frequencies.
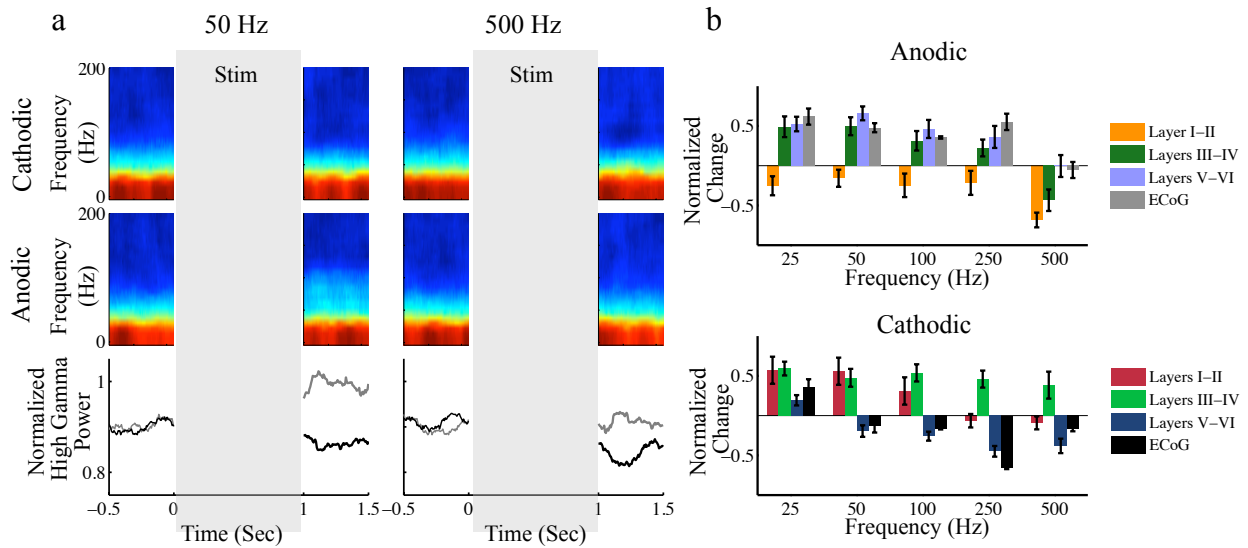
Figure 3.5. Effects of the frequency of stimulation on ECoG regardless of stimulation amplitude. a) The top plot shows the normalized ECoG spectrograms of the corresponding LFPs and units shown in Figure 3.4 averaged across trials for frequencies of 50Hz (left column) and 500Hz (right column) following Cathodic stimulation. The middle plot shows the normalized ECoG spectrograms following Anodic stimulation. Time is on the x-axis; frequency is on the y-axis; power is color-coded in a log scale (hot colors represent high power, cold colors represent low power). The bottom plot shows the normalized high gamma power (60-120 Hz) of the ECoG averaged across trials. Vertical shaded bars represent the 1 second stimulus pulse train in which no activity was recorded. b) The mean of the averaged normalized change of high gamma power in all ECoG recorded signals from baseline in the first 500ms interval after the offset of stimulation in comparison with unit activity as a function of stimulation frequency for anodic and cathodic stimulation.

3.4.3. CES amplitude

Anodic vs. cathodic post-stimulus effects on gamma power of LFPs and high gamma power of ECoGs observed in upper and lower layers were also amplitude-dependent (p<0.01, Figure 3.6). In Figure 3.6a, the mean of the normalized change of unit activity (solid-colored bars) across all units and LFP gamma power change (30-120 Hz) across all LFPs (white bars) as the function of stimulation amplitude of Anodic and Cathodic stimulation is shown. As can be seen in this Figure, the change in the gamma power of LFP was highly correlated with the change in unit activity following all amplitudes of stimulation in each of the layer categories (r>0.95).

The change in the high gamma power of ECoGs was also highly correlated with the change in unit activity of the lower layers (V-VI) following all amplitudes of stimulation (Figure 3.6b). In this figure, the mean of the normalized change of unit activity (solid-colored bars) across all units is shown with the high gamma power (30-120 Hz) change of ECoGs across all ECoGs as the function of stimulation amplitude.
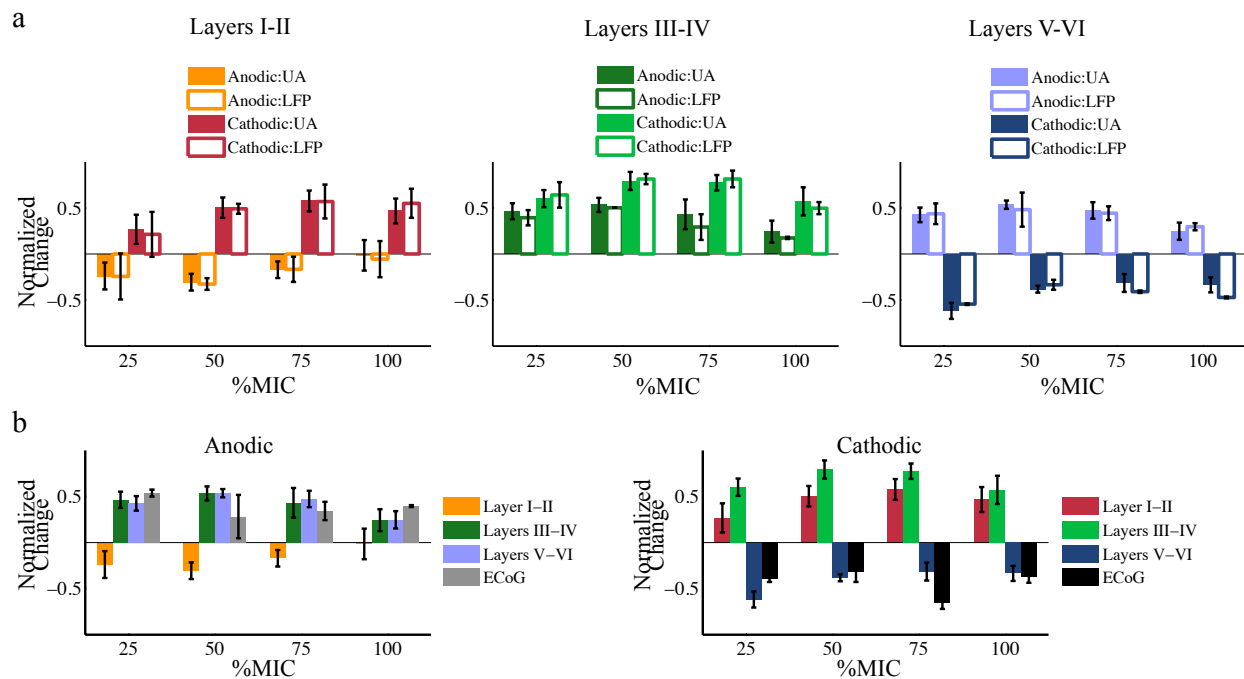
Figure 3.6. Effects of the amplitude of stimulation on LFP and ECoG regardless of stimulation frequency. a) The mean of the normalized change of unit activity (solid-colored bars) across all units and LFP gamma power (30-120 Hz) change (white bars) across all LFP as the function of stimulation amplitudes for Anodic-first (light shading) and Cathodic-first (dark shading) stimulation consistent with the color coding in previous figures. b) The mean of the averaged normalized change of high gamma power in all ECoG recorded signals (increase, positive deviation; decrease, negative deviation) from baseline in the first 500ms interval after the offset of stimulation (white bars) in comparison with unit activity as a function of stimulation amplitude.

3.5. Discussion

3.5.1. Effects of CES parameters on LFPs

The results of time-frequency spectral analysis on LFPs showed that Anodic and Cathodic stimulation pulses had a significantly different post-stimulus effect on the gamma power (30-120 Hz) of LFPs recorded from upper and lower cortical layers. The changes observed in the gamma power of LFPs as the result of stimulation were highly correlated with the effects of stimulation in unit activity. These results were also frequency and amplitude-dependent. LFPs are defined as low-frequency component (<200Hz) of the recorded neural activity and reflect the spatial and temporal superposition of the synaptic input to a local population surrounding the electrode[14]. These signals are thought to represent the synaptic activity of a few thousand neurons, depending on the tip diameter used for the recording[15,16]. While lower-frequency activity in the LFPs are thought to be due to the activity of a larger population of neurons, higher frequencies typically reflect a smaller population[15]. Frequencies higher than 300 Hz are probably dominated by action potential currents[17]. Therefore, it is expected to see a high correlation between the high-frequency activity in LFPs with the firing of a few neurons located close to the recording electrode[2]. Our results agree with this hypothesis as we see a high correlation between the gamma power of LFPs with the unit activity in each of the cortical layers. However, previous studies have shown that power in a frequency range of high gamma (60–200 Hz) is tightly coupled to the firing rates of a small population of neurons[2,5]. The high correlation that we see in the low gamma range (30-60Hz) as well as the high gamma range with unit activity in our results could be due to synchronization induced in the network by the stimulation. While an increase in high-gamma could be attributable to an increase in spike synchronization within the neural population, an increase in low gamma power could be attributable to an increase in

71

synchronization in synaptic inputs, because synaptic activity is correlated with the low-gamma frequency range[2]. These results suggest that we introduce a synchronization in both spiking activity and synaptic input of the affected cortical region by electrical stimulation at the cortical surface. The higher frequency components of LFPs (>120Hz) probably have a greater relative contribution from the generation of action potentials, whereas the size of the neural population (that generates the activity at that frequency) decreases with increasing frequency[15]. Therefore, based on our results, the broad gamma frequency range (30–120 Hz) appears to be well suited for studying the spiking activity of a relatively small population of neurons in LFP recordings following cortical electrical stimulation.

3.5.2. Effects of CES parameters on ECoGs

The results of time-frequency spectral analysis on ECoGs showed a significantly different post-stimulus effect on the high gamma (60-120 Hz) power following Anodic versus Cathodic stimulation. The changes observed in the high gamma power of ECoGs, as the result of stimulation, were highly correlated with the effects of stimulation on unit activity of the lower layers (V-VI) only. These results were also frequency and amplitude-dependent. As reported in previous studies, LFP high-gamma activity represents the average firing of neurons near the microelectrode from which the LFP activity is recorded, weighted according to their distance from the electrode[2]. If LFP high-gamma activity is a measure of neural firing of the population near the microelectrode, ECoG high-gamma activity should be an indicator of the firing properties of the entire neural population beneath the ECoG electrode. In other words, while LFP high-gamma activity may only reflect the firing rate of the neural population near the microelectrode, at a larger level of integration such as ECoG, it is possibly an index of neural

synchrony in the underlying cortical neurons. It has been shown that the change in high-gamma power in the ECoG signal is due to changes in firing rate or synchronization in the underlying neural population[2,3]. Most of the power recorded by the ECoG electrode is due to synaptic activity[15,16], so it is hypothesized that the contribution of the action potentials is small and limited to the higher frequencies only. Our results agree with this hypothesis, however the surprising result is that we only see correlation between the high gamma power of ECoGs with the unit activity of the lower cortical layers. As high frequency activity does not travel far spatially, we were expecting to see a high correlation between the high gamma power of ECoGs with the unit activity of the upper cortical layers. It is important to keep in mind that the dipoles in upper layers are much less organized than the dominant pyramidal cells in lower layers. As the high gamma activity in ECoG represents the neural synchrony in the underlying cortical neurons, these highly organized pyramidal cells play a more dominant role in this frequency band. Another possibility is that the ECoGs are recording electrical activity from the apical dendrites of the pyramidal cells. This however, raises the question as to why we don't see this signature in the LFP recordings in the upper cortical layers. There are two possible explanations for these results. One is that ECoG electrodes are placed in a different orientation than the LFP electrodes with respect to the neural population and their resultant dipoles. The other is that the surface area of the ECoGs are ~20,000x larger than the LFP recording sites. This means that we are "listening" to the neural activity of a much larger population of neurons using ECoGs compared to LFP recordings. Our results suggest that high-gamma activity in electrophysiological recordings of a large population (like ECoG) could be a useful indicator of the firing dynamics of the neural population whose activity is being altered by stimulation. This key finding could potentially be used to characterize the effects of stimulation in the underlying neural activity, particularly layers

V-VI.

That ECoG signals are highly correlated with population dynamics in the output layers of cortex are highly important. Several arguments suggest that ECoG signals might be preferable for neuropresthetic and neurorehabilitation applications over unit or LFP recordings where understanding or controlling a population of units is desired. One argument is that ECoG electrodes do not penetrate the cortical surface and therefore reduce the risk for brain tissue damage. In contrast to unit spike data, which reflect single cell activity, ECoG (and LFP) measure population activity, which offers a better prospect of long-term recording stability. In addition, ECoG (as LFP) requires lower sampling rates for data acquisition and doesn't need specialized spike detection and sorting algorithms, therefore reducing the computational costs associated with single-unit recordings. It is also important to point out that clinical investigation using the ECoG signals are regularly performed for days in patients who are candidates for surgical resection of epileptic foci[18].

3.5.3. Implications for closed-loop stimulation

Although a wide range of electrical stimulation parameters have been successfully used for a number of neuroprosthetics applications, their employment has been as "open-loop" control systems. Open-loop refers to stimulation that is independent of brain activity at any particular point in time such that the dynamics of neuronal behavior are not incorporated in the generation of stimulation protocols[19]. In open-loop stimulation systems, the stimulation is kept periodically on and off following preset programming, regardless of the state of the brain[19]. However the exact nature and timing of these cycles are sometimes very critical. Under normal conditions in which no pathologic state is present, chronically stimulated neurons could easily get fatigued

under such long term activation, resulting in alteration of normal brain function[19-21]. Alternatively, constant stimulation could lead to an alteration in synaptic efficacy in the affected region, changing network characteristics in possibly a deleterious way[19-22]. To address such concerns, studies have been done to incorporate "feedback" in seizure control for epilepsy patients[19,23-26] and pain control[27] through a number of applications using EEG signals. In general, "closing the loop" would permit precisely timed stimulation with specific parameters that could adjust appropriately to the dynamic of the brain region of interest. The results of our time-fequency analysis on ECoGs provide a promising potential to use surface recordings (such as ECoG) and monitor the signatures of the underlying neural population activity before, during, and after the stimulation to modify subsequent stimulus pulses in such closed-loop stimulation systems. These findings show that future cortical stimulation studies could lean towards less invasive control systems that incorporate surface stimulation and recording configurations.

3.5.4. Implications for TMS and tDCS

Although the results of the study presented in this chapter and chapter 2, could be related to epidural and subdual motor cortex stimulation applications, there are important differences between our results relative to the use of conventional, non-invasive cortical stimulation methods. Transcranial magnetic stimulation (TMS) and Transcranial direct current stimulation (tDCS) are two of the most important applications of cortical stimulation in neurorehabilitation given their non-invasiveness[28-33]. There are important differences between electric and magnetic stimulation of the brain. First, during magnetic stimulation, the direction of the electric field is approximately tangential (parallel to the surface of the skull). However, during electric

stimulation the electric field has both radial and tangential components[34]. Therefore, the distribution of the electric field as the result of electric and magnetic stimulation and consequently the excited elements are different. There are also latency differences in surface-recorded electromyographic responses following electric and magnetic stimulation of the brain[35-36]. The response latency in the contracting muscle during magnetic stimulation was found to be longer than electrical stimulation. These findings suggest that magnetic stimulation activates neurons trans-synaptically, while electric stimulation activates them directly[34,37]. Because of these differences we suggest that the results presented in these two chapters may not be related to TMS applications.

It is also important to point out that there are major differences between CES and tDCS. Although in tDCS the electrodes attached to the scalp can be used to activate neurons in the brain, the high resistance of the skull shunts most of the current through the scalp[34]. In addition tDCS approaches have a low spatial specificity and induce a modulation in a large cortical area[38]. CES on the other hand, permits high spatial specificity to targeted neuronal populations[39]. Therefore due to these differences between our studues and tDCS, the spatial distribution of electric fields are likely significantly different.

3.5.5. Considerations

In this chapter and chapter 2 we used the rat model of CES because rat's cortex is well defined [63] and often used in neuroprosthetics and neurorehabilitation research [40-43]. Therefore, the rat's cortex will help us to begin to understand the effects of stimulation in vivo without the confounding factors of sulci and gyri. However in interpreting and comparing the results of

these studies for human applications, it is important to keep in mind that following the fold of the gyrus, the orientation of the neurons with respect to the electrode changes [44]. Bending axons exhibit abrupt changes in the profile of membrane voltage along the axon at the sites of the bends[40,45] and therefore the excitation conditions are altered [44].

One of the important choices in designing stimulation paradigms is the choice of the waveform and whether to use voltage or current controlled pulses. We used current-controlled pulses because the effects of current pulse stimulation are more tractable than the effects of voltage pulse stimulation, for which the (current-induced) electric field depends upon the complex impedance of the stimulation electrode[31]. Another constraint was to use charge-balanced stimulation to avoid injection of net charge and prevent electrode and cell damage[46]. To be able to compare the effects of anodic versus cathodic stimulation on different neurons in the motor cortex, we used a monopolar stimulation configuration that used biphasic pulse trains consisting of a square leading phase and a decaying exponential phase to balance charge. A third constraint was the width of the leading phase of the stimulus pulses. In this study the leading phase pulse width was fixed at 100 μs as this pulse width is typically used for neural stimulation [41,42,47,48]. There have been several investigations to optimize the stimulus waveform in order to maximize the injected charge through the electrode interface while keeping the activation threshold at a minimum[49-51]. It has been shown that this optimization varies as a function of the stimulus waveform and stimulating electrode material[49]. Further investigation is needed to determine if alternative waveforms can provide similar results with the same polarity, frequency and amplitude of stimulation as used in the studies presented in this chapter and chapter 2.

3.6. Conclusion

In this chapter we investigated the effects of CES on LFPs and ECoGs recorded from the rat primary motor cortex and compared the results with the CES effects on the simultaneous recorded unit activity (reported in the previous chapter). Our results showed a significant different post-stimulus effect on the gamma power of LFPs and the high gamma (60-120 Hz) power of ECoGs following Anodic versus Cathodic stimulation. Time-frequency analysis of LFPs showed high correlation of gamma power with unit activity in corresponding layers. On the other hand, high gamma power of ECoG signals only showed high correlation with the unit activity in lower layers. Time-frequency correlations, which were found between LFPs, ECoGs and unit activity were also frequency- and amplitude- dependent. The data demonstrates that the poststimulus effects in neural activity after manipulation of CES parameters changes according to the location (depth) of the recorded neural activity in motor cortex. The signature of the neural activity observed in LFP and ECoG signals provides a better understanding of the effects of stimulation on the affected network and has a promising potential to be used in closed-loop control stimulation systems. These results demonstrate that the neurorehabilitation and neuroprosthetic applications of CES can be further improved by optimizing CES parameters.

3.7. References

1. Mitzdorf U. Properties of the evoked-potential generators current-source-density analysis of visually evoked-potentials in the cat cortex. International Journal of Neuroscience. 1987;33(1-2):33-59.

2. Ray S, Crone NE, Niebur E, Franaszczuk PJ, Hsiao SS. Neural Correlates of High-Gamma Oscillations (60-200 Hz) in Macaque Local Field Potentials and Their Potential Implications in Electrocorticography. The journal of neuroscience : the official journal of the Society for Neuroscience. 2008;28(45):11526.

3. Crone NE, Sinai A, Korzeniewska A. High-frequency gamma oscillations and human brain mapping with electrocorticography. Event-related duynamics of brian oscillations. 2006;159:275-95.

4. Logothetis NK, Kayser C, Oeltermann A. In Vivo Measurement of Cortical Impedance Spectrum in Monkeys: Implications for Signal Propagation. Neuron. 2007;55(5):809.

5. Belitski A, Gretton A, Magri C, Murayama Y, Montemurro MA, Logothetis NK, et al. Low-Frequency Local Field Potentials and Spikes in Primary Visual Cortex Convey Independent Visual Information. The journal of neuroscience : the official journal of the Society for Neuroscience. 2008;28(22):5696.

6. Pesaran B, Pezaris JS, Sahani M, Mitra PP, Andersen RA. Temporal structure in neuronal activity during working memory in macaque parietal cortex. Nature Neuroscience. 2002;5(8):805-11.

7. Spinks RL, Kraskov A, Brochier T, Umilta MA, Lemon RN. Selectivity for Grasp in Local Field Potential and Single Neuron Activity Recorded Simultaneously from M1 and F5 in the Awake Macaque Monkey. The journal of neuroscience : the official journal of the Society for Neuroscience. 2008;28(43):10961.

8. Mukamel R, Gelbard H, Arieli A, Hasson U, Fried I, Malach R. Coupling Between Neuronal Firing, Field Potentials, and fMRI in Human Auditory Cortex. Science. 2005;309(5736):951.

9. Kipke D, Vetter R, Williams J, Hetke J. Silicon-Substrate Intracortical Microelectrode Arrays for Long-Term Recording of Neuronal Spike Activity in Cerebral Cortex. IEEE transactions on neural systems and rehabilitation engineering : a publication of the IEEE Engineering in

Medicine and Biology Society. 2003;11(2):151.

10. Mitra PP, Ogawa S, Hu X, Ugurbil K. The Nature of Spatiotemporal Changes in Cerebral Hemodynamics As Manifested in Functional Magnetic Resonance Imaging. Magnetic resonance in medicine : official journal of the Society of Magnetic Resonance in Medicine. 1997;37(4):511.

11. Prechtl JC, Cohen LB, Pesaran B, Mitra PP, Kleinfeld D. Visual stimuli induce waves of electrical activity in turtle cortex. Proceedings of the National Academy of Sciences of the United States of America. 1997;94(14):7621.

12. Mitra, P. P. & Pesaran, B. Analysis of dynamic brain imaging data. *Biophys J* **76**, 691-708 (1999).

13. Slepian, D. & Pollack, H. O. Prolate spheroidal wavefunctions: Fourier analysis and uncertainty I. *Bell System Tech Journal* **40**, 43-63 (1961).

14. Mitzdorf U. Current-source-density method and application in cat cerebral-cortex-Investigation of evoked-potentialsl and EEG phenomena. Physiological Reviews. 1985;65(1):37-100.

15. Nunez PL (1981) Electrical fields of the brain: the neurophysics of EEG. New York: Oxford UP.

16. Nunez PL (1995) Neocortical dynamics and human EEG rhythms. Oxford: Oxford UP.

17. Logothetis N. The neural basis of the blood-oxygen-level-dependent functional magnetic resonance imaging signal. Philosophical Transactions: Biological Sciences. 2002;357(1424):1003-37.

18. Pistohl T, Ball T, Schulze-Bonhage A, Aertsen A, Mehring C. Prediction of arm movement trajectories from ECoG-recordings in humans. Journal of neuroscience methods. 2008;167(1):105.

19. Li Y, Mogul D. Electrical Control of Epileptic Seizures. Journal of clinical neurophysiology : official publication of the American Electroencephalographic Society. 2007;24(2):197.

20. Fregni F, Boggio PS, Silva MT, Marcolin MA, Pascual-Leone A, Barbosa ER. Rapid-rate repetitive transcranial magnetic stimulation and cognitive function in Parkinson's disease patients: A safety study. Movement disorders. 2004;19:S240-S1.

21. Michelucci R, Valzania F, Passarelli D, Santangelo M. Rapid-rate transcranial magnetic stimulation and hemispheric language dominance: Usefulness and safety in epilepsy. Neurology. 1994;44(9):1697.

22. Jahanshahi M, Ridding MC, Limousin P, Profice P. Rapid rate transcranial magnetic stimulation - a safety study. Electroencephalography and clinical neurophysiology. 1997;105(6):422.

23. Nakagawa M, Durand D. Suppression of spontaneous epileptiform activity with applied currents. Brain research. 1991;567(2):241-7.

24. Krauss G, Fisher R. Cerebellar and Thalamic Stimulation for Epilepsy. Advances in neurology. 1994;63:231-46.

25. Warren RJ, Durand DM. Effects of applied currents on spontaneous epileptiform activity induced by low calcium in the rat hippocampus. Brain research. 1998;806(2):186.

26. Sun FT, Morrell MJ, Wharen RE. Responsive cortical stimulation for the treatment of epilepsy. Neurotherapeutics. 2008;5(1):68-74.

27. Ativanichayaphong T, He JW, Hagains CE, Peng YB, Chiao JC. A combined wireless neural stimulating and recording system for study of pain processing. Journal of neuroscience methods. 2008;170(1):25.

28. Nitsche MA, Schauenburg A, Lang N, et al. Facilitation of Implicit Motor Learning by Weak Transcranial Direct Current Stimulation of the Primary Motor Cortex in the Human. Journal of Cognitive Neuroscience. 2003;15(4):619-26.

29. Kincses TZ, Antal A, Nitsche MA, Bartfai O, Paulus W. Facilitation of probabilistic classification learning by transcranial direct current stimulation of the prefrontal cortex in the human. Neuropsychologia. 2004;42(1):113-7.

30. Fregni F, Boggio PS, Nitsche M, et al. Anodal transcranial direct current stimulation of prefrontal cortex enhances working memory. Experimental brain research. 2005;166(1):23.

31. Marshall L, Molle M, Hallschmid M, Born J. Transcranial Direct Current Stimulation during Sleep Improves Declarative Memory. The journal of neuroscience: the official journal of the Society for Neuroscience. 2004;24(44):9985.

32. Lefaucheur JP. Repetitive transcranial magnetic stimulation (rTMS): insights into the treatment of Parkinson's disease by cortical stimulation. Clinical Neurophysiology. 2006;36(3):125-33.

33. Fitzgerald PB, Huntsman S, Gunewardene R, Kulkarni J, Daskalakis ZJ. A randomized trial of low-frequency right-prefrontal-cortex transcranial magnetic stimulation as augmentation in treatment-resistant major depression. The International Journal of Neuropsychopharmacology. 2006;9(6):655-66.

34. Basser PJ, Roth BJ. New currents in electrical stimulation of excitable tissues. Annual review of Biomedical Engineering. 2000;2:377-97.

35. Rothwell J, Burke D, Hicks R, Stephen J. Transcranial electrical stimulation of the motor cortex in man: further evidence for the site of activation. The Journal of physiology. 1994(481):243.

36. Day BL, Thompson PD, Dick JP, Nakashima K, Marsden CD. Different sites of action of electrical and magnetic stimulation of the human-brain. Neuroscience letters. 1987;75(1):101-6.

37. Edgley SA, Eyre JA, Lemon RN, Miller S. Excitation of the corticospinal tract by electromagnetic and electrical stimulation of the scalp in the macaque monkey. The Journal of physiology. 1990;425:301-20.

38. Alappat JJ. Motor cortex stimulation for chronic pain: Systematic review and meta-analysis of the literature - To the Editor. Neurology. 2009;72(6):577.

39. Cherney LR, Erickson RK, Small SL. Epidural cortical stimulation as adjunctive treatment for non-fluent aphasia: preliminary findings. Journal of neurology, neurosurgery and psychiatry.81(9):1014-21.

40. Iles JF. Simple models of stimulation of neurones in the brain by electric fields. Progress in biophysics and molecular biology. 2005;87(1):17-31. Electroencephalography and clinical neurophysiology. 1992;85(5):291-301.

41. Teskey GC, Flynn C, Goertzen CD, Monfils MH, Young NA. Cortical stimulation improves skilled forelimb use following a focal ischemic infarct in the rat. Neurological research. 2003;25(8):794.

42. Butovas S, Schwarz C. Spatiotemporal Effects of Microstimulation in Rat Neocortex: A Parametric Study Using Multielectrode Recordings. Journal of neurophysiology. 2003;90(5):3024.

43. Thomson AM, Deuchars J, West DC. Large, Deep Layer Pyramid-Pyramid Single Axon EPSPs in Slices of Rat Motor Cortex Display Paired Pulse and Frequency Dependent Depression, Mediated Presynaptically and Self-Facilitation, Mediated Postsynaptically. Journal of neurophysiology. 1993;70(6):2354.

44. Manola L, Holsheimer J, Veltink P, Buitenweg JR. Anodal vs cathodal stimulation of motor cortex: A modeling study. Clinical neurophysiology : official journal of the International Federation of Clinical Neurophysiology. 2007;118(2):464.

45. Wongsarnpigoon A, Grill WM. Computational modeling of epidural cortical stimulation. Journal of Neural Engineering. 2008;5(4):443-54.

46. Wagenaar DA. Effective parameters for stimulation of dissociated cultures using multi-electrode arrays. Journal of neuroscience methods. 2004;138(1):27.

47. Brown JA, Lutsep HL, Weinand M, Cramer SC. Motor Cortex Stimulation for the Enhancement of Recovery from Stroke: A Prospective, Multicenter Safety Study. Neurosurgery. 2006;58(3):464.

48. Bossetti CA, Birdno MJ, Grill WM. Analysis of the quasi-static approximation for calculating potentials generated by neural stimulation. Journal of Neural Engineering. 2008;5(1):44-53.

49. Sahin M, Tie Y. Non-rectangular waveforms for neural stimulation with practical electrodes. Journal of Neural Engineering. 2007;4(3):227-33.

50. Blair HA. On the intensity-time relations for stimulation by electric currents. I: The Rockefeller University Press.

51. Ayers GM, Aronson SW, Geddes LA. Comparison of the ability of the lapicque and exponential strength-duration curves to fit experimentally obtained perception threshold data. Australasian Physical and Engineering Sciences in Medicine. 1986;9(3):111-6.

Chapter 4

Estimation of electrode location in rat motor cortex by laminar analysis of electrophysiology and intracortical electrical stimulation

4.1. Abstract

While the development of microelectrode arrays has enabled access to disparate regions of cortex for neurorehabilitation, neuroprosthetic, and basic neuroscience research, accurate interpretation of the signals and manipulation of the cortical neurons depend upon the anatomical placement of the electrode arrays in layered cortex. Toward this end, this report compares two in vivo methods for identifying the placement of electrodes in a linear array spaced 100 μm apart based on in situ laminar analysis of (1) ketamine-xylazine-induced field potential oscillations in rat motor cortex and (2) intracortical electrical stimulation-induced movement threshold. The first method is based on finding the polarity reversal in laminar oscillations which is reported to appear at the transition between layer IV/V in laminar "high voltage spindles" of the rat cortical column. Analysis of histological images in our data set indicate that polarity reversal is detected 150.1±104.2 μm below the start of layer V. The second method compares the intracortical microstimulation currents that elicit a physical movement for anodic versus cathodic stimulation. It is based on the hypothesis that neural elements perpendicular to the electrode surface are preferentially excited by anodic stimulation while cathodic

stimulation excites those with a direction component parallel to its surface. With this method, we expect to see a change in the stimulation currents that elicits a movement at the beginning of layer V when comparing anodic versus cathodic stimulation as the upper cortical layers contain neuronal structures that are primarily parallel to the cortical surface and lower layers contain structures that are primarily perpendicular. Using this method, there was a 78.7±68 µm offset in the estimate of the depth of the start of layer V. The polarity reversal method estimates the beginning of layer V within ±90 µm with 95% confidence and the intracortical stimulation method estimates it within ±69.3 µm. We propose that these methods can be used to estimate the in situ location of laminar electrodes implanted in rat motor cortex.

4.2. Introduction

The development of microelectrode arrays has enabled access to disparate regions of cortex for neurorehabilitation, neuroprosthetic, and basic neuroscience research[1-4]. The mammalian neocortex has a regular structure consisting of six layers that is similar across different brain areas[5]. Microelectrode array technology has enabled us to span the entirety of the six layer cortex allowing simultaneous electrophysiological recordings and stimulation in different depths and layers[3-4].

One exciting application of these electrodes is in the neuroprosthetic field where neural signals are acquired from motor cortex to control external devices[6-8]. Previous neuroprosthetic studies have targeted neurons in the lower layers of the motor cortex (layers V and VI)[9-11] to obtain a control signal because the large pyramidal Betz cells in these layers project to the spinal cord, and their large dipole fields result in higher

recording quality relative to other cells[12]. Parikh et. al[13] have shown that units in the lower layers are significantly more likely to encode direction information as compared to units in the upper layers. Advances in electrode technology and the ability to conduct long-term, simultaneous, multi-site recordings have made it possible to evaluate event-related action potentials from different cortical layers for movement and direction information[13,14].

Another application of these electrodes is in intracortical microstimulation (ICMS) for neurorehabilitation applications[15,16]. It has been shown that for specific neurorehabilitation applications it is important to target deep cortical layers (specifically layer V)[17]. Studies on the neurorehabilitation applications of cortical electrical stimulation have shown that stimulation differentially affects neuronal activity of deep and superficial layers of motor cortex[18]. Therefore, advances in techniques to determine the location and type of cell recorded in an awake, behaving preparation via extracellular recordings will help validate proposed cortical microcircuits and the functional role of the different cells across layered cortex[14].

Accurate interpretation of the signals recorded with these electrodes depends upon having a firm understanding of the neural signal and accurate placement of the electrodes[13,19-23]. Often, the placement of the electrodes can only be evaluated through histological and electrolytic lesioning techniques, which practically can only be done post-mortem by explanting the brain[24-25]. Although these electrodes can be visualized in situ during electrode placement at specialized institutions using MRI or CT[26-27], the small size of these electrodes and the cost of MRI and CT makes it more difficult for visualization in animal models. An in vivo method for identification of correct placement of electrodes is

necessary to determine in situ electrode placement for use in the development of clinical neuroprosthetic and neurorehabilitation devices in animal models of human disorders.

In the first in vivo method for electrode localization described here, the depth of an electrode array was estimated by laminar analysis of the field potential oscillations. This method is based on the field potential polarity reversal, which appears 100-300μm below layer IV of cortex[28] in laminar ketamine-xylazine-induced high voltage spindles (HVS) of rat cortical column. HVSs consist of a rhythmic series of spike and wave components in local field potentials and occur in the resting or sleeping states in rats[28-29]. The intraepisodic frequency of HVSs in the anesthetized animal varies from 2–6 Hz[28]. Single fibers of thalamocortical neurons provide input mainly to layer IV but also give off collaterals to layers V and VI [30,31]. This contributes to a polarity reversal observed 100-300μm below layer IV of cortex[28] which was used as a biological marker to estimate the depth of the implanted electrode in this method. The depth of polarity reversal in these oscillations was calculated and compared to the start of layer V based on histological analysis. The electrode recording site in which polarity reversal appeared, was identified by estimating the instantaneous phase of each recording site using the Hilbert Transform.

In the second in vivo method, the depth of the electrode array was estimated by electrically stimulating through each electrode site and comparing the minimum current that induced a threshold movement for cathodic vs. anodic pulse shapes. When an electrical stimulus is applied within the brain, cells and fibers over an unknown volume of tissue are activated[32]. To make accurate inferences about anatomic structures involved in electrical stimulation, we must know which elements are stimulated. Previous clinical, animal, and modeling studies have shown that neural elements perpendicular to the

electrode surface are preferentially excited by anodic stimulation while cathodic stimulation excites those with a direction component parallel to its surface[18,33-35]. Previous investigations on the effects of extracellular anodic and cathodic stimulation on cortical neurons have inferred that the differences obtained are due to the opposing membrane potential changes induced between oppositely directed poles (dendrite and axon) of the neurons[36-40]. In addition, it has been reported that the site of excitation is dependent on the polarity of the stimulus, with cathodic stimuli resulting in lower thresholds of activation for electrode positions closer to the axon and anodic stimuli resulting in lower thresholds for electrode positions closer to the cell body and dendrites[41-43]. The layer V of rat motor cortex contains large pyramidal neurons which are primarily perpendicular to the surface of the brain[44-45] and therefore parallel to the stimulating electrode sites. Upper cortical layers contain neuronal structures that are primarily parallel to the cortical surface and perpendicular to the implanted electrode surface[45]. Considering the structure of cortical layers and the implantation of microelectrode arrays in rat motor cortex, we hypothesize that lower motor thresholds can be obtained by anodal stimulation in upper layers of motor cortex compared to cathodal and vice versa in layers V/VI. To test this hypothesis, we designed an experiment to measure the motor thresholds by sequentially stimulating across different electrodes (and hence different cortical layers) of the rat motor cortex through a linear array of equally spaced electrodes.

The estimated depths from both methods were tested against the histological images. The results of both methods demonstrate placement of the electrode sites in the upper and lower cortical layers with less than ±100 μm error in a linear array with sites spaced 100

89

μm apart. These results suggest that both methods are suitable for *in situ* electrode localization for neuroprosthetic research that has typically targeted neurons in the lower layers of the motor cortex[9-11,13].

4.3. Methods

4.3.1. Animal Procedures

Fourteen normal male rats weighing 275-450g (Charles River Laboratories) were used for this study. A craniotomy was performed over the neck (n=6) or forelimb (n=8) representation of primary motor cortex (MI) in the right hemisphere. The dura was cut and folded back to allow insertion of a micro-scale penetrating electrode array (NeuroNexus Technologies) consisting of 16-electrodes linearly spaced 100 μm apart[3] (figure 4.1(a)-(b)) with site areas of 413, 703, or 1250 $μm^2$ on an array-by-array basis. The electrodes were inserted by hand with the aid of a dissecting microscope until the top recording site was even with the brain surface such that a maximum number of electrodes span six-layer neocortex. The probes were then secured using dental cement and the subjects were allowed 5-10 days to recover.

4.3.2. Extracellular Field Potential Recordings

Extracellular field potential recordings were obtained under condition of ketamine-xylazine anesthesia. The rats were anesthetized with a mixture (1.8 mg/kg) of ketamine (50 mg/ml) and xylazine (5 mg/ml). Neural electrophysiological signals were simultaneously amplified and bandpass filtered (3-90 Hz or 1-500 Hz) and sampled at

500 or 1000 Hz using a Multichannel Neuronal Acquisition Processor (Plexon Inc, Dallas, TX).
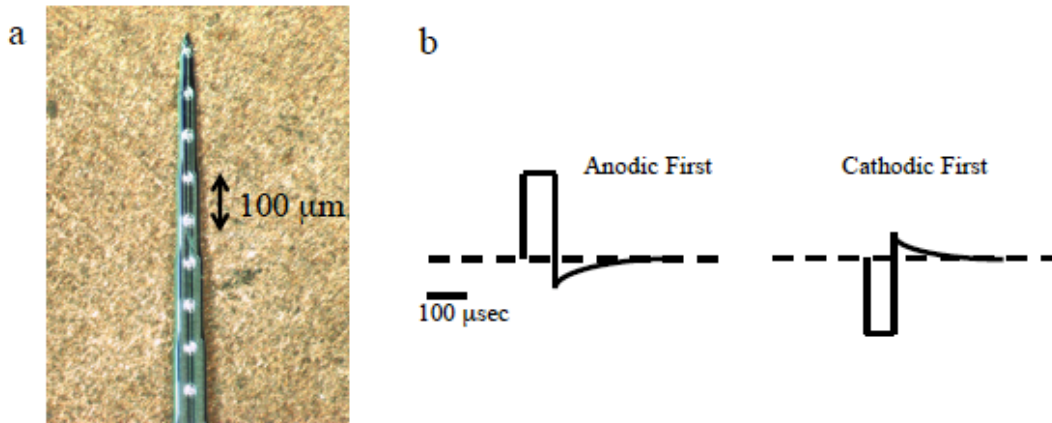
Figure 4.1. a) silicon electrode array on top of an American penny. b) Pulse shapes: Constant current CES was delivered in two configurations, cathodic or anodic consisting of pulse trains. Pulses consisted of square leading phase (100 μsec) followed by an exponentially decaying second phase to balance charge. The pulse width of the leading phase was fixed at 100 μsec and length of the trailing phase dependent upon current amplitude.

4.3.3. Polarity Reversal Method

In this method, we use the field potential polarity reversal, which appears 100-300μm below layer IV of cortex[28] in laminar ketamine-xylazine-induced HVSs of rat cortical column. The polarity reversal was found based on instantaneous phase calculations of the recorded local field potentials (LFPs) of each electrode site. LFP phase estimation steps are shown in figure 4.2 and described as follows:

The Hilbert Transform permits a direct estimation of the instantaneous phase of a signal[46-47]. In this method, the phase of a signal can be obtained by means of the analytic signal concept originally introduced by Gabor (1946)[48] and recently investigated for model systems as well as for experimental data[49]. For an arbitrary signal s(t), the analytic

signal $\zeta(t)$ is a complex function of time defined as:

(4.1)
$$\zeta(t) = s(t) + j\tilde{s}(t) = A(t)e^{j\varphi(t)}$$

where the function $\tilde{s}(t)$ is the Hilbert transform of s(t):

(4.2)
$$\tilde{s}(t) = \frac{1}{\pi} P.V. \int_{-\infty}^{+\infty} \frac{s(t)}{t - \tau} d\tau$$

P.V. indicates that the integral is taken in the sense of the Cauchy principal value. The instantaneous amplitude A(t) and the instantaneous phase $\varphi(t)$ of the signal s(t) are thus uniquely defined by Equation (4.1)[46].

An important advantage of this approach is that the phase can be easily obtained for an arbitrary broad-band signal. Nevertheless, application of the Hilbert Transform to the unfiltered signal gives analytic phase values resembling a "random walk". Effective use of the Hilbert transform with LFPs must be preceded by filtering to separate the frequency band of interest from the background brain activity[50-52].

To capture the polarity reversal appearing in the ketamine-xylazine-induced field potential oscillations, corresponding to each electrode site, the field potential signal of the most superficial site ($s_1(t)$: reference site) was passed through a zero-phase-lag band pass filter (4-6 Hz)[28]. The Hilbert transform, and therefore the instantaneous phase of the filtered signal ($\varphi_1(t)$), were calculated (figure 4.2). To calculate the phase reversal, we averaged the LFPs of all sites ($s_i(t)$; i=1:16) with respect to the instantaneous phase of the most superficial signal ($\varphi_1(t)$) in $-\pi$ to $+\pi$ range with $2\pi/100$ steps (figure 4.2). The

averages over -π to π phase duration were smoothed by fitting to sine waves. The phase of the smoothed signal ($\varphi_2(i)$) was calculated for each recording site. The highest phase difference corresponds to the site of polarity reverse. Since we are expecting to see a polarity reversal at this site, the phase difference should be about 180 degrees. We have considered a 60 degrees margin for the polarity reversal. Any phase difference less than 60 degrees is considered not indicative of a polarity reversal.
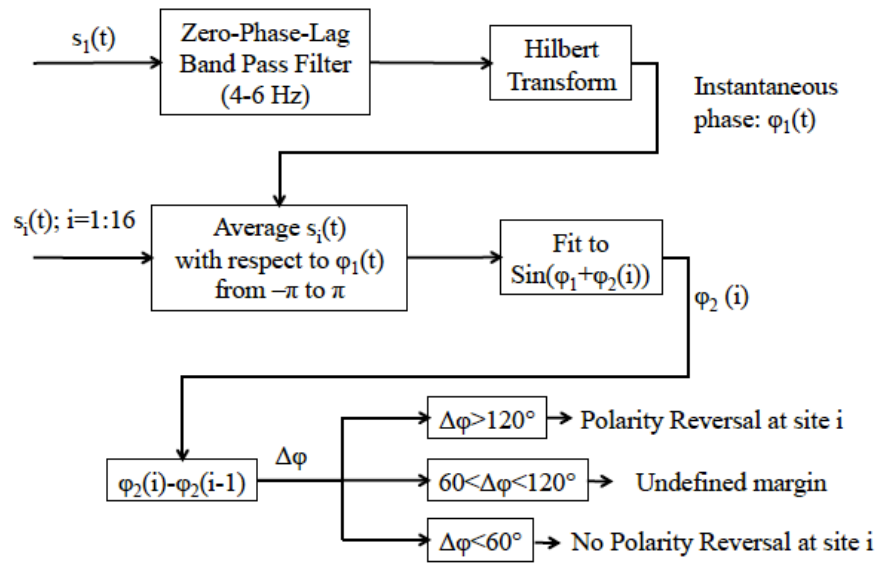
Figure 4.2. Block diagram of the Polarity Reversal Method. The field potential signal of the most superficial site (s1(t): reference site) was passed through a zero-phase-lag band pass filter (4-6 Hz). The Hilbert transform and therefore the instantaneous phase of the filtered signal ($\varphi_1(t)$) were calculated. To calculate the phase reversal, we averaged the signal of all sites (si(t); i=1:16) with respect to the instantaneous phase of the most superficial signal ($\varphi_1(t)$) in - π to +π range with 2π/100 steps. The averages over -π to π phase duration were smoothed by fitting to sine waves. The phase of the smoothed signal ($\varphi_2(i)$) was calculated for each recording site. The corresponding electrode sites with phase differences higher than 120° are considered the polarity reversal site.

To demonstrate the independence of our method to the referenced (most superficial) site, a virtual depth experiment was designed in which the most superficial site was changed from site 1 progressively to site 16 and the polarity reversal site was recalculated based

93

on the method described above.

4.3.4. Intracortical Stimulation Method

For the second proposed method, the depth of the electrode array is estimated by stimulating through each electrode site and comparing the minimum current that induces a movement for cathodic vs. anodic pulse shapes. Constant current intracortical microstimulaltion was delivered in two configurations, cathodic or anodic consisting of 1 second pulse trains at the frequency of 100 Hz. Pulses consisted of square leading phase (100 μsec) followed by an exponentially decaying second phase to balance charge of length dependent upon the amplitude of the leading phase. Current-Induced Movements (CIMs) were determined as the weakest current passed through the cortical electrode that caused a forced movement in 50% of test pulses[53-56]. The anodic and cathodic CIMs then were compared. In cases in which anodic CIM was higher than cathodic CIM it was concluded that the corresponding electrode site was located in upper cortical layers (I-IV). On the other hand, when anodic CIM was lower than cathodic CIM, it was concluded that the electrode site was located in the lower cortical layers (V-VI). In cases in which anodic CIM was equal to cathodic CIM, it was concluded that no information on cortical location could be obtained.

4.3.5. Comparing two Methods

To compare these methods, the depth of layer V for each animal was estimated based on the data from all other animals. In this comparison we evaluated the reliability of each

94

method by assuming that we have just implanted that animal and estimated the depth of layer V based on each method proposed without a priori knowledge of that animal's histology. This was done by leave-one-out cross-validation (LOOCV). Cross-validation involves partitioning a sample of data into complementary subsets, performing the analysis on one subset (called the training set), and validating the analysis on the other subset (called the validation set or testing set). LOOCV uses a single animal from the original sample as the validation data, and the remaining animals as the training data[57]. This is repeated such that each observation in the sample is used once as the validation data.

4.3.6. Histology

Upon completion of the experiment, electrolytic lesions were made followed by histological analysis to determine the electrode site locations within the different cortical layers[13]. Three electrode sites that were approximately at the top, middle and bottom of each electrode array that had low impedances were chosen for lesioning. At these selected sites we passed 35 μA DC for 2 seconds using a potentiostat (AUTOLAB, EcoChemie, Netherlands) to create micro-lesions[13]. Animals were deeply anesthetized before lesioning. Lesion marks, on average were 40, 60 and 70 μm in diameter for electrode site diameters of 23, 30 and 40 μm. Serial 100 μm coronal slices were stained with a standard cresyl-violet (Nissl) staining method (figure 4.3(c)-(e)). The slices were then analyzed under a microscope and images were taken to reconstruct the position of the electrode array based on the shank track, centroid of the lesion marks, and the known geometry of the probe. In all cases, electrodes extracted from the brain were intact and

were kept attached to the skull/headcap. The angle, location and length of the intact electrodes were calculated through the images taken from these headcaps (figure 4.3a-b). To make a more precise estimation of the probe location and angle, exact stereotaxic positions of lesion marks and probe tracts were identified by co-registering the results of histological image analysis to the estimated probe locations from the images taken from the intact arrays[13]. After determining the location of the electrode array, we identified the location of the boundary between the upper and lower layers (the start of layer V) by analyzing the gray-level index values of the images using ImageJ (RSB, NIH: http://rsb.info.nih.gov/ij/).

4.4. Results

4.4.1. Polarity Reversal Method

The results of each analysis steps for one animal (M2) is shown in figure 4.4. Figure 4.4(a) shows the ketamine-xylazine-induced field potential oscillations recorded from motor cortex. Sites are arranged such that site 1 is located closest to the cortical surface. The peak amplitude shown on top sites (1,2,3) starts to decrease and it disappears completely at site 6. figure 4.4(b) shows the average of filtered LFPs with respect to the first site of the recording electrode (site 1). In figure 4.4(c) the phase of each of the recording sites for a sample recording ($\varphi 2(i)$) is shown. These data demonstrate a clear phase shift that occurs between sites 4 and 5 for this rat. figure 4.4(d) shows the phase differentiation from site to site (Differentiation of plot 4c). The highest amplitude corresponds to site 5 for this rat. This site is used to determine the depth of layer V in this method.
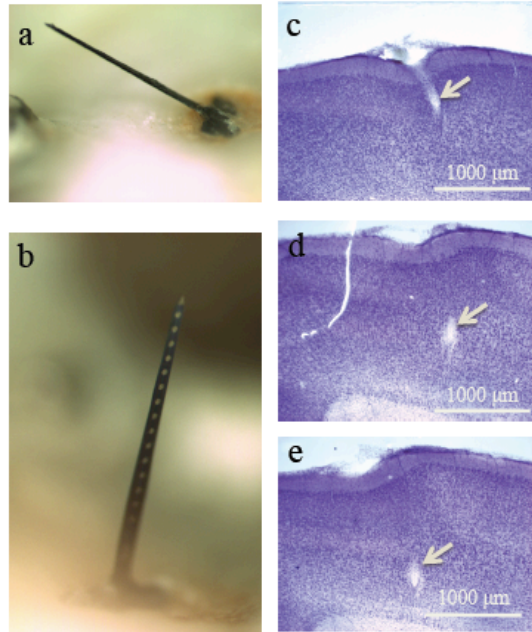
Figure 4.3. a,b) The angle and depth of the silicon probe was estimated using these images of intact skulls/headcaps. Individual electrodes can be seen along the silicon shank in (c). c-e) Histology images from one rat. Three lesion marks are shown in the different depths where the electrode was implanted. The lesion marks are used to reconstruct the trajectory of the silicon probe and depth of layer V relative to each site in the array.

The results of our analysis for the polarity reversal method for all animals are listed in Table 4.1. We found polarity reversal in LFPs recorded in 7 of 8 rats. For animal M4, we did not find a polarity reversal in the recorded LFPs as the most superficial electrode was located deeper than the start of layer V. The average depth of polarity reversal was calculated to be 928.4±110.4 µm. The offset is calculated based on the start of layer V from histological analysis (Table 4.1). Our results show that polarity reversal appears 150.1±104.2 µm below the start of layer V.

97
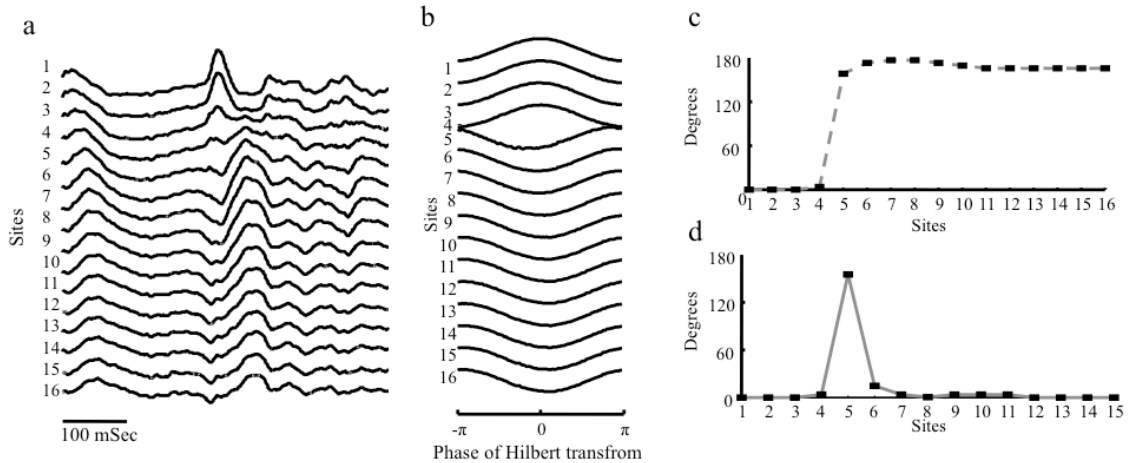
Fig 4.4. a) 16 channel ketamine-xylazine-induced field potential oscillations recorded from motor cortex of a single rat. The peak amplitude shown on top sites (1,2,3) starts to decrease and it disappears completely at site 6. Sites are arranged such that site 1 is located closest to the cortical surface. b) Average of filtered LFPs with respect to the first site of the recording electrode (site 1). c) Phase of each of the recording sites for a sample recording. These data demonstrate a clear phase shift that occurs between sites 4 and 5. d) Phase differentiation from site to site (Differentiation of plot c). The highest amplitude corresponds to site 5 for this rat (M2 in Table 4.1). This site is used to determine the depth of layer V in the polarity reversal method. This figure was originally printed in 18 (© 2007 IEEE).

The results of changing the reference site in a virtual depth experiment from site 1 (the most superficial) to site 16 (the deepest) are shown in figure 4.5. Changing the reference (most superficial) site from site 1 to the site demonstrating the polarity reversal showed the previously detected polarity reversal site as the site in which we see a phase difference higher than 120 degrees. We therefore determined this site to be the most accurate polarity reversal site. Changing the reference site from the polarity reverse site to site 16, being the most deep electrode in the array relative to the surface of the cortex, showed no polarity reversal. These results demonstrate the independence of our phase calculating method to the reference site.

98

Table 4.1. Results based on histology and the Polarity Reversal Method.   Averages indicate mean ± SD. Column C shows the offset of the estimation of depth of layer V for this method in comparison with histological analysis. The polarity reversal was exclusively observed below layer V. The estimate of the polarity reversal (E) was obtained with the LOOCV method for each validation animal, calculated from the training data. The error of the LOOCV method (F) is the difference between the estimate and the actual location of layer V based on histology. Data are in μm.

Animal ID	Polarity Reverse (Site)	(A) Depth of Polarity Reverse	(B) Depth of Layer V (Histology)	(C) Offset (A-B)	(D) Mean of offset For the training dataset	(E) Estimate of Layer V (A-D)	(F) Error (E-B)
M1	8	1101	819	282	128	973	153
M2	5	842	775	67	164	678	-97
M3	11	1052	758	294	126	926	167
M4	No PR	-	680	-	150	-	-
M5	9	903	762	141	151	752	-10
M6	9	910	802	108	157	753	-49
N4	9	791	776	15	172	619	-157
N8	12	901	757	144	151	750	-7
Average		928.6±110.4	766.1±41.1	150.1±104.2	150.1±16.1	778.4±127.4	SD:±121.5
							95% Confidence Interval: ±90
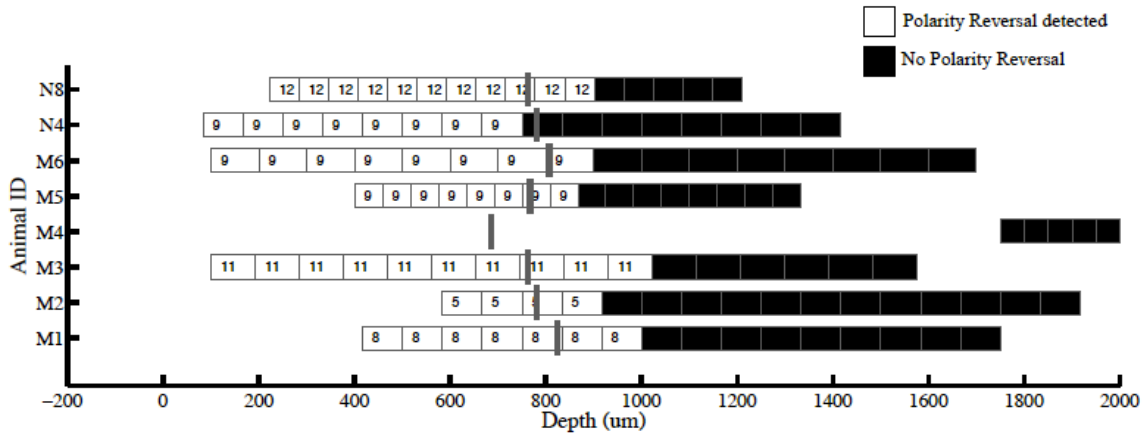
Figure 4.5. Virtual Depth experiment: for each electrode, the reference site was changed from 1-16 (site 1 being closest to the cortical surface) and the polarity reversal was calculated. Each square depicts one electrode site in the array. The widths of squares are consistent within each "array" and are based on the angle of the electrode relative to layered cortex. White squares show that the polarity reversal was detected with respect to sites located deeper. The number on that square indicates the site number of the polarity reversal. Black squares indicate that no polarity reversal was detected by choosing those sites as reference with respect to the sites located deeper. The gray bar indicates the depth of layer V as determined through histology. In animal M4, no polarity reversal was observed as every electrode in this array was located deeper than layer V.

4.4.2. Intracortical Stimulation Method

The results of the intracortical stimulation method are summarized in figure 4.6 and Table 4.2. Figure 4.6 shows the anodic and cathodic CIM threshold difference as a function of cortical depth. Table 4.2 lists the electrode site number and depth of the CIM threshold change for anodic and cathodic stimulation. The threshold change indicates the electrode in the array at which anodic intracortical stimulation had a higher threshold for eliciting a movement than cathodic stimulation. The average estimated depth of CIM threshold change based on this method was 812±81.8 μm, corresponding to the 687-916 μm start of layer V. The offset is calculated based on the difference of the depth of CIM threshold change and the histological indication of the depth of layer V. Our results show that CIM change appears with a 78.8±68 μm offset below the start of layer V.
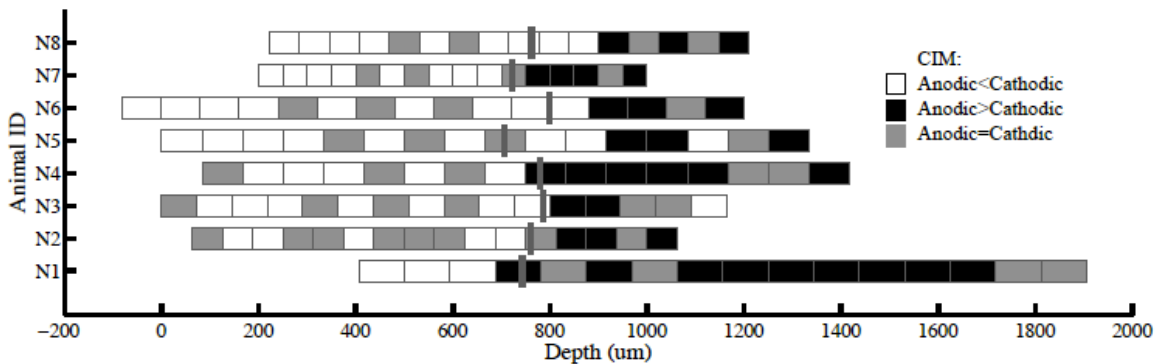
Figure 4.6. Anodic and Cathodic CIM threshold differences: Each square indicates the threshold for inducing a movement with anodic intracortical stimulation relative to cathodic stimulation. The widths of the squares are consistent within each "array" and are based on the angle of the electrode relative to layered cortex. As one moves from superficial electrodes (left) to deep electrodes (right), the threshold for inducing a movement with anodic stimulation becomes higher than the threshold for inducing movement with cathodic stimulation. The location of this change is used to estimate the location of layer V with the Intracortical Stimulation Method. The gray bar indicates the depth of layer V as determined through histology.

Table 4.2. Results based on histology and the Intracortical Stimulation Method.   Averages indicate mean ± SD. Column C shows the offset of the estimation of depth of layer V for this method in comparison with histological analysis. A negative offset indicates the movement threshold change occurred superficial to layer V. The estimate of the CIM change (E) was obtained with the LOOCV method for each validation animal, calculated from the training data. The error of the LOOCV method (F) is the difference between the estimate and the actual location of layer V based on histology. Data are in μm.

Animal ID	CIM Change (Site)	(A) Depth of CIM Change (μm)	(B) Depth of Layer V (Histology)	(C) offset (A-B)	(D) Mean of offset For the training dataset	(E) Estimate of Layer V (A-D)	(F) Error (E-B)
N1	4	687	738	-51	75	612	-126
N2	13	812	755	57	59	753	-3
N3	12	800	781	19	65	735	-47
N4	9	750	776	-26	71	679	-98
N5	12	916	702	214	37	879	176
N6	13	880	793	87	55	825	31
N7	12	750	718	32	63	687	-32
N8	12	901	757	144	47	854	96
Average		812±81.8	752.5±31.6	59.5±87.6	59.5±12.5	752.5±93.6	SD:±99.9
							95% Confidence Interval: ±69.3

4.4.3. Comparing two Methods

We evaluated the reliability of each method by leave-one-out cross-validation (LOOCV) described above. We used the data from a single animal as the validation data, and the remaining animals as the training data. This was repeated such that the data from each animal from the data set was used once as the validation data (each row in tables 4.1 & 4.2). We used the average of the offset (column C) from tables 4.1 and 4.2 from all of the animals excluding the validation animal as the training data. This average is shown in column (D) in these tables. This column is the average offset for each method in comparison to the start of layer V for each training set. To estimate the depth of layer V for each method we subtracted this offset from the depth of biological marker (column A) used for each method (column E). To calculate the error of each LOOCV we compared

101

these estimations with the histology results (column F). The estimation results, along with the 95% confidence intervals in the estimation, are shown in figure 4.6 and represent the estimate of layer V without a priori knowledge of the actual depth of layer V. These results indicated that we can estimate the depth of the start of layer V within ±90 µm for the polarity reversal method and ±69 µm for the intracortical stimulation method with 95% confidence relative to the physical location of the start of layer V.

In two animals (N4, N8), both methods were used for estimating the depth of the start of Layer V. The depth of polarity reversal estimated for N4 was 619 µm which was 157 µm above the beginning of layer V (757 µm), while the depth of CIM threshold change for this rat was estimated to be 679 µm, 98 µm above the start of layer V. Alternatively, the depth of polarity reversal estimated for N8 was 750 µm which was located 7 µm above the start of layer V (757 µm), while the depth of MT change for this rat was estimated to be 854 µm, 96 µm below the start of layer V. Both of these methods, when used together in these animals, predicted the depth of the beginning of layer V within the 95% confidence intervals of both methods.

4.5. Discussion

4.5.1. Electrophysiological-based laminar Analysis

The polarity reversal of cortical field potentials appears 100-300 µm below layer IV of motor cortex[28]. The motor cortex in the rat has a small but distinct layer IV (~100 µm thick) which receives thalamic inputs and begins around 650 µm and ends around 750 µm below the surface of the brain[58]. Therefore we expect to find the polarity reversal at a depth of 850-1050 µm. Our results showed that the average depth was calculated to be

928.4±110.4 μm which lies in the reported range of polarity reversal in cortical column for HVS[28]. Also, as reported in Table 4.1, this method can estimate the depth of the start of layer V within ±90 μm with 95% confidence. As electrode recording sites in the probes used in this project were spaced at 100 μm, this gives us a laminar resolution of 100 μm along the 1500 μm shank and allows us to tolerate up to 50 μm error in polarity reversal and structural depth estimation with respect to the expected range for each method. Recording electrodes with lower site spacing may give us more laminar resolution, reduce the error and provide a more accurate estimation.
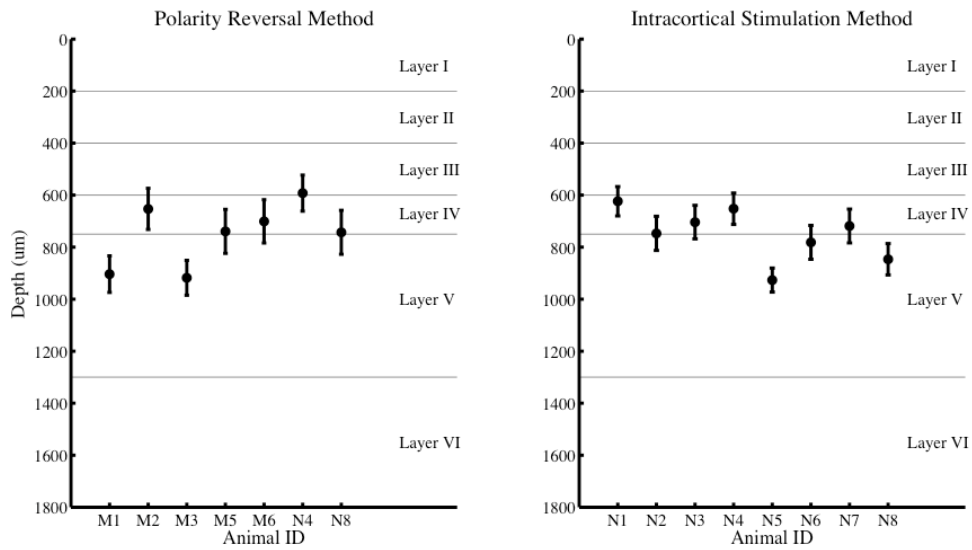
Figure 4.7. In Situ estimation of layer V based on the Polarity Reversal Method (left) and Intracortical Stimulation Method (right). Data are plotted on a schematic of layered rat motor cortex with relative distances between layers (Skoglund et al. 1997). The markers are the estimation of layer V as reported in columns F of Tables 4.1 and 4.2 without a priori knowledge of the depth of layer V. The bars show the 95% confidence interval based on the dataset excluding the representative animal from the dataset using the LOOCV method.

No polarity reversal was found for animal M4 by calculating the phase difference of its electrode recording sites. Considering the electrode configuration we concluded that the electrode was placed so deep in motor cortex that the first site was passed the polarity reverse point (beginning of layer V). Histological analysis showed that the depth of first site for this rat was 1,826 µm below the cortical surface, which confirms our prediction.

As described in the text, the independence of our method to the referenced site was evaluated. The results showed that the phase difference of the HT of each electrode site and the referenced site is high (>120 degrees) when the referenced site is located superficial to the polarity reversal and low (<60 degrees) for when the referenced site is located deeper than the polarity reversal. This demonstrates the robustness of the polarity reversal method due to the independence of the referenced site.

4.5.2. Intracortical stimulation

In the intracortical stimulation method, the depth of the electrodes in the array is estimated by comparing the minimum current that induces a movement for cathodic vs. anodic pulse polarity. This method is based on previous studies that show that neural elements perpendicular to the electrode surface are preferentially excited by anodic stimulation while cathodic stimulation excites those with a direction component parallel to its surface[33-35]. Upper cortical layers contain the neuronal structures that are primarily parallel to the cortical surface while lower layers of rat motor cortex contain large pyramidal neurons which are primarily perpendicular to the surface of the brain[45]. We

used this stimulation method to detect the structural change that appears at the beginning of layer V.

Previous investigations on the effects of extracellular anodic and cathodic stimulation on cortical neurons have inferred that the differences obtained are due to the opposing membrane potential changes induced between oppositely directed poles (dendrite and axon) of the neurons[36-40]. Upper cortical layers contain the neuronal structures that are primarily parallel to the cortical surface and therefore perpendicular to the stimulating electrode surface[45]. When stimulating through the perpendicularly implanted microelectrode array in these layers, anodic current is thought to hyperpolarize the dendrites while depolarizing cell body and axonal portions of neurons located in these layers. An opposite sequence of depolarizing-hyperpolarizing events is thought to occur during cathodic current flow[59]. Therefore it is expected to see lower anodic currents to induce movements in these layers in comparison with cathodic currents.

Previous modeling studies have suggested that cathodic stimulation excites the neural elements with a direction component parallel to the surface of stimulation[34-35]. The layer V of rat motor cortex contains large pyramidal neurons which are primarily perpendicular to the surface of the brain[44,45] and therefore parallel to the stimulating electrode sites of the implanted microelectrode array. We expected to see lower cathodic currents to induce movements in layer V in comparison with anodic currents. In addition it has been reported that the site of excitation is dependent on the polarity of the stimulus, with cathodic stimuli resulting in lower thresholds for electrode positions closer to the axon and anodic stimuli resulting in lower thresholds for electrode positions closer to the cell body and dendrites[41-43]. Pyramidal cell neurons located within the layer V in the primary

105

motor cortex send their axons down to the spinal cord. They have apical, perisomatic and basal dendrites that project into all cortical layers[44-60]. Therefore, their dendrites are located in upper layers (I-IV) while their axons are located in lower layers (V-VI) of motor cortex. This will also contribute to our hypothesis of having lower CIM for cathodic stimulation in these layers in comparison with anodic stimulation. Our results from the intracortical stimulation method agree with these previous findings and support our hypothesis.

Since, on average, layer V of cortex starts 750-800 μm below the surface of the cortex[58], we therefore expect to see a change in the difference of anodic and cathodic CIMs in this range due to the large neural elements of pyramidal cells traveling the depth of a cortical column. The depth of CIM change in our results was in the range of 812±81.8 μm below the surface of the brain, which is below the expected range. As reported in Table 4.2, this method can estimate the depth of the start of layer V to within ±69.3 μm with 95% confidence. In this method, recording electrodes with lower site spacing may give us more laminar resolution, reduce the error and provide a more accurate estimation.

The high error in some cases in our results can be explained in part by the angle of the electrode in the brain relative to the organization of layered cortex. We attempted to implant the electrodes as perpendicular to the surface of the brain as possible, however, in some cases they were implanted at an angle. Because this method is sensitive to the orientation of the electrode site surface with respect to the orientation of fibers, this angle can cause additional errors in the depth estimation. As it has been suggested by Wongsarnpigoon and Grill[35], to predict the response of the neural elements located in different angles with respect to the stimulation surface, further modeling studies need to

106

be conducted. However, because our results are also described by the site of excitation in addition to the direction of the neuronal fibers, this error will be limited when the stimulation electrode site is proximate to the axonal parts of the layer V neurons[41-43].

4.5.3. Comparing the two methods

The polarity reversal method gives a 90 μm confidence interval for the estimation of the start of layer V while the intracortical stimulation method gives a 69 μm confidence interval, suggesting that the intracortical stimulation method can provide a more accurate estimate.

In two animals (N4 and N8), we were able to apply both methods for localizing layer V. The polarity reversal method gave a more accurate estimation for N8 while the intracortical stimulation method gave a more accurate estimation for N4. This could be explained in part by the large angle of the electrode array N8 in comparison to N4 relative to the cortical layers. As the hypothesis behind the intracortical stimulation method is based on the direction of the cortical fibers, this method is more sensitive to the angle of the electrode compared to the polarity reversal method. We can conclude that in the cases in which we have *a priori* knowledge of the electrode array implanted at an angle, the polarity reversal method will give a more accurate estimation of the depth of the start of layer V.

Although we consider the neocortex in many species and cortical areas to be built according to a stereotypic cortical architecture[61], it has to be taken into consideration that there are certain variations between different cortical areas in both architecture and

107

particularly in the layout of horizontal connections[62]. Furthermore, across the cortical surface, within and/or between neighboring areas, distinct discontinuities of horizontal connections exist[63]. Such variability might affect the biological markers in our proposed methods and deserves attention in each case in which these methods are used. Nevertheless, in view of a common architecture of neocortex, the present results obtained in rat motor cortex provide reliable methods for estimating the depth of the implanted linear electrode array for other cortical areas and/or species.

4.5.4. *Accuracy of the histological localization and layer estimation*

The depth of the beginning of layer V was calculated with the program ImageJ which has a high accuracy for identifying the change in light density of nissl-stained images associated with the start of dense pyramidal cell bodies in layer V[13]. Given the micro-scale of these electrode arrays it is necessary to make three lesion marks along the shank to get accurate electrode placement by aligning a three-dimensional vector between "points" indicating the lesion. Therefore, it is likely that the majority of the errors recorded in these measurements are attributed to the limitations of each of the individual methods rather than localizing the electrodes relative to layer V. While the centroid of each electrode was space 100 μm apart, the addition of the diameter of each electrode meant that the true distance between electrodes was 77, 70 and 60 μm for electrode site diameters of 23, 30 and 40 μm, respectively. Ideally, each electrode would be an infinitely small "point-source" relative to the size of the neural elements being measured or activated in order to make a precise measurement. However, each of the methods

described here involve the activity of more than just one neuron or neural element. In the phase reversal method, we are recording changes in the local electrical fields. These fields are highly susceptible to the orientation and type of neural element coursing through each of the neural layers that are a likely source of error in this method. In the CIM method, charge is activating a number of output neurons innervating muscle to affect an easily observable muscle "twitch". The size and shape of the electric fields generated at the stimulated electrode are likely complex and have a degree of overlap between neighboring electrodes. It remains to be seen if reducing the diameter and spacing of the electrodes will improve the accuracy of these techniques or if the error inherent to each technique is too great for further improvement. Ultimately, these techniques achieves the goal of identifying the electrode in an array closest to the output layer of motor cortex and thus most effective for neuroprosthetics and neurorehabilitation research.

4.6. Conclusion

In this study we propose and compare two in vivo methods for estimation of electrode depth in rat primary motor cortex in situ. The results of both methods demonstrate their utility to define the placement of the electrode sites in the upper and lower cortical layers. The proposed methods are reliable candidates for targeting deep and superficial layers within three electrodes in an array of electrodes spaced 100 μm spanning layered motor cortex. This has important implications for neuroprosthetic and neurorehabilitation research that has typically targeted neurons in the lower layers of the motor cortex[9-11, 13, 14].

4.7. References

1. Cogan SF. Neural Stimulation and Recording Electrodes. Annual review of biomedical engineering. 2008;10:275.

2. Mercanzini A, Cheung K, Buhl DL, Boers M, Maillard A, Colin P, et al. Demonstration of cortical recording using novel flexible polymer neural probes. Sensors and actuators A, Physical. 2008;143(1):90.

3. Kipke DR, Vetter RJ, Williams JC, Hetke JF. Silicon-Substrate Intracortical Microelectrode Arrays for Long-Term Recording of Neuronal Spike Activity in Cerebral Cortex. IEEE transactions on neural systems and rehabilitation engineering : a publication of the IEEE Engineering in Medicine and Biology Society. 2003;11(2):151.

4. Vetter RJ, Williams JC, Hetke JF, Nunamaker EA, Kipke DR. Chronic neural recording using silicon-substrate microelectrode arrays implanted in cerebral cortex. IEEE Transactions on Biomedical Engineering. 2004;51(6):896-904.

5. DeFelipe J, Alonso-Nanclares L, Arellano JI. Microstructure of the neocortex: Comparative aspects. Journal of Neurocytology. 2002;31(3-5):299-5.

6. Levine SP, Huggins JE, BeMent SL, Kushwaha RK, Schuh LA, Rohde MM, et al. A direct brain interface based on event-related potentials. IEEE Transactions on Rehabilitation Engineering. 2000;8(2):180-5.

7. Wessberg J, Stambaugh CR, Kralik JD, Beck PD, Laubach M, Chapin JK, et al. Real-time prediction of hand trajectory by ensembles of cortical neurons in primates. Nature. 2000;408(6810):361.

8. Carmena JM, Lebedev MA, Crist RE, O'Doherty JE, Santucci DM, Dimitrov DF, et al. Learning to control a brain-machine interface for reaching and grasping by primates. PLOS Biology. 2003;1(2):193-208.

9. Serruya MD, Hatsopoulos NG, Paninski L, Fellows MR, Donoghue JP. brief communications - Brain-machine interface: Instant neural control of a movement signal. Nature. 2002;416(6877):141.

10. Taylor DM, Helms Tillery SI, Schwartz AB. Information Conveyed Through Brain-Control: Cursor Versus Robot. IEEE transactions on neural systems and rehabilitation engineering : a publication of the IEEE Engineering in Medicine and Biology Society. 2003;11(2):195.

11. Donoghue JP. Connecting cortex to machines: recent advances in brain interfaces. NATURE NEUROSCIENCE. 2002;5:1085-8.

12. Humphrey DR, Schmidt EM, Thompson WD. Predicting measures of motor performance from multiple cortical spike trains. Science. 1970;170(NN395):758-&.

13. Parikh H, Marzullo TC, Kipke D, R. Lower layers in the motor cortex are more effective targets for penetrating microelectrodes in cortical prostheses: Institute of Physics Publishing; 2009.

14. Du J, Riedel-Kruse IH, Nawroth JC, Roukes ML, Laurent G, Masmanidis SC. High-Resolution Three-Dimensional Extracellular Recording of Neuronal Activity With Microfabricated Electrode Arrays. Journal of neurophysiology. 2009;101(3):1671.

15. Taub E, Uswatte G, Elbert T. New treatments in neurorehabiliation founded on basic research. 2002:Nature.

16. Friel K, Barbay S, Frost S, Plautz E, Stowe A, Dancause N, et al. Effects of a Rostral Motor Cortex Lesion on Primary Motor Cortex Hand Representation Topography in Primates. Neurorehabilitation and Neural Repair. 2007;21(1):51-61.

17. Gradinaru V, Mogri M, Thompson KR, Henderson JM, Deisseroth K. Optical Deconstruction of Parkinsonian Neural Circuitry. SCIENCE. 2009;324(5925):354-9.

18. Yazdan-Shahmorad A, Gage GJ, Marzullo TC, Kim E, Kipke DR. Linear electrode depth estimation in rat motor cortex by laminar analysis of Ketamine-Xylazine-Induced oscillations. 2007 3rd International IEEE/EMBS Conference on Neural Engineering, Vols 1 and 2. 2007:646-9.

19. Schwartz AB, Cui XT, Weber DJ, Moran DW. Brain-controlled interfaces: Movement restoration with neural prosthetics. NEURON. 2006;52(1):205-20.

20. Anderson W, Kudela P, Cho J, Bergey G, Franaszczuk P. Studies of stimulus parameters for seizure disruption using neural network simulations. Biological Cybernetics. 2007;97(2):173-94.

21. Marzullo TC, Miller CR, Kipke DR. Neural Engineering - Suitability of the Cingulate Cortex for Neural Control. IEEE transactions on neural systems and rehabilitation engineering : a publication of the IEEE Engineering in Medicine and Biology Society. 2006;14(4):401.

22. Gage GJ, Ludwig K, A., Otto KJ, Ionides EL, Kipke D, R. Naive coadaptive cortical control: Institute of Physics Publishing; 2005.

23. Musallam S, Corneil BD, Greger B, Scherberger H, Andersen RA. Cognitive control signals for neural prosthetics. Science. 2004;305(5681):258-62.

24. Brozoski TJ, Caspary DM, Bauer CA. Marking multi-channel silicon-substrate electrode recording sites using radiofrequency lesions. Journal of neuroscience methods. 2006;150(2):185.

25. Townsend G, Peloquin P, Kloosterman F, Hetke JF, Leung LS. Recording and marking with silicon multichannel electrodes. Brain research protocols. 2002;9(2):122-9.

26. Larson PS, Richardson RM, Starr PA, Martin AJ. Magnetic Resonance Imaging of Implanted Deep Brain Stimulators: Experience in a Large Series. Stereotactic and Functional Neurosurgery. 2008;86(2):92-100.

27. Ferroli P, Franzini A, Marras C, Maccagnano E, rsquo, Incerti L, et al. A Simple Method to Assess Accuracy of Deep Brain Stimulation Electrode Placement: Pre-Operative Stereotactic CT + Postoperative MR Image Fusion. Stereotactic and Functional Neurosurgery. 2004;82(1):14-9.

28. Kandel A, Buzsaki G. Cellular-synaptic generation of sleep spindles, spike-and-wave discharges, and evoked thalamocortical responses in the neocortex of the rat. Journal of Neuroscience. 1997;17(17):6783-97.

29. Jando G, Carpi D, Kandel A, Urioste R. Spike-and-wave epilepsy in rats: sex differences and inheritance of physiological traits. Neuroscience. 1995;64(2):301.

30. Bodegreuel KM, Singer W, Aldenhoff JB. A current source density analysis of field potentails-evoked in slices of visual-cortex. Experimental Brain research. 1987;69(1):213-9.

32. Ranck JB, Jr. Which elements are excited in electrical stimulation of mammalian central nervous system: A review: Elsevier; 2006.

31. Jensen KF, Killackey HP. Terminal arbors of axons projecting to the somatosensory cortex of the adult-rat. Journal of Neuroscience. 1987;7(11):3529-43.

33. Nitsche MA, Paulus W. Excitability changes induced in the human motor cortex by weak transcranial direct current stimulation. The Journal of physiology. 2000;527:633-40.

34. Manola L, Holsheimer J, Veltink P, Buitenweg JR. Anodal vs cathodal stimulation of motor cortex: A modeling study. Clinical neurophysiology : official journal of the International Federation of Clinical Neurophysiology. 2007;118(2):464.

35. Wongsarnpigoon A, Grill WM. Computational modeling of epidural cortical stimulation. Journal of Neural Engineering. 2008;5(4):443-54.

36. Bishop GH, Oleary JL. The effects of polarizing currents on cell potentials and ther significance in the interpretation of central nervous system activity. Electroencephalography and clinical neurophysiology. 1950;2(4):401-16.

37. Creutzfeldt O, Fromm GH, Kapp H. Influence of transcortical D-C current on cortical neuronal activity. Experimental Neurology. 1962; 5 :436-452.

38. Hern JE, Landgren S, Phillips CG, Proter R. Selective excitation of corticofugal neurones by surface-anodal stimulation of the baboon's motor cortex. The Journal of physiology. 1962;161:73-90.

39. Landau WM, Bishop GH, Clare MH. Analysis of form + distribution of evoked cortical potentials under influence of polarizing currents. Journal of Neurophysiology. 1964;27(5):788.

40. Libet B, Gerard RW. Steady potential fields and neurone activity. Journal of Neurophysiology. 1941;4(6):438-55.

41. Yeomans JS, Maidment NT, Bunney BS. Excitability properties of medial forebrain-bundle axons of A9 and A10 dopamine cells. Brain Research. 1988;450(1-2):86-93.

42. Matthews G. Neural substrate for brain-stimulation reward in rat- cathodal and anodal strength-duration properties. Journal of comparative and physiological psychology. 1977;91(4):858-74.

43. McIntyre CC, Grill WM. Electrophysiology - Excitation of Central Nervous System Neurons by Nonuniform Electric Fields. Biophysical journal. 1999;76(2):878.

44. Elston GN. Cortex, Cognition and the Cell: New Insights into the Pyramidal Neuron and Prefrontal Function. Cerebral Cortex. 2003;13(11):1124-38.

45. Brodmann, K. Brodmann's Localisation in the cerebral cortex / translated with editorial notes and an introduction by Laurence J. Garey. 1999; London: Imperial College

46. Le Van Quyen M, Foucher J, Lachaux J-P, Rodriguez E, Lutz A, Martinerie J, et al. Comparison of Hilbert transform and wavelet methods for the analysis of neuronal synchrony. Journal of neuroscience methods. 2001;111(2):83.

47. Shaw JC. The Electroencephalogram: Its Patterns and Origin. By John S. Barlow. Journal of psychophysiology. 1996;10(2):174.

48. Gabor D. Theory of communication. Electrical Engineers. 1946; 93: 429–57

49. Rosenblum M, Pikovsky A, Schafer C, Tass PA, Kurths J. Phase Synchronization: From Theory to Data Analysis. 1999://www.agnl.

50. Freeman WJ. Origin, structure, and role of background EEG activity. Part 2. Analytic phase. Clinical neurophysiology : official journal of the International Federation of Clinical Neurophysiology. 2004;115(9):2089.

51. Freeman WJ. Origin, structure, and role of background EEG activity. Part 3. Neural frame classification. Clinical neurophysiology : official journal of the International Federation of Clinical Neurophysiology. 2005;116(5):1118.

52. Freeman WJ. Origin, structure, and role of background EEG activity. Part 4: Neural frame simulation. Clinical Neurophysiology. 2006;117(3):572-89.

53. Teskey GC, Flynn C, Goertzen CD, Monfils MH, Young NA. Cortical stimulation improves skilled forelimb use following a focal ischemic infarct in the rat. Neurological research. 2003;25(8):794.

54. Adkins-Muir DL and Jones TA. Cortical electrical stimulation combined with rehabilitative training: Enhanced functional recovery and dendritic plasticity following focal cortical ischemia in rats. Neurological research. 2003; 25: 780.

55. Brown JA, Lutsep HL, Weinand M, Cramer SC. Motor Cortex Stimulation for the Enhancement of Recovery from Stroke: A Prospective, Multicenter Safety Study. Neurosurgery. 2006;58(3):464.

56. Plautz EJ. Post-infarct cortical plasticity and behavioral recovery using concurrent cortical stimulation and rehabilitative training: A feasibility study in primates. Neurological research. 2003;25(8):801.

57. Picard R and Cook D. Cross-Validation of Regression Models. Journal of the American Statistical Association. 1984; 79: 575–583

58. Skoglund T, Pascher R, Berthold C. The existence of a layer IV in the rat motor cortex. Cerebral Cortex. 1997;7(2):178-80.

59. Gorman ALF. Differential patterns of activation of pyramidal system elicited by surface anodal and cathodal cortical stimulation. Journal of Neurophysiology. 1966;29(4):547-&.

60. Franceschetti, S.Sancini G, Panzica F, Radici C. Postnatal differentiation of firing properties and morphological characteristics in layer V pyramidal neurons of the sensorimotor cortex. Neuroscience. 1998;83(4):1013.

61. Braitenberg V, Schuz A. Anatomy of the cortex : statistics and geometry. 1991 New York : Springer-Verlag.

62. Lund JS, Yoshioka T, Levitt JB. Comparison of intrinsic connectivity in different areas of Macaque monkey cerebral-cortex. Cerebral Cortex. 1993;3(2):148-62.

63. Manger PR, Woods TM, Munoz A, Jones EG. Hand/face border as a limiting boundary in the body representation in monkey somatosensory cortex. Journal of Neuroscience. 1997;17(16):6338-51.

Chapter 5

Conclusion and future directions

5.1. Conclusions

The work presented in this dissertation was focused on investigating the effects of electrical stimulation on the affected neural population located in the layered structure of rat primary motor cortex. The purpose of these studies was to help identify the effects of electrical stimulation on cortical neural tissue, elucidate mechanisms of action and ultimately to optimize the parameters used for neurorehabilitation and neuroprosthetic applications. We were able to use linear electrode arrays in these studies that enabled us to record and target different depths and layers of the primary motor cortex and investigate the effects of stimulation on these locations. In the studies presented in this dissertation we used both surface stimulation and intracortical microstimulation methods. We also were able to investigate the effects of stimulation of several brain signals such as spiking activity, local field potentials and electrocorticograms. The general findings of the three studies presented here was that the polarity of cortical electrical stimulation differentially affects the neural signals of the superficial and deep cortical layers.

In Chapter 2, the goal was to design a set of experiments and test the influence of CES pulse polarity of various frequencies and amplitudes on the imposed volume of rat primary motor cortex. The results suggested that neurons in lower layers have a higher probability of being excited following anodic stimulation. Similarly neurons located in

upper cortical layers have a higher probability of being excited following cathodic stimulation. The opposing effects observed after anodic vs. cathodic stimulation in upper and lower layers were frequency- and amplitude-dependent. In addition, our results demonstrate that the changes in neural activity following manipulation of CES parameters is time-dependent according to the location (depth) of the recorded units.

In chapter 3, we investigated the effects of CES on LFPs and ECoGs recorded from the rat primary motor cortex and compared the results with the CES effects on the simultaneous recorded unit activity (reported in chapter 1). Our results showed a significant different post-stimulus effect on the gamma (30-120 Hz) power of LFPs and the high gamma (60-120 Hz) power of ECoGs following Anodic versus Cathodic stimulation. Time-frequency analysis of LFPs showed high correlation of gamma power with unit activity in corresponding layers. On the other hand, high gamma power of ECoG signals only showed high correlation with the unit activity in lower layers. Time-frequency correlations, which were found between LFPs, ECoGs and unit activity were also frequency- and amplitude- dependent. The signature of the neural activity observed in LFP and ECoG signals provides a better understanding of the effects of stimulation on the affected network and has a promising potential to be used in closed-loop control stimulation systems. These results demonstrate that the neurorehabilitation and neuroprosthetic applications of CES can be further improved by optimizing CES parameters. It is clear that more quantitative data about intracortical distribution of projections and their target, as well as variation of electrical properties of cortical circuits are needed before the specific effects observed in chapters 1 and 2 can be fully understood, especially in the context of maximizing efficacy of CES for

neurorehabilitation and neuroprosthetic applications.

In chapter 4, we proposed an intracortical microstimulation method for estimation of electrode depth in rat primary motor cortex in situ and compared it with another method based on the laminar analysis of the local field potentials. The results of both methods demonstrate their utility to define the placement of the electrode sites in the upper and lower cortical layers. The proposed methods are reliable candidates for targeting deep and superficial layers within three electrodes in an array of electrodes spaced 100 μm spanning layered motor cortex. This has important implications for neuroprosthetic and neurorehabilitation research that has typically targeted neurons in the lower layers of the motor cortex.

5.2. Future Directions

In the three studies presented in this dissertation we showed that polarity of cortical electrical stimulation differentially affects the neural signals of the superficial and deep cortical layers. In the other words, we have shown that by changing the stimulation parameters we can target a specific group of neurons in the cortex. This means that we can optimize the targeting of the electrical stimulation by choosing the right parameters from the available parameter space. Also in the first two studies that we have used surface stimulation, we have shown that by choosing the appropriate set of parameters we can control the effect of stimulation on the neurons located in the upper and lower cortical layers. Therefore we have shown that by using a specific set of parameters we can have the spatial resolution and focality of intracortical microstimulation without producing any damage to the cortical integrity. These results can be used in the

neurorehabilitation and neuroprosthetic applications that are design to target the neurons in the lower layers of the motor cortex. One of the future directions of this dissertation would be to test the results presented here in the diseased animal models and monitor the therapeutic effects as the result of stimulation. As it has been proposed and shown in 1 deep layer V neurons are the sufficient targets for Parkinson's disease, surface stimulation could be a better alternative for Parkinson's disease treatment in comparison to deep brain stimulation methods. This could be investigated using the result of the studies presented here to target the layer V neurons in the Parkinson's animal models.

Another factor that needs to be considered in choosing the stimulation paradigms for the neurorehabilitation applications is the duration of stimulation. As mentioned in the previous chapters of this dissertation, the duration of stimulation plays an important role in the therapeutic effects observed as the result of stimulation. Under normal conditions in which no pathologic state is present, chronically stimulated neurons could easily get fatigued under such long term activation, resulting in alteration of normal brain function[2-4]. Alternatively, constant stimulation could lead to an alteration in synaptic efficacy in the affected region, changing network characteristics in possibly a deleterious way[2-5]. Therefore it is very important to investigate the effect of duration of stimulation on the affected brain region as well and monitor the neural behavior in time.

Also since the distribution of electrical stimulation cannot be precisely controlled, the stimulation may spread into unexpected brain areas and include mechanisms and neural populations into the therapeutic mechanisms that we don't anticipate. In addition electrical stimulation does not provide cell type–specific, manipulations. Electrical stimulation also does not allow highly controlled inhibition and causes electrical

interference that hampers the simultaneous electrical recording of neural signals from the same site. To get a better insight about the effects of stimulation on the therapeutic aspects of electrical stimulation it would be helpful to use a more precise method of stimulating neurons and compare it with the effects of electrical stimulation. Optogenetics addresses these challenges by introducing into neurons light-sensitive proteins that regulate the ion conductance of the membrane[6]. These proteins, encoded by microbial opsin genes, are derived from sources such as archaebacteria and algae. They allow optical excitation[7,8] or inhibition[9,10] of specific neuron types based on their expression or projection patterns. Moreover, optogenetics allows simultaneous artifact-free electrical recording of action potentials[11-13]. Therefore it would be very interesting to investigate the effects of electrical stimulation by using the cell-specific manipulations of optogenetics techniques.

5.3. References

1**.** Gradinaru V. Optical Deconstruction of Parkinsonian Neural Circuitry. SCIENCE. 2009;324(5925):354-9.

2. Li Y. Electrical Control of Epileptic Seizures. Journal of clinical neurophysiology : official publication of the American Electroencephalographic Society. 2007;24(2):197.

3. Fregni F. Rapid-rate repetitive transcranial magnetic stimulation and cognitive function in Parkinson's disease patients: A safety study. Movement disorders. 2004;19:S240-S1.

4. Michelucci R. Rapid-rate transcranial magnetic stimulation and hemispheric language dominance: Usefulness and safety in epilepsy. Neurology. 1994;44(9):1697.

5. Jahanshahi M. Rapid rate transcranial magnetic stimulation - a safety study. Electroencephalography and clinical neurophysiology. 1997;105(6):422.

6. Diester I, Kaufman MT, Mogri M, Pashaie R, Goo W, Yizhar O, et al. An optogenetic toolbox designed for primates. Natute Neuroscience.14(3):387-97.

7. Boyden ES, Zhang F, Bamberg E, Nagel G, Deisseroth K. Millisecond-timescale, genetically targeted optical control of neural activity. Natute Neuroscience. 2005;8(9):1263-8.

8. Zhang F. Channelrhodopsin-2 and optical control of excitable cells. NATURE METHODS. 2006;3(10):785-92.

9. Zhang F. Multimodal fast optical interrogation of neural circuitry. Nature. 2007;446(7136):633.

10. Gradinaru V. eNpHR: a Natronomonas halorhodopsin enhanced for optogenetic applications. Brain Cell Biology. 2008;36(1-4):129-4.

11. Gradinaru V, Thompson KR, Zhang F, Mogri M, Kay K, Schneider MB, et al. Targeting and Readout Strategies for Fast Optical Neural Control In Vitro and In Vivo. The journal of neuroscience : the official journal of the Society for Neuroscience. 2007;27(52):14231.

12. Zhang F, Gradinaru V, Adamantidis AR, Durand R, Airan RD, de Lecea L, et al. Optogenetic interrogation of neural circuits: technology for probing mammalian brain structures. Nature Protocols.2010; 5(3):439-56.

13. Zhang JY, Laiwalla F, Kim JA, Urabe H, Van Wagenen R, Song YK, et al. Integrated device for optical stimulation and spatiotemporal electrical recording of neural activity in light-sensitized brain tissue. Journal of Neural Engineering. 2009;6(5).

Appendix A

Model Fitting and Data Analysis

Before settling on the model defined by equation (3), we varied the possible model classes and looked for an optimal trade-off between the number of parameters in the model and the maximum likelihood cost of the fitted model. We computed the Aikaike's criterion (AIC), which is 2*(the number of parameters-log likelihood of the model), for each possible model class (Table 1). This criterion provides a way to rank different candidate models. It is an estimate between a distribution given by an approximating model and the distribution of the true underlying process generating the data[17].

The model can be fit to the neural spike trains using general linear model (GLM) methods[17]. The GLM is an extension of the multiple linear regression model in which the variable being predicted, in this case spike times, need not be Gaussian[17]. GLM provides an efficient computational scheme for model parameter estimation and a likelihood framework for conducting statistical inferences based on the estimated model[20-21].

We used Kolmogorov-Smirov (KS) plots based on the time-rescaling theorem to assess model goodness-of-fit. The time-rescaling theorem is a well known result in probability theory which states that any point process with an integrable CIF may be transformed into a Poisson process with unit rate[21]. A KS plot, which plots the empirical cumulative distribution function (CDF) of the transformed spike times versus the CDF of a unit rate

exponential, is used to visualize the goodness-of-fit for each model. We computed 95%

confidence bounds for the degree of agreement using the distribution of the KS statistic[17].

Time was discretized by partitioning the time interval (0,T] into 1 msec bins and the

discretized CIF was estimated. Finally, maximum-likelihood estimates and confidence

intervals of θ were computed for each neuron using the glmfit.m function in MATLAB.
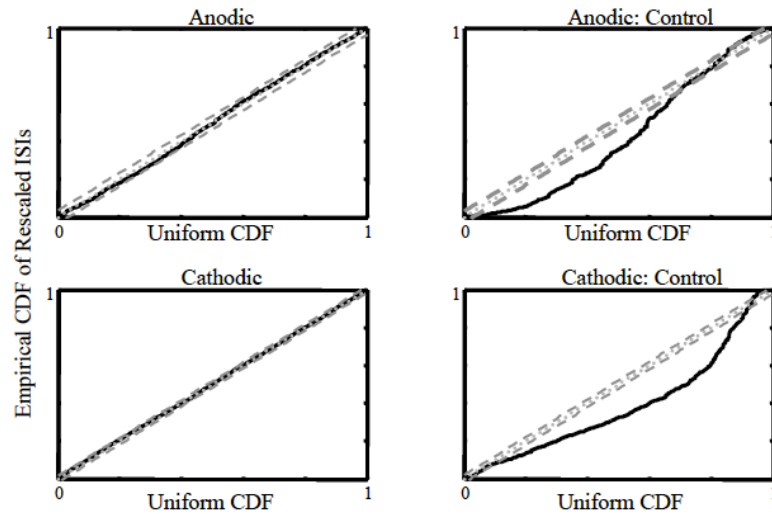

Fig 1. KS-plots (solid lines) with 95% confidence intervals (dotted lines) for stimulation and control (no-stimulation) sessions for anodic and cathodic first stimulation.

Table 1. Aikaike's criterion (AIC), is 2× (the number of parameters-log likelihood of the model). DEV is -2×log likelihood of the model and the number of parameters for four models of a single neuron following anodic and cathodic stimulation.

Model classes	# of parameters	Anodic		Cathodic	
		DEV (-2loglik)	AIC	DEV (-2loglik)	AIC
Proposed Model	45	52657	52747	63285	63375
Amplitude Only	20	52745	52785	63380	63410
Frequency Only	25	52783	52833	63320	63380
Separate each parameter set	100	52601	52801	63260	63460

Short-term temporal effects of CES (Cathodic stimulation)

To investigate the post-stimulus effects of CES for cathodic stimulation after 2 seconds following the offset of stimulation, we have done further analysis. We have formulated another CIF and have included the 2000-2500ms interval after the offset of stimulation as another time interval to equation (2.3) for the Cathodic stimulation. The new equation is:

$$(1) \qquad \lambda(t \mid H_t) = \exp\{\sum_{i=1}^{6}\sum_{a=1}^{4}\alpha_{i,a}I_{i,a}(t) + \sum_{i=1}^{6}\sum_{f=1}^{5}\beta_{i,f}I_{i,f}(t)\}$$

where time was divided into six intervals of 500 ms with variable i, where i=1 corresponds to the 500ms before the onset of stimulation and i={2,3,4,5,6} correspond to (0-500), (500-1000), (1000-1500), (1500-2000) and (2000-2500) ms time intervals after the offset of the stimulation. Here we also scaled the ($\{\alpha_{i,a}\}$ and $\{\beta_{i,f}\}$) to have values between -1 and 1 using the equations (2.4) and (2.5). The differences of these scaled parameters for all of the five time intervals defined in the model were calculated (equations (2.6) and (2.7)).

We performed a t-test of the null hypothesis that data in the 2000-2500 ms after the offset of stimulation are a random sample from a normal distribution with mean 0 and unknown variance, against the alternative that the mean is not 0. The null hypothesis was accepted for this time interval for Cathodic stimulation (p=0.16). Considering that the null hypothesis was rejected for the 1500-2000 ms time interval after the offset of stimulation, we conclude that the effects of Cathodic CES on unit activity lasts 2 sec following the offset of stimulation.

Appendix B

Electrochemical reaction

We have assessed the electrochemichal reaction at the stimulation site based on the method proposed by Shanon 1992[1]. Shanon demonstrates that the following relation can be used to determine the parameters for safe stimulation.

$$\log(Q/A) = k - \log(Q)$$

Where Q is charge in µC and A is surface area in cm^2 and tissue damage has been shown to occur conservatively when $k > 1.5$. In this study we have the following parameters:

Material = stainless steel

Diameter of the cathode = 1.6 mm

Area of the cathode = 0.02 cm^2

Diameter of the anode = 5.33 mm

Area of the Anode = 0.0573 cm^2

If we assume our maximum current is 5 mA and take the leading phase of the stimulation pulse to be 100 µs then Q will be 0.5 µC. According to the equation above we will have the following:

$$\text{Log}(25) = k - \log(0.5)$$

$$1.4 = k - -0.3$$

$$k = 1.1 \text{ which is} < 1.5$$

It should also be noted that 25 μC/cm^2 is below the maximum reversible charge storage capacity of stainless steel (40 – 50 μC/cm^2)[2].

However, we recognize that the equation of Shannon is relevant for 50 Hz stimulation only and the fact that we are using a screw as the cathode does not take into account that local concentrations of charge density may be present around the threads of the screws, representing local discontinuities in the electrode that may affect charge distribution[3]. This would suggest that the highest concentration of charge density occurs in a ring around the diameter of the electrode (screw).   Since these concentrations of charge density could have occurred in a smaller geometric surface area, it may be that charge density exceeded safe limits.   Inspection of the tissue directly below the stimulating electrodes following histology did not reveal any gross tissue damage, however tissue damage was not quantified in this study. Furthermore the voltage at the electrode during constant current stimulation was not monitored and could have exceeded ±1 V, the limits for irreversible faradaic reactions at the electrode-tissue interface for stainless steel electrodes.   However, the impedance of these electrodes at the electrode-tissue interface was likely << 1 KΩ suggesting that it would take <1 V to drive the maximum of 5 mA.

References

1. Shannon RV. A model of safe levels for electrical stimulation. IEEE Trans Biomed Eng 1992;39(4):424–6.

2. Merrill DR, Bikson M, Jefferys JG. Electrical stimulation of excitable tissue: design of efficacious and safe protocols.J Neurosci Methods. 2005 141(2):171-98.

3. McIntyre CC, Grill WM. Finite element analysis of the current-density and electric field generated by metal microelectrodes. Ann Biomed Eng. 2001 29(3):227-35.